DNV·GL

Final Report

Technical Root Cause Analysis of Delmont Line 27 Failure – April 29, 2016

Spectra Energy Partners, LP
Houston, Texas

Report No.: OAPUS307KKRA (PP158894)
October 14, 2016

Project Name:	Technical Root Cause Analysis of Delmont Line 27 Failure – April 29, 2016
Customer:	Spectra Energy Partners, LP
Contact Person:	J. Andrew Drake, P.E.
Date of Issue:	October 14, 2016
Project No.:	PP158894
Organization Unit:	Incident Investigation
Report No.:	OAPUS307KKRA

DET NORSKE VERITAS (U.S.A.), INC. (DNV GL)
Oil & Gas
Materials & Corrosion Technology Center
Incident Investigation
5777 Frantz Road
Dublin, OH 43017-1886
United States
Tel: (614) 761-1214
Fax: (614) 761-1633
www.dnvgl.com

Task and Objective:

Please see Executive Summary.

Prepared by

Katherine M. Buckingham, Ph.D.
Principal Engineer

Verified by

John A. Beavers, Ph.D., FNACE
Senior Principal Engineer

Approved by

David M. Norfleet, Ph.D., P.E.
Head of Section –
Incident Investigation

Thomas A. Bubenik, Ph.D.
Senior Principal Engineer

☐ Unrestricted Distribution (internal and external)
☐ Unrestricted Distribution within DNV GL
☐ Limited Distribution within DNV GL after 3 years
☐ No Distribution (confidential)
☐ Secret

Keywords

Rev. No.	Date	Reason for Issue:	Prepared by:	Verified by:	Approved by:
0	2016-10-06	First Issue			
1	2016-10-14	Final			

Executive Summary

Spectra Energy Partners, LP (Spectra) retained Det Norske Veritas (U.S.A.), Inc. (DNV GL) to perform a technical root cause failure analysis (RCFA) on a 30-inch nominal diameter natural gas transmission pipeline (Line 27) that experienced an in-service failure. The pipeline that failed is part of the Penn-Jersey System, which transports natural gas approximately 265-miles from Delmont, PA to Lambertville, NJ. The system is owned and operated by Texas Eastern Transmission, LP (TETLP), a subsidiary of Spectra Energy, and consists of three (3) parallel pipelines (Line 12, Line 19, and Line 27) and one (1) pipeline with multiple loops (Line 28).

The failure occurred at 8:13 AM EDT on April 29, 2016 at a location approximately 1.6 miles downstream (D/S) of the Delmont, PA Compressor Station at Milepost (MP) 2.06, Survey Station 108+90. During the failure, a 25.87-foot long section of pipe was ejected from the pipeline. The ejected section contained a portion of a girth weld (GW), identified as GW 2470, which was adjacent to the failure origin.

The failure occurred in a mostly rural area in a region where the topography is hilly. During excavation of the failed pipe, multiple French drains were observed in the vicinity of the failure. The presence of multiple French drains in the area indicates that the failure occurred in an area prone to high moisture.

The portion of the pipeline that failed is comprised of 30-inch nominal diameter by 0.404-inch nominal wall thickness, API 5L Grade X65 line pipe steel that was manufactured by U.S. Steel Corporation and contains a double submerged arc welded (DSAW) longitudinal seam. The pipeline was installed in 1981 and is externally coated with a mill-applied fusion bonded epoxy (FBE) coating along the pipe body and a field-applied polyethylene tape coating system at the girth welds (GWs). The pipeline has an impressed current cathodic protection (CP) system.

The maximum operating pressure (MOP) of the line is 1,050 psig, which corresponds to 60.0% of the specified minimum yield strength (SMYS) at the failure location. The normal operating pressure ranged between 900 to 1,040 psig, which corresponds to 51.4% to 59.4% of SMYS at the location. The pressure at the time and location of failure was 1,039 psig, which corresponds to 59.3% of SMYS.

The portions of the pipeline that contained the failure location, as well as sections containing girth welds near the failure, were removed and sent to DNV GL for metallurgical analysis to determine the immediate cause of the failure. The metallurgical report was previously issued to Spectra and PHMSA on July 5, 2016. The results of the metallurgical analysis indicate that "*the rupture initiated at the 5:30 o'clock orientation at a region of external*

corrosion near Girth Weld 2470. The rupture initiated in the axial direction and then propagated axially and circumferentially. Final failure was ductile in nature." Supplemental analyses identified evidence of wet-dry cycling that contributed to the observed external corrosion.

The objective of the RCFA, per the amended corrective action order issued by PHMSA, was to "*document the decision making process and all factors contributing to the failure*" and "*include findings and any lessons learned and whether the findings and any lessons learned are applicable to other locations within Spectra's PJS System*." The analysis focused on Delmont Section 1 of Line 27 (Isolated Segment), which contained the Failure and extended from Delmont Station to approximately MP 15. The conclusions and recommendations for this RCFA are based on the findings from the metallurgical report, supplemental analyses performed by DNV GL, as well as information obtained from Spectra.

DNV GL identified two technical root causes of the failure. The root causes are associated with the occurrence or absence of actions / decisions that either resulted in or worsened the failure. DNV GL reserves the right to modify or supplement these conclusions should new information become available.

1. ***Selection and use of tape coatings at girth welds did not mitigate external corrosion at the failure location.***

   Basis:

   Based on the presence of external corrosion at the failure location, the polyethylene tape coating was compromised. The tape coating failed to prevent moisture from reaching the pipe steel, allowing the external corrosion process to occur. The cathodic protection was also not beneficial in mitigating corrosion at the failure location.

   The external corrosion was exacerbated by

   - The mode of coating failure
   - The occurrence of wet/dry cycling

   Additional possible contributing factors include (1) the operating temperature of the line and (2) the possibility of elevated chloride levels.

2. ***The high corrosion growth rate of the feature that failed was not recognized, based on the available information. Thus, the use of applicable regulatory and industry standards (ASME B31.8S), and the implicit corrosion growth rate therein, resulted in a non-conservative***

estimate of the remaining life of the feature. Accordingly, the feature that failed was not prioritized for remediation.

Basis:

- The most likely corrosion growth rate associated with the feature that failed was approximately 45 mpy.
- The corrosion growth rate associated with the feature that failed was much higher (five or more times higher) than the rate implicit in ASME B31.8S Figure 4, which was used by Spectra to determine remediation priorities. Thus, the failure location was not prioritized for remediation.
- It is unlikely that Spectra could have identified the rate associated with the failure based on available data and information before the failure.

The RCFA identified improvements (Lessons learned) that could be made within the integrity management program. These observations are given below.

1. For new construction and field repairs, avoid the use of wraps/coatings that can disbond and shield CP.
2. Improve understanding and recognition of mechanisms and conditions under which extreme damage rates can occur
    - Investigating locations where corrosion is occurring under disbonded GW coating may provide insights needed to identify extreme value corrosion growth rates. Although data existed in 2012 indicating corrosion under GW coatings was not being controlled by CP, additional investigative efforts were not triggered. However, using only the 2012 ILI results and Figure 4 in ASME B31.8S, approximately 800 locations were prioritized for remediation before the failure location.
3. As stated in ASME B31.8S, Figure 4 is applicable for a “reasonably anticipated or scientifically proven rate of corrosion” and is routinely used for the general threat of external corrosion. Once a threat with an accelerated corrosion rate, such as disbonded coating combined with wet dry cycling, is identified, an alternative threat assessment should be performed to handle the specific threat.
4. Enhance review, interpretation, and comparison of in-line inspection results to better identify areas with high growth rates or the possibility for high growth rates.
5. Incorporate lessons learned within the integrity management plan and risk models to improve identification of unusual integrity threats on pipelines.
    - Treat specific damage mechanisms (e.g., corrosion under disbonded coatings at girth welds) not addressed by general categories (e.g., external corrosion) as separate threats to be managed within an integrity management program.

- Consider the distribution of damage rates (including extreme values) instead of average or typical rates for a mechanism.
- Integrate data from corrosion, inspection, and risk management programs and combine knowledge of subject matter experts in these disciplines.

Table of Contents

1.0 INTRODUCTION 1
1.1 Background 1
2.0 TECHNICAL APPROACH 2
2.1 Methodology 2
2.2 Approach 3
3.0 METALLURGICAL CAUSE 4
4.0 SUPPLEMENTAL ANALYSES 5
4.1.1 Analysis of Tape Coatings from Adjacent Girth Welds 6
4.1.2 Corrosion Product Analyses 7
4.1.2.1 X-ray Diffraction 7
4.1.2.2 Energy Dispersive Spectroscopy 7
4.1.2.3 Corrosion Product Cross Section 7
4.1.3 Examination of External Wall Loss at Adjacent Girth Welds 8
4.1.4 Soil and Ground Water Analyses 8
5.0 TIMELINE OF EVENTS 9
6.0 TECHNICAL ROOT CAUSE ANALYSIS 12
6.1 Technical Root Cause 1 12
6.1.1 Primary Factors 13
6.1.2 Possible Contributing Factors 14
6.1.3 Role of Cathodic Protection System 15
6.1.3.1 CP and 2005 ILI in the Vicinity of the Failure 16
6.1.3.2 CP and 2012 ILI in the Vicinity of the Failure 17
6.2 Technical Root Cause 2 18
6.2.1 ILI Background 18
6.2.2 Corrosion Growth Rates 20
6.2.2.1 Corrosion Growth Rates at the Failure Location 20
6.2.2.2 Corrosion Growth Rates Distributions 20
6.2.2.3 Statistical CGR Analysis 21
6.2.2.4 Combined CGR and ILI Tolerance Analysis 22
6.2.3 Application of ASME B31.8S-2004 Figure 4 23

Table of Contents (continued)

7.0 SUMMARY AND CONCLUSIONS 24

8.0 LESSONS LEARNED 25

Appendices

Appendix A – References

Appendix B – Additional Tape Coating Photographs

Appendix C – ILI to ILI Master Methodology

List of Tables

Table 1. Summary of dimensional analyses performed on areas of external corrosion on Line 27 GWs 2440 – 2520 in the vicinity of the failure. 27

Table 2. Results of compound analyses, using X-ray diffraction, performed on representative corrosion products removed from GWs on Line 27 in the vicinity of the failure. 28

Table 3. Results of elemental analyses, using EDS, performed on external corrosion deposits removed from GWs on Line 27, in the vicinity of the failure. 29

Table 4. Summary of results of analyses performed on soil samples removed along Line 27 after the failure and analyzed by DNV GL. 30

Table 5. Summary of risk rankings[1], performed by Spectra, between 2011 and 2015 for a portion of the Isolated Segment that contained the Failure. 31

Table 6. Summary of the ILI as-called depths and measured feature depths associated with the failure location. 32

Table 7. Summary of statistical parameters associated with the corrosion growth rate distributions determined from the ILI datasets and Field-measured dataset. Data shown in Figure 36. 32

Table 8. Summary of probability calculations based on an initial feature depth of 0.101 mils or 25% wall thickness. 33

List of Figures

Figure 1. Photographs of the Failure Site showing the failure crater, the ejected pipe section, the U/S and D/S termini of the failure, and the locations where soil samples were collected. 34

Figure 2. Field photographs showing the topography in the vicinity of the Failure Site. 35

Figure 3. Photographs showing the ends of a French drain within the excavation site near the Failure. 36

Figure 4. Drawing (Left) and satellite imagery (Right) showing locations of French drains relative to the Failure Site. The blue lines on the drawing (Left) correspond to locations of French drains. The white and red dots identified in the satellite imagery (Right) correspond to GPS coordinates obtained for French drains and the failure crater, respectively. The red line corresponds to the location of Line 27 and the yellow star corresponds to the failure origin in the satellite imagery. 37

Figure 5. Photographs (top) and color map from laser scanning (bottom) showing region of external wall loss at the failure origin following cleaning the pipe with a solvent. The tape measure indicates distance CW from the 12:00 o'clock orientation at GW 2470. 38

Figure 6. Photograph showing the region of external wall loss at GW 2460 (Left) and color map showing the remaining wall thickness (viewed from the OD surface) from laser scan data (Right). The tape measure indicates distance CW from the 12:00 o'clock orientation at GW 2460. 39

Figure 7. Photographs showing the regions of external wall loss at GW 2480 and color maps showing the remaining wall thickness (viewed from the OD surface) from laser scan data: wall loss region near 3:00 o'clock orientation (Left) and wall loss region near 9:00 o'clock orientation (Right). The tape measure indicates distance CW from the 12:00 o'clock orientation at GW 2460. 40

Figure 8. Schematic and a google map image showing girth welds on Line 27 in the vicinity of the failure. The locations where metallurgical, tape coating, corrosion deposit, soil, and ground water samples were taken for various analyses are identified on the schematic. 41

Figure 9. Photographs showing the tape coating and the pipe surface at GW 2450 before and after removal of the tape from the pipe. 42

List of Figures (continued)

Figure 10. Photographs (Top) and light photomicrographs (Bottom) showing the polyethylene tape and mastic surfaces of tape coatings from GW 2440 and GW 2450. 43

Figure 11. FTIR spectral comparison of representative tape sample removed from GW 2450 to a standard spectrum for chlorinated polyethylene. 44

Figure 12. EDS data collected from a representative cross sectional mount of the tape coating from GW 2520. Numbers in photographs indicate locations of analyses..... 45

Figure 13. EDS data collected from a representative cross sectional mount of corrosion products from GW 2440 (100X magnification). Numbers in photographs indicate locations of analyses. 46

Figure 14. EDS data collected from a representative cross sectional mount of corrosion products from GW 2440 (500X magnification). Numbers in photographs indicate locations of analyses. 47

Figure 15. Plot showing chloride content (ppm) identified in soil samples collected along the Isolated Segment in the vicinity of the Failure. 48

Figure 16. Timeline showing key events for Line 27 (Isolated Segment only) from the time of construction January 1, 2010. The timeline includes dates for (1) construction (Black x and brackets), (2) CP related activities (blue circles, brackets, and blocks), (3) integrity related assessments (orange triangles and brackets), and (4) ILI related digs (Green squares). 49

Figure 17. Timeline showing key events for Line 27 (Isolated Segment only) from January 1, 2010 until the failure on April 29, 2016. The timeline includes dates for (1) construction (Black x), (2) CP related activities (blue circles, brackets, and blocks), (3) integrity related assessments (orange triangles), (4) ILI related digs (Green squares), (5) aerial patrol (red circles), and (6) the April 29, 2016 failure (purple X)..... 50

Figure 18. Satellite imagery showing the failure site coincident with an area of probable high moisture content: Imagery from 4/1994 (Left) and 4/2016 (Right). Red dotted lines identify the perimeter of the failure crater and yellow arrows point to high moisture areas. 51

Figure 19. Plot showing the elevation profile for Line 27 in the vicinity of the Failure. The vertical green line on the plot identifies the location of the April 29, 2016 failure. 52

List of Figures (continued)

Figure 20. Plot showing Delmont discharge temperatures between 2012 and 2016. 53

Figure 21. Line 27 Delmont discharge in the vicinity of the failure: External metal loss depths reported in 2005 In-Line inspection report aligned to least negative pipe-to-soil potentials between 1983 and 2005. 54

Figure 22. Line 27 Delmont discharge in the vicinity of the failure: External metal loss depths reported in 2012 In-Line inspection report aligned to least negative pipe-to-soil potentials between 2005 and 2012. 55

Figure 23. Line 27 Delmont discharge in the vicinity of the failure: External metal loss (orientations and depths) reported in 2005 In-Line inspection report between test stations located upstream and downstream of the 2016 failure. (Figure 7) 56

Figure 24. Line 27 Delmont discharge in the vicinity of the failure: External metal loss (orientations and depths) reported in 2012 In-Line inspection report between test stations located upstream and downstream of the 2016 failure. 57

Figure 25. 2005 ILI results (depths) versus distance downstream of Delmont Compressor Station. 58

Figure 26. 2012 ILI results (depths) versus distance downstream of Delmont Compressor Station. 59

Figure 27. Metal loss depth unity plot from digs following 2005 ILI run. Data provided by Spectra [Ref. 57]. 60

Figure 28. Metal loss depth unity plot from 2012 - 2015 digs following 2012 ILI run. Data provided by Spectra [Ref. 57] 60

Figure 29. External ILI calls from the 2005 and 2012 ILI runs showing a strong correlation with girth weld locations (vertical lines). 61

Figure 30. Distribution of feature depths determined from 2016 digs performed between May 17, 2016 and August 20, 2016 on the Isolated Segment and the depths determined for features near GWs at and near the failure location vs. ILI log distance 62

Figure 31. Distribution of corrosion rates determined from 2016 digs performed between May 17, 2016 and August 20, 2016 on the Isolated Segment and the corrosion rates determined for features on GWs at and near the failure location vs. ILI log distance. Corrosion rates determined based on comparison to 2012 ILI results. 63

List of Figures (continued)

Figure 32. Histogram showing the distribution of corrosion rates determined from 2016 digs performed between May 17, 2016 and August 20, 2016 on the Isolated Segment and the corrosion rates determined for features on GWs at and near the failure location. Corrosion rates determined based on comparison to 2012 ILI results. 64

Figure 33. Histogram showing the distribution of corrosion rates determined from the ILI-ILI Master dataset. Corrosion rates determined based on comparison of the 2005 ILI data to the 2012 ILI data. 65

Figure 34. Distribution fit of a 3-Parameter Lognormal to the corrosion growth rates determined from the comparison of the 2016 Field measurements and 2012 ILI data. 66

Figure 35. Distribution fit of a 3-Parameter Lognormal to the corrosion growth rates determined from the comparison of the 2005 and 2012 ILI data. 66

Figure 36. Combined histogram showing the previous two figures overlaid onto each other (i.e. 2005 - 2012 ILI data distribution overlaid with 2012 ILI data – 2016 Field measurement distribution. 67

Figure 37. Plot showing the probability of a given CGR, the corresponding probability for an undercall, and the combined probability. 68

Acronyms and Definitions

Term	Definition
ACAO	Amended Corrective Action Order [Ref. 1]
BSCAT™	Barrier-based Systematic Cause Analysis Technique
CGR	Corrosion Growth Rate
CP	Cathodic Protection
CP Shielding	1) Preventing or diverting the cathodic protection current from its intended path. NACE Standard RP0169-2007, Control of External Corrosion on Underground or Submerged Metallic Piping Systems. 2) High resistance or non-conducting material preventing cathodic protection current from reaching the structure, or low resistance material diverting the current away from the structure to be protected. PHMSA Corrosion Enforcement Guidance, p. 4 (12/7/2015), http://www.phmsa.dot.gov/staticfiles/PHMSA/Pipeline/TQGlossary/Glossary.html.
DSAW	Double Submerged Arc Welded
DNV GL	Det Norske Veritas (U.S.A), Inc.
D/S	Downstream
EDS	Energy Dispersive Spectroscopy
EDT	Eastern Daylight Time
Failure	Incident that occurred on April 29, 2016 on Line 27 of the Penn-Jersey System, located at MP 2.06, Survey Station 108+90, Girth Weld 2470, Wheel Count 8680.93 from 2012 ILI Survey, Lat: 40.39682924, Lon: -79.52351279.
Failure Location	The failure origin adjacent to GW 2470
Failure Site	The geographical area in proximity of the Failure Location
FBE	Fusion bonded epoxy
Failure Pressure Ratio (FPR)	Failure Pressure Ratio (FPR) is a ratio of the predicted failure pressure of the metal loss anomaly reported by the ILI tool divided by the maximum allowable operating pressure (MAOP) of the pipeline segment.
FTIR	Fourier Transform Infrared
GW	Girth weld
ICCP	Impressed Current Cathodic Protection
ILI	In-line Inspection
IMP	Integrity Management Plan

Term	Definition
Isolated Segment (Delmont Section 1)	The 15-mile segment of Line 27, running from the discharge of the Delmont Compressor Station (MP 0.41) in Delmont, Pennsylvania, to the Conemaugh River Valves (MP 15.45). It is the portion of Line 27 that was shut-in after the Failure by closing main line valve MLV 27-263 and cross-over valves 27-917 and 27-273 downstream of the Failure Site, and MLV 27-289 upstream of the Failure Site. [Ref. 1, pg 2]
MFL	Magnetic Flux Leakage
MP	Mile Post
Penn-Jersey System	The pipeline system operated by Texas Eastern Transmission, LP, consisting of four (4) parallel pipelines (the 30 and 36-inch Line 27, the 24-inch Line 12, the 30-inch Line 19, and the 36-inch Line 28 with multiple loops) that transport natural gas from Delmont, Pennsylvania, to Lambertville, New Jersey, for approximately 263 miles. Also referred to as the Affected Segment and defined in the ACAO. [Ref. 1, pg 2]
PE	Polyethylene
PHMSA	Pipeline and Hazardous Materials Safety Administration
Root Cause	The basic, underlying causal factor in the Failure, which, if removed, would have prevented it from occurring. *PHMSA Pipeline Glossary:* https://primis.phmsa.dot.gov/comm/Glossary/index.htm#RootCause.
RCFA	Root Cause Failure Analysis
ROW	Right-of-Way
SEM	Scanning Electron Microscopy
SOP	Standard Operating Procedure
SMYS	Specified Minimum Yield Strength
TETPL	Texas Eastern Transmission, LP
U/S	Upstream

1.0 INTRODUCTION

1.1 Background

Spectra Energy Partners, LP (Spectra) retained Det Norske Veritas (U.S.A.), Inc. (DNV GL) to perform a technical root cause failure analysis (RCFA) on a 30-inch nominal diameter natural gas transmission pipeline (Line 27) that experienced an in-service failure. The pipeline that failed is part of the Penn-Jersey System, which transports natural gas approximately 265-miles from Delmont, PA to Lambertville, NJ. The system is owned and operated by Texas Eastern Transmission, LP (TETLP), a subsidiary of Spectra Energy, and consists of three (3) parallel pipelines (Line 12, Line 19, and Line 27) and one (1) pipeline with multiple loops (Line 28).

The failure occurred at 8:13 AM EDT on April 29, 2016 at a location approximately 1.6 miles downstream (D/S) of their Delmont, PA, Compressor Station, at Milepost (MP) 2.06, Survey Station 108+90. During the failure, a 25.87-foot long section of pipe was ejected from the pipeline; see Figure 1. The ejected section contained a portion of a girth weld (GW), identified as GW 2470, which was adjacent to the failure origin. The failure occurred along the side of a hill, in a mostly rural area where the topography is hilly; see Figure 2. During excavation of the failed pipe, multiple French drains were observed in the vicinity of the failure. Figure 3 contains photographs showing the proximity of one of the French drains, relative to the failure location. Spectra confirmed the locations of multiple French drains in the area, providing drawings of the French drains in the vicinity of the failure as well as GPS coordinates for the French drains identified in the field; see Figure 4. The presence of multiple French drains in the area indicates that the failure occurred in an area prone to high moisture.

The portion of the pipeline that failed is comprised of 30-inch nominal diameter by 0.404-inch nominal wall thickness, API 5L Grade X65 line pipe steel that was manufactured by U.S. Steel Corporation and contains a double submerged arc welded (DSAW) longitudinal seam. The portion of the pipeline was installed in 1981 and is externally coated with a mill-applied fusion bonded epoxy (FBE) coating along the pipe body and a field-applied polyethylene tape coating system at the girth welds (GWs). The pipeline has an impressed current cathodic protection (CP) system.

The maximum operating pressure (MOP) of the line is 1,050 psig, which corresponds to 60.0% of the specified minimum yield strength (SMYS) at the failure location. The normal operating pressure ranged between 900 to 1,040 psig, which corresponds to 51.4% to 59.4% of SMYS at the location. The pressure at the time and location of failure was 1,039 psig, which corresponds to 59.3% of SMYS.

The portions of the pipeline that contained the failure location, as well as sections containing girth welds near the failure, were removed and sent to DNV GL for metallurgical analysis to determine the immediate cause of the failure. The metallurgical report was previously issued to PHMSA on July 5, 2016 [Ref. 2].

The objective of the RCFA, per the amended corrective action order (ACAO) issued by PHMSA, was to "*document the decision making process and all factors contributing to the failure*" and "*include findings and any lessons learned and whether the findings and any lessons learned are applicable to other locations within Spectra's PJS System*." [Ref. 1]. The analysis focused on Delmont Section 1 of Line 27 (Isolated Segment), which contained the Failure and extended from Delmont Station to approximately MP 15. The conclusions and recommendations for this RCFA are based on the findings from the metallurgical report, supplemental analyses performed by DNV GL, as well as information obtained from Spectra. The information obtained from Spectra, and considered as part of the RCFA, is referenced in Appendix A.

DNV GL reserves the right to modify or supplement the conclusions presented herein should new information become available.

2.0 TECHNICAL APPROACH

2.1 Methodology

DNV GL utilized two methods/processes to determine the technical root cause(s) of the Delmont Line 27 Failure. Both methodologies are based on causal analysis, which is the core of an incident investigation. The methods utilize systematic approaches of processing evidence gathered during an investigation in order to identify the barriers or causal factors that led to the failure. Although the approaches differ, both methods assisted in the identification of root causes presented and the development of corrective and/or remedial measures.

One of the methods used by DNV GL for this investigation was the Barrier-based Systematic Causal Analysis Technique (BSCAT™). This method identifies barriers that contributed to an incident. Barriers are factors in place to prevent or mitigate threats from escalating into an incident. The BSCAT™ method specifically combines the DNV GL's Loss Causation Model and BowTie diagrams to identify and assess the effectiveness and/or existence of barriers within a system to prevent specific threats from escalating into an incident.

The second method used for this investigation was TapRoot®. This method identifies causal factors that contributed to an incident. Causal factors are the occurrence or absence of decisions / actions prior to or during an incident that either resulted in or worsened the

incident. Taproot is a systematic process used to identify these causal factors, identify root causes associated with each causal factor, and develop corrective and/or remedial measures to mitigate the reoccurrence of similar failures.

2.2 Approach

DNV GL performed supplemental analyses, reviewed various materials obtained from Spectra (i.e. technical documents, manuals, maps, and data) as well as performed interviews with Spectra personnel. The materials and interviews are grouped into the following categories:

- Incident Related Documents - References 1 - 25,
- Design and Construction Related Documents - References 26 - 39,
- Integrity Related Documents – References 40 – 99,
- Dig and Repair Historical Documents - References 100 – 119,
- Management of Change Documents – References 120 – 121,
- Cathodic Protection Records – References 122 – 128,
- Leak Detection Documents – References 129 – 142,
- Operations Related Documents – References 143 – 151,
- Other Documents – References 152 - 155, and
- Interviews – References 156 - 160.

A complete list of the materials reviewed for the RCFA is provided in Appendix A.

The documents listed above were used for the following tasks:

- Metallurgical cause determination for the failure.
- Timeline creation of events leading up to the failure.
- Technical root cause(s) determination for the failure.

It is important to note that the analyses described within this report were only performed for the Isolated Segment of the pipeline affected by the failure (i.e. Line 27 Delmont Section 1). The findings and discussion presented in this report are not necessarily representative or indicative of all pipeline systems and programs covered by Spectra and Spectra subsidiaries.

3.0 METALLURGICAL CAUSE

DNV GL performed a metallurgical analysis on the portions of the pipeline associated with the failure and indicate that "*the rupture initiated at the 5:30 o'clock orientation at a region of external corrosion near Girth Weld 2470. The rupture initiated in the axial direction and then propagated axially and circumferentially. Final failure was ductile in nature*."[Ref 2] Figure 5 contains photographs of the failure origin, provided in the metallurgical report, after cleaning and alignment of the failed pipe sections. The region of external corrosion associated with the failure extended 12 inches in the longitudinal direction and 55 inches in the circumferential direction (i.e. 58% around the circumference of the pipe at the girth weld). The maximum depth of the external corrosion was 75% of the measured wall thickness at the failure origin (i.e. 0.303 inches in depth based on a nominal wall thickness of 0.404 inches).

During the investigation, external corrosion features were identified at the failure location (GW 2470), as well as at GWs located U/S and D/S from the failure (i.e. GWs 2460 and 2480, respectively). Figure 6 and Figure 7 are photographs, provided in the metallurgical report, showing the areas of external corrosion at GW 2460 and GW 2480, respectively, and Table 1 summarizes dimensional analyses performed on the areas. As shown in the figures, one area of external corrosion was identified near GW 2460 and two regions of external corrosion were identified near GW 2480.

The area of external corrosion at GW 2460 spanned between the 3:44 and 7:55 o'clock orientation, measuring approximately 5.2 inches in length longitudinally and 32.6 inches in length circumferentially (i.e. 35% around the circumference of the pipe). The maximum depth of the corrosion was 0.099 inches, which corresponds to a wall loss of 24%, based on a nominal wall thickness of 0.404 inches.

Two areas of external corrosion were identified at GW 2480: one centered at the 3:00 o'clock orientation and one centered at the 9:00 o'clock orientation. The area of external corrosion at the 3:00 o'clock orientation spanned between the 1:37 and 4:19 o'clock orientations, measuring 7.2 inches in length longitudinally and 21.1 inches in length circumferentially (i.e. 22% around the circumference of the pipe). The maximum depth of corrosion was 0.174 inches, which corresponds to a wall loss of 43%, based on a nominal wall thickness of 0.404 inches. The area of external corrosion at the 9:00 o'clock orientation spanned between the 7:10 and 9:30 o'clock orientations, measuring 6.3 inches in length longitudinally and 18.4 inches in length circumferentially (i.e. 20% around the circumference of the pipe). The maximum depth of corrosion was 0.104 inches, which corresponds to 26% wall loss, based on a nominal wall thickness of 0.404 inches.

As a consequence of the failure, the field joint coatings at the failure location (GW 2470) and GWs 2460 and 2480 were not available for examination. However, the fact that the corrosion exists at these three girth welds indicates that the field girth weld coatings were compromised.

Additional findings from the metallurgical analysis include:

- The soil samples removed from the U/S end of the crater and the failure origin are classified as lean clay with sand and silty gravel with sand, respectively.
- The soils are mild to moderately corrosive, based on measured resistivities.
- There was no evidence of crack-like indications, using magnetic particle inspection, on the internal and external surfaces of the pipe in the vicinity of GWs 2460, 2470, and 2480.
- There was no evidence of any metallurgical defects in the line pipe steel, with the exception of fire damage that occurred after the failure.
- There was no evidence of external corrosion on the pipe beneath the mill applied FBE coating in the vicinity of the failure, with the exception of those regions beneath the field applied girth weld coating.
- There was no evidence of secondary cracking, internal corrosion, or other integrity threats identified on the pipe sections examined.
- The tensile properties of Joint 2510 meet tensile requirements for API 5L Grade X65 line pipe steel in place at the time of construction.
- The chemistries of Joints 2440 - 2520 meet composition requirements for API 5L Grade X65 line pipe steel in place at the time of construction.

4.0 SUPPLEMENTAL ANALYSES

As a consequence of the failure, field joint coatings and corrosion products were not available at or near the origin of failure for the metallurgical analysis. To gain insight into the likely coating condition and corrosion products present at the failure location, tape coatings and corrosion products from GWs, on Line 27, that were in the vicinity of the failure were examined. Figure 8 is a schematic and Google Earth image showing the GWs adjacent to the failure, as well as the locations where supplemental samples were collected for analysis. As part of the analyses, ground water samples and additional soil samples in the vicinity of the failure were collected and analyzed to determine whether there was evidence of corrosive species in the vicinity of the failure that could account for why the failure occurred at that specific location.

Details of the analyses are provided below.

4.1.1 Analysis of Tape Coatings from Adjacent Girth Welds

Figure 9 contains representative photographs showing the tape coating (i.e. coating at the field joints) and pipe surface from GW 2450 on Line 27, which was two joints U/S of the failure origin. During the failure investigation, six (6) sections of pipe containing GWs 2440, 2450, and 2490 - 2520 were removed from the pipeline and brought to Delmont Station for examination. The purpose of the examination was to assess the condition of the field coatings in the vicinity of the failure to gain insight into the likely failure mode of the coating at the failure location.[1] At the time of the examination, the field joint coatings were photographed, removed, and collected for further analysis at DNV GL. As seen in Figure 9, coating damage in the form of wrinkles and lack of adhesion of the tape was observed. Similar observations were made for GWs 2440 and 2490 - 2520. The extent of the coating damage on these other GWs varied; see Appendix B. In some cases, corrosion products were present beneath the tape coatings, which indicates that water reached the pipe steel.

As installed, the tape coating for all six girth welds consisted of two (2) wraps of tape with an overlap width that ranged from 1.5 to 3 inches. Each wrap was approximately 6.25 inches wide with a total width of 9 to 11 inches. The average tape thickness was 22 mils and the average thickness of the combined tape and mastic was approximately 40 mils.

The tape coating at each of the six GWs was similar in appearance, with a brown/maroon colored tape on the external surface and a black mastic material on the internal surface of the tape coating. Figure 10 contains photographs and light photomicrographs showing the external surface (tape) and internal surface (mastic surface) of representative coatings. As shown, the external tape surface appears brown and the internal mastic surface appears black.

Fourier transform infrared (FTIR) spectroscopy was performed on tape coating removed from the six GWs in order to identify the composition of the coating. All six coatings consisted of a chlorinated polyethylene (PE) tape and a polyvinyl chloride (PVC) based mastic material. Figure 11 contains a representative FTIR spectral comparison of the tape from GW 2450 to a standard spectrum for chlorinated PE. The matched peaks are a positive indication of chlorinated PE.

1 Although a coating sample was not recovered from GW 2470 (i.e. near the failure origin) as a consequence of the failure, the corrosion profile is consistent with the upstream and downstream girth welds indicating that a coating was most likely present prior to the failure.

Based on the fact that the tape was identified as a chlorinated PE, further analysis was performed on a representative tape sample (i.e. tape from GW 2520) to determine whether the chlorine present in the tape may have contributed to the corrosion. Figure 12 contains the results of energy dispersive spectroscopy (EDS) scans performed in a representative areas through the thickness of the chlorinated PE tape and the mastic. The chlorinated PE tape contained slightly higher amounts of chlorine than the mastic material. There was no clear evidence, based on multiple scans through the thickness of the chlorinated PE tape, to indicate that there was selective leaching of chlorine from the tape.

4.1.2 Corrosion Product Analyses

4.1.2.1 X-ray Diffraction

X-ray diffraction (XRD) was performed on representative corrosion products collected from GWs 2420, 2440, 2450, and 2500 to identify the compounds present and to determine the likely mechanism for the corrosion. Due to the limited amount of corrosion deposits available from the other GWs, those deposits were not analyzed using XRD. The results of the analyses are summarized in Table 2. The primary compounds identified for all four samples were goethite (FeOOH) and magnetite (Fe_3O_4). Goethite is one of the most thermodynamically stable iron oxides under aerobic (high oxygen) conditions. Conversely, magnetite is a metastable phase formed under low oxygen conditions.

4.1.2.2 Energy Dispersive Spectroscopy

Elemental analyses of the corrosion products associated with GWs 2420, 2440, 2450, 2490 - 2520 were also performed using EDS to determine the composition and identify the presence of any corrosive species that may have played a role in the corrosion. The results of the EDS analyses are summarized in Table 3. The two primary constituents found in all of the samples analyzed are iron (Fe) and oxygen (O). Based on the results of the XRD analyses, the high amounts of iron and oxygen are likely in the form of iron oxides. Varying quantities of chlorine (Cl) were identified within the deposits, likely associated with chlorides. Elevated concentrations of chlorine were detected in samples removed from the U/S and D/S GWs in the vicinity of the failure origin.

4.1.2.3 Corrosion Product Cross Section

A representative layered corrosion product from GW 2440 was mounted in epoxy, polished and examined in a scanning electron microscope (SEM). This corrosion product was selected as it was relatively thick and solid. In the cross section, alternating light and dark layers were observed within the deposits. Energy dispersive spectroscopy was performed on the layered regions to characterize their elemental compositions. Figure 13 and Figure 14 contain the results of EDS scans performed on the layered regions identified

in the deposits. The two primary constituents are iron (Fe) and oxygen (O), which are characteristic of iron oxides. The light area in Figure 13, Scans 4 – 6, has an average O content of approximately 24.8 wt.%, while the darker bands, Scans 1 – 3, have an average O content of 31.4 wt.%. Similar results were obtained when the product was examined at higher magnifications; see Figure 14. At higher magnifications, the average O content in the light and dark regions were 29 wt% and 32.9 wt %, respectively. Given that the XRD analyses identified goethite and magnetite as the two compounds associated with the corrosion products, these values were compared to the calculated oxygen content for goethite (36 wt.%) and magnetite (28 wt.%). These values closely correlate, indicating that the light areas are likely magnetite and the darker areas are likely goethite.

The presence of goethite and magnetite in a layered morphology is consistent with aqueous corrosion under wet-dry cycling.[2] Goethite is the stable oxide when oxygen transport is high, such as during the drying stages when the electrolyte is relatively thin. Magnetite is predominant during saturated conditions or when oxygen is limited (i.e. thick products). The alternating nature of the layers suggests that external variables, such as rain, drainage, and operating temperature contributed to the corrosion process.

4.1.3 Examination of External Wall Loss at Adjacent Girth Welds

Table 1 is a summary of the external wall loss regions identified at GWs 2440 to GW 2520. A rectangle was drawn around the wall loss regions and the maximum axial lengths and circumferential widths were reported. A rectangle was not drawn around GW 2510, as the only feature identified was a negligible anomaly in the cap of the weld at the approximate 6:00 o'clock orientation. As shown in the table, wall loss regions identified at the GWs, excluding GW 2510, ranged from 1.8 to 12.0 inches in the axial direction and 6.1 to 55.0 inches in the circumferential direction. The maximum axial and circumferential lengths were both identified at the failure location (i.e. GW 2470). The maximum axial and circumferential lengths, excluding both GW 2470 and 2510, were 7.2 inches and 34.9 inches, respectively. The maximum depth of corrosion, excluding GW 2470 and 2510, ranged from less than 0.051 inches to 0.217 inches (i.e. wall losses of <12.5% to 54%).

4.1.4 Soil and Ground Water Analyses

Soil analyses were presented in the Metallurgical Report. The two soils taken near the failure site were at 2470 (taken 18 ft off the ROW and at pipe depth) and 2460 (taken below pipe). These are very different soils with respect to water permeability; a high clay / silt content soil (2460) will have a lower permeability than a low clay / silt content soil

2 Nasrazadani, S. and Raman, A., *Formation and Transformation of Magnetite (Fe3O4) on steel surfaces under Continuous and Cyclic Water Fog Testing*, Corrosion, 1993.

(2470). These soils were characterized as 9% clay / 11% silt / 28 % sand / 52% gravel and 39% clay / 34% silt / 25 % sand / 2% gravel for soils at GWs 2470 and 2460 respectively. Note that soil sample 2470 was taken off the Line 27 ROW because of the crater created by the failure. Therefore, it is not possible to characterize the soil right at the failure. For purposes of the failure investigation, water permeability of the soil is important to the wet-dry cycling contributing cause; a higher permeability soil is expected to support this mechanism more than a low permeability soil. There is no data in the literature to quantify the effect of water permeation in soil on the wet-dry cycling corrosion mechanism.

Chlorides are a possible contributing cause to the high corrosion experienced at the failure site. Chlorides may be introduced from several sources: i.e. soil chemistry, water run-off, and materials in contact with the pipe (tape coating, mastic, or primer). Chlorides measured in the soil samples ranged from a few to 31 ppm depending on the location (Table 4). The chloride analyses for the different lines and their relationship relative to the failure are shown in Figure 15. For Line 27, there is a trend of higher chlorides between 50 to 150 feet U/S from the failure location (highest 50 ft upstream). As a consequence of the failure, a soil sample could not be taken from the failure origin. Therefore, a sample was collected 18 ft off the ROW, which exhibited low chloride levels.

At the two locations where ground water was analyzed (Table 4), the chlorides measured in the ground water were higher than measured in the soil samples. The chlorides measured in the ground water were 52 and 108 ppm compared to chlorides in the soil of 13 and 22 ppm respectively.

Although these chloride concentrations are not abnormally high, the presence of chloride could have an effect on the corrosion process by reacting with the iron corrosion products and decreasing the effectiveness of the corrosion products forming protective films that could limit the corrosion rate.

5.0 TIMELINE OF EVENTS

Historical timelines were developed to help visualize and to identify the action/events that occurred leading up to the failure on April 29, 2016 that may have contributed to the failure. The timelines incorporate key events that occurred on the Isolated Segment of Line 27 (Delmont Section 1), unless otherwise noted, between the time of construction and the day of the failure. This segment of Line 27 consists of 15 miles of pipeline that starts at the discharge side of the Delmont Station. Information provided by Spectra was used to populate the timeline with relevant information.

Figure 16 and Figure 17 contain multiple timelines showing key events for the Isolated Segment on Line 27 from the time of construction to the day of the failure. The timelines include dates for: (1) construction (Black x and brackets), (2) CP related activities (blue circles, brackets, and blocks), (3) integrity related assessments (orange triangles and brackets), (4) ILI related digs (green squares), (5) the last aerial patrol prior to the failure (red circles), and (6) the April 29, 2016 failure (purple x).

Construction activities for this line segment started with procurement and manufacture of the line pipe. Spectra contracted with US Steel Corp. in McKeesport, PA to manufacture the line pipe, placing the order on March 2, 1981 [Ref. 39]. The order was part of the Phase I and II expansion activities (identified as the SS-II Expansion) of the Penn-Jersey System. Pipe joints with varying wall thicknesses and steel grades were ordered for the Isolated Segment. The portion of this line segment that failed was comprised of Grade X65 line pipe steel with a 0.404 inch nominal wall thickness and was manufactured between June 20, 1981 and June 28, 1981 [Ref. 38]. Installation of the Isolated Segment occurred between August 3, 1981 and November 10, 1981 (i.e. during the Phase I and II work of the Penn Jersey expansion activities) [Ref. 32]. French drains were identified in the vicinity of the 2016 Failure Location prior to construction of the Isolated Segment. In 1968, repairs were made to French drain tracks 7 and 9a, near Lines 12 and 19 and in the vicinity of the 2016 Failure. After coolers were installed at Delmont Station in 2014.

Cathodic protection (CP) in the form of an impressed current system was applied to the Isolated Segment of Line 27; however, a new CP system was not constructed when Line 27 was installed. Rather, CP was applied via direct connection to the existing CP rectifiers in use for the protection of Line 12 and Line 19 (i.e., a rectifier at MP 0.45, which was installed in 1968, and a rectifier at MP 9.30, which was installed in 1955) [Ref 124]. The CP system in use during the time of installation was impressed current remote ground beds, situated along the pipeline.

Starting in 1983, CP system upgrades and additions have been implemented along the Isolated Segment. In August of 1983, a CP survey was performed on Phase I, II, and III of the Penn Jersey Expansion Program SS-II [Ref. 123]. Since that time, a distributed ground bed was installed at MP 15.43 and a remote ground bed was installed at MP 15.44 in 1985 [Ref. 124]. In 2007, the remote ground bed at MP 9.30 was upgraded [Ref. 124]. In 2008 and 2013, linear anodes were installed at MP 13.62 and MP 0.56, respectively [Ref. 124]. Thus, the impressed current cathodic protection system on the Isolated Segment consists of a mixture of ground bed designs (i.e. remote ground beds, distribute anode beds, and linear anode systems). Periodic operational data were provided for the rectifiers along the line

segment between 1991 and 2002 [Ref. 122]. The dates when the data were acquired are shown in Figure 16. Bimonthly operational data for the rectifiers were obtained; See Figure 16 and Figure 17. Annual pipe-to-soil potential surveys (test station surveys) were also performed on the segment [Ref. 126]. Between 2000 and 2012, on-potentials were acquired during the annual surveys. Starting in May of 2013, on/off potentials were acquired during the surveys.

Multiple integrity assessments including a hydrotest, in-line-inspections (ILIs), periodic threat/risk evaluations, and risk rankings were performed on the Isolated Segment. The first assessment was performed after the segment was installed, during the mainline hydrostatic testing of the SS-II Expansion between October and December of 1981 [Ref. 63]. The portion of the line segment that contained the failure (identified as Section 3 in the hydrotest report) was hydrotested between the afternoon of October 20, 1981 and the morning of October 21, 1981 [Ref. 63].

Three ILIs were performed on Isolated Segment of Line 27 between 1986 and 2012 [Ref 43]. The ILIs were run in 1986, 2005, and 2012 by Tuboscope, Rosen, and GE/PII, respectively. In 1986, a standard resolution ILI was performed [Ref 43]. The results from this inspection were not available. In 2005, Spectra contracted with Rosen Inspection Technologies to run two tools on the line: (1) an electronic geometry pig and (2) a magnetic flux leakage (MFL) pig [Ref 46]. Based on the results of these runs, nine digs were performed on the line between October of 2005 and September of 2007 (see green squares between these dates on the timeline) [Refs. 109 and 110]. In 2012, Spectra contracted with GE/PII North America, Inc. to run two more tools on the line: (1) a multi-channel caliper tool and (2) a Hi-resolution MFL tool with an inertial measurement unit (IMU) [Ref. 44]. Based on the results of these runs, nine digs were performed on the line between September of 2012 and September of 2015 (see green squares between these dates on the timeline), prior to the failure [Refs. 112 - 115]. Additional digs have been performed on the line segment following the failure.

As part of their integrity management program, Spectra performs annual threat/risk assessment evaluation meetings of the Isolated Segment [Ref. 41]. These meetings are performed near the end of the year. Dates for these meetings are shown in Figure 17 for the years 2013, 2014, and 2015. Similar meetings were performed in previous years, but are not shown on the timelines. The last meeting prior to the failure occurred on December 8, 2015 [Ref. 41]. Following the threat/risk evaluation meetings, annual risk ranking meetings are held in the first quarter of the subsequent year. The last risk ranking meeting

for the Isolated Segment was performed in March of 2016 [Ref. 41]. The results of the risk rankings for 2016 as well as those performed in 2011 - 2015 are shown in Table 5 [Refs. 41 and 64]. The primary risks identified for this segment between 2011 and 2015 were external corrosion and outside force.

As part of the leak detection methods used by Spectra, routine aerial patrols are performed along Line 27. The last patrol took place on April 19, 2016 – ten days before the failure. No leaks were identified during that patrol [Ref 129].

6.0 TECHNICAL ROOT CAUSE ANALYSIS

Two technical root causes were identified for the April 29, 2016 failure. The root causes are associated with the occurrence or absence of actions / decisions that either resulted in or worsened the failure.

The two technical root causes of the failure identified by DNV GL are:

1. ***Selection and use of tape coatings at girth welds did not mitigate external corrosion at the failure location.***
2. ***The high corrosion growth rate of the feature that failed was not recognized, based on the available information. Thus, the use of applicable regulatory and industry standards (ASME B31.8S), and the implicit corrosion growth rate therein, resulted in a non-conservative estimate of the remaining life of the feature. Accordingly, the feature that failed was not prioritized for remediation.***

These root causes are discussed in detail in the subsequent sections.

6.1 Technical Root Cause 1

The first technical root cause identified for the April 29, 2016 failure is that the ***selection and use of tape coatings at girth welds did not mitigate external corrosion at the failure location***. This root cause is based on the metallurgical analysis [Ref 2] that reported that the failure occurred at an area of external metal loss at the girth weld, due to corrosion, that ultimately failed by ductile overload at the operating pressure. The presence of external corrosion at the failure location (GW 2470) indicates that the field joint coating was compromised.

Buried carbon steel pipelines are normally protected against external corrosion by a combination of an external coating and cathodic protection (CP). The external coating serves to prevent exposure of the external pipe surface to the surrounding soil environment

and potentially corrosive conditions. The CP system is used to counteract the natural electrochemistry of corrosion that can occur at defects in the external coating through the application of a direct current. Both an external coating and CP system were in place on Line 27 to minimize the threat of external corrosion.

Based on the results of the supplemental analyses reported in Section 4.0, the coating at the failure location was likely a PE tape. PE tape coatings can fail in a mode that can lead to corrosion and shield CP. For situations where the mode of coating failure shields CP, changes to the CP system typically do not improve the mitigative benefits of CP to the pipeline at these locations. Thus, the PE tape coating at the failure location (GW 2470) played a larger role in the failure than the CP system.

6.1.1 Primary Factors

Two primary factors were identified that exacerbated the corrosion at the failure location. These factors include:

- The mode of coating failure
- The occurrence of wet / dry cycling.

The first factor that exacerbated the corrosion at the failure location is the mode of coating failure. As shown in Figure 9 and Appendix B, tape coatings in the vicinity of the failure exhibited evidence of wrinkling and disbonding. This failure mode was likely affected by soil stresses acting on the tape coating and elevated temperatures. Both of these factors can enhance disbondment of the tape coating. The soil stresses may be attributed to settlement of the soil after installation, movement of the pipe, and changes in the soil due to moisture content. In order for the corrosion to occur beneath the tape at GW 2470, the tape coating had to disbond from the steel surface. Once the coating disbonded, groundwater was allowed to reach the pipe surface providing an environment conducive to corrosion. Although disbonded PE tape coatings do not necessarily shield CP, the mode of coating failure at the failure location and at other taped GWs along this line resulted in shielding of CP current and subsequent corrosion beneath the disbonded coating.

The second factor that exacerbated the corrosion is the occurrence of wet/dry cycling. The presence of goethite and magnetite in a layered morphology is consistent with aqueous corrosion under wet-dry cycling.[3] Higher corrosion rates have been reported under these conditions and thus likely contributed to the high corrosion rate at this location. The

3 Nasrazadani, S. and Raman, A., *Formation and Transformation of Magnetite (Fe3O4) on steel surfaces under Continuous and Cyclic Water Fog Testing*, Corrosion, 1993.

alternating nature of the layers suggests that external variables, such as rain, drainage, and operating temperature contributed to the corrosion process. As previously stated, the area where the failure occurred is prone to high moisture based on the presence of multiple French drains within the area. In retrospect, this is further supported by satellite imagery of the failure location from 1994 and 2016 that shows a possible band of high moisture coincident with the location of the failure; see Figure 18 The portion of the Isolated Segment that contains the failure may also be more prone to wet-dry cycling based on the fact that it is located (1) along the side of a hill and (2) midway between a local low point and a local high point along the pipeline; see Figure 19.

6.1.2 Possible Contributing Factors

Two additional factors were identified that may have contributed to an accelerated corrosion process, which include: (1) the operating temperature of the line and (2) the possibility of elevated chloride levels at the failure site.

The operating temperature may have contributed to the corrosion process in three possible ways:

- Elevated temperatures can influence adhesion and coating disbondment of cold-applied tape coatings. The failure location is 1.6 miles D/S of the compressor station. Figure 20 is a plot showing the Delmont discharge temperatures between 2012 and 2016. Prior to 2014, the pipeline primarily operated at temperatures greater than 100 °F.

- Corrosion rates follow an Arrhenius relationship, increasing with increasing temperature. The elevated temperature could also increase the drying cycle, which would increase the corrosion rate until either the oxygen is significantly depleted in the solution or the solution has dried.

- The addition of after coolers in 2014 reduced the operating temperature of the line. After 2014, the operating temperature of the pipeline ranged between 80 and 100 °F. The drop seen in the operating temperature starts in 2014 and coincides with the installation of after coolers at Delmont station. The corrosion growth rates calculated between 2012 and 2016 are higher than those calculated between 2005 and 2012 (discussed in 6.2.2), suggesting that a segment-wide change occurred that accelerated the corrosion growth rate.

  Recognizing that this is contrary to the Arrhenius relationship, the reduction in temperature might have altered the environment in a way that increased corrosion rate related to wet/dry cycling. Given the complicated nature of the multiple factors

leading to high corrosion rates from wet/dry cycling, it is difficult to determine what mechanistically occurred at the failure location.

Elevated chloride levels may have contributed to an accelerated corrosion process at the failure location. Higher chlorine levels were detected in corrosion products near or adjacent to the failure location; see Section 4.1.2.2. Dunn et al.[4] have reported that the presence of chlorine can contribute to accelerated corrosion rates during wet / dry cycling. A source of the chlorides was not identified.

6.1.3 Role of Cathodic Protection System

Documentation and information provided by Spectra were reviewed to determine if the cathodic protection (CP) system was functioning as intended at the failure location in the years leading up to the failure. NACE International Standard Practice SP0169 "Control of External Corrosion on Underground or Submerged Metallic Piping" [Ref. 156] indicates coating supplemented with CP is a proven method of external corrosion control and it should be provided in the initial design and maintained during the service life of the piping system. Cathodic protection is intended to mitigate external corrosion at exposed coating holidays. Spectra Standard Operating Procedure (SOP) 2-2200 "Application of Cathodic Protection Criteria" [Ref 79], indicates a cathodic protection system shall be installed and placed into service as soon as possible but within one year of completion of installation, for buried or submerged pipelines installed after July 31, 1971. Data provided by Spectra indicate both of these requirements were met for Line 27 [Ref 123].

SOP 2-2180 "Annual Corrosion Control Survey" [Ref 78] indicates the corrosion control survey of pressurized gas piping shall be conducted annually, with intervals not to exceed 15 months but at least once each calendar year. This SOP (2-2180) also indicates one of the purposes of the annual corrosion control survey is to determine adequacy of CP for onshore pipelines and SOP 2-2200 describes the requirements for achieving cathodic protection as provided in US Title 49 CFR Part 192, Appendix D, for buried or submerged steel pipeline systems.

SOP 2-2200 includes the following acceptance criteria for cathodic protection:

- "-0.850 VDC "ON" Acceptable Criterion
- "-0.850 VDC "OFF" Acceptable Criterion

4 Dunn, DS., Bogart, MB, Brossia, CS, and Cragnolino, GA, *Corrosion of Iron Under Alternating Wet and Dry Conditions*, Corrosion, 2000. Vol. 56., No. 5. P.471 - 481.

- 100 mVDC Polarization Acceptable Criterion

CP operational data, annual pipe-to-soil potential records, field data collected at digs, and external metal loss data from ILI runs were reviewed and analyzed to develop the external corrosion control information included in the timelines presented in Figure 16 and Figure 17.

Structure-to-electrolyte potential data recorded between Years 1983 and 2016, at CP test stations located along Line 27 downstream of the Delmont Discharge [Ref 122], were provided for review and analysis. These data included "ON" VDC structure-to-electrolyte potentials prior to 2013, and "ON" and "OFF" VDC structure-to-electrolyte potentials since 2013. Spectra staff indicated [Ref 128] that, for Line 27 at the Delmont Discharge, the -0.850 VDC "ON" (with consideration of IR drop) was utilized as the acceptance criteria prior to 2013 and that the -0.850 VDC "OFF" acceptance criteria has been utilized since 2013 to assess the CP effectiveness. Prior to 2013, Spectra used the following two methodologies to consider IR drop in structure-to-electrolyte potential measurements:

- Reference cell placement, and
- A targeted "ON" structure-to-electrolyte potential criterion of -1.00 VDC measured versus a copper-copper sulfate reference electrode.

Structure-to-electrolyte potentials measured at the test stations located immediately upstream and downstream of the 2016 failure site met Spectra CP acceptance criteria between 1983 and 2016. Figure 21 and Figure 22 are data plots showing the least negative potential measurements for the year ranges 1983-2005 and 2005-2012, respectively, aligned with the respective In-Line Inspection (ILI) data set that was acquired within each date range. These are all plotted as a function of distance along the pipeline, between approximate Stations 81+00 and 115+00. The aligned ILI data analysis indicates that, although the annual pipe-to-soil potential data were meeting Spectra's acceptance criteria for adequate CP, corrosion growth continued. This indicates that CP was not mitigating corrosion at the failure site.

6.1.3.1 CP and 2005 ILI in the Vicinity of the Failure

The 2005 ILI results near the location of failure, MP 2.06, were evaluated. A total of 29 external metal loss features were reported by the 2005 ILI run between Station Numbers 81+84 (test station at MP 1.6) and 115+48 (test station at MP 2.2). Twenty eight (28) of the 29 features were located within 0.5 feet of a girth weld. The depths of23 of the 29 external metal loss anomalies reported in this section were equal to or less than 20%[5] of

5 A minimum depth of 10% was reported, which corresponds to 0.040 inches.

the nominal wall thickness and the depths of the remaining six (6) external metal loss anomalies were greater than 20% and less than 50% of the pipe nominal wall thickness. The maximum wall loss depth reported by the 2005 ILI inspection between Station Numbers 81+84 and 115+48 was 0.121 inch (30%[6] of the nominal wall thickness - 0.404 inch). The depth and orientation around the circumference of the pipe of the metal loss features reported by the 2005 ILI inspection between Station Numbers 81+84 and 115+48 are presented Figure 23.

Assuming external metal loss between Station Numbers 81+84 and 115+48 initiated when Line 27 was installed in 1981 and external metal loss occurred at a constant rate until 2005, an average corrosion rate range can be calculated from the minimum (0.040 inch) and maximum (0.121 inch) external metal loss depths reported and the operational life of the line (2005 - 1981 = 24 years). Based on the assumptions mentioned above, the corrosion rate ranges from 1.7 to 5.0 mils per year (mpy). This observed corrosion occurred despite meeting Spectra CP criteria [Ref. 79].

6.1.3.2 CP and 2012 ILI in the Vicinity of the Failure

The 2012 ILI near the location of failure, MP 2.06, were evaluated. A total of 112 external metal loss features were reported by the 2012 ILI run between Station Numbers 81+84 (test station at MP 1.57) and 115+10 (test station at MP 2.18). Not considering the lengths of the features, 86 of the metal loss features (i.e. 77% of the features identified) were located within 0.5 feet of a girth weld. The depths of 79 of the 112 external metal loss anomalies reported in this section were equal to or less than 20% of the nominal wall thickness and the depths of the remaining 33 external metal loss anomalies were greater than 20% and less than 50% of the pipe nominal wall thickness. The maximum wall loss depth reported by the 2012 ILI inspection between Station Numbers 81+84 and 115+10 was 0.204 inch (42%[7] of the nominal wall thickness - 0.485 inch). The depth and orientation around the circumference of the pipe of the metal loss features reported by the 2012 ILI inspection between Station Numbers 81+84 and 115+10 are presented in Figure 24.

The corrosion growth rate for each feature identified in the 2012 ILI dataset was estimated and is discussed in Section 6.2.2. The estimated corrosion rate ranged from 0 to 24 mpy. The aligned ILI data analysis indicates that, although the annual pipe-to-soil potential data were meeting Spectra's acceptance criteria for adequate CP, corrosion growth continued. This indicates that CP was not mitigating corrosion at the failure site.

6 Feature identified at Station Number 115+47.
7 Feature identified at Station Number 114+52, nominal wall thickness of pipe at feature is 0.485 inches

6.2 Technical Root Cause 2

The second root cause identified in this study is that ***the high corrosion growth rate of the feature that failed was not recognized, based on the available information. Thus, the use of applicable regulatory and industry standards (ASME B31.8S) resulted in a non-conservative estimate of the remaining life of the feature, which was not prioritized for remediation***.

Spectra uses Figure 4 of ASME B31.8S-2004 to establish "due dates" for reported anomalies. The due dates are based on the results of an in-line inspection. This approach is consistent with industry practice, and is required in 49CFR192. The implicit corrosion growth rate in Figure 4 for this portion of the pipeline is 8 mpy. Evidence existed of a maximum corrosion growth rate of 24 mpy on Segment 1 between 2005 and 2012. The feature that failed exhibited a corrosion growth rate of 45 mpy between 2012 and the time of failure; see Section 6.2.2. Therefore, the use of Figure 4 led to a non-conservative estimate of the remaining life for the feature that failed.

6.2.1 ILI Background

Documentation and information provided by Spectra pertaining to prior in-line inspections (ILI) were reviewed to assess the corrosion damage identified along Delmont Segment 1 and to determine if the severity of corrosion damage had changed between successive ILI runs. Spectra conducted three in-line inspections of the subject pipeline in 1986, 2005, and 2012 as part of its integrity management program. Records from the 1986 inspection were not available. The 2005 inspection identified 656 external metal loss anomalies[8] on the Isolated Segment, with a maximum depth of 58% of the wall thickness [Ref. 45]. The 2012 inspection identified 4,015 external metal loss anomalies on the Isolated Segment. The maximum reported depth was 47% of the wall thickness (nominal wall thickness is 0.434 inches at this location) [Ref. 44]. The data from the 2005 and 2012 ILI runs (Isolated Segment) are presented in Figure 25 and Figure 26, respectively, as the measured percent wall thickness versus wheel count or stationing.

Spectra performed nine (9) digs between October 21, 2005 and September 28, 2007, following the 2005 ILI run; see Figure 16. Three digs were performed in 2005, one dig was performed in 2006, and five digs were performed in 2007. Eleven (11) field depth measurements were matched by Spectra to features identified in the 2005 ILI run. The measured field depths were plotted vs. the reported ILI depths to validate the results of the ILI. Figure 27 is plot, provided and generated by Spectra, showing the correlation of the

8 Identified as metal-loss corrosion and cluster features in the 2005 pipeline listing

field depth data to the ILI reported depths. The blue line in the figure corresponds to a one to one correlation of the data. The yellow and red lines correspond to variations in the data that fall within a 10% and a 20% tool tolerance, respectively. The data all fall within the red lines, which correspond to a tool tolerance of 20%.

Similar validations were performed based on the 2012 ILI run. Spectra performed nine (9) digs between September 11, 2012 and September 23, 2015; see Figure 17. Five (5) digs were performed in 2012, one (1) dig was performed in 2013, one (1) dig was performed in 2014, and two (2) digs were performed in 2015. Twenty five (25) field depth measurements were matched by Spectra to features identified in the 2012 ILI run. A comparison of the data is shown in a unity plot provided in Figure 28. The majority of the data falls within the yellow lines, which assumes a tool tolerance of 10% of the wall thickness. These results show a relatively good correlation between the field and ILI data. Per API Standard 1163, the performance specification is a "plausible description of performance for the population of ILI measurements."

The 2012 inspection identified many more anomalies than the 2005 inspection. This, in itself, is not unusual (newer inspections often report more anomalies due to improvements and advances in the algorithms and technologies used). A high percentage of the anomalies reported by both in-line inspections were in proximity to girth welds. Figure 29 is a plot showing an approximate 200 foot span, containing the failure origin, from the same ILI data presented in Figure 25 and Figure 26 with the vertical lines representing the girth weld locations. As shown, there is a strong correlation between the locations of the ILI calls and the GWs. This information indicates that the girth weld coatings along the line were failing, allowing corrosion to occur under the damaged (disbonded) girth weld coatings.

A metric used by Spectra to assess the severity of metal loss is a tolerance-corrected failure pressure ratio (the ratio of the estimated failure pressure, after accounting for depth tolerance, divided by the maximum allowable operating pressure). Using this metric, there were no anomalies with a failure pressure ratio below 1.25 in 2005; there was one anomaly with a failure pressure ratio between 1.25 and 1.39 and ten anomalies between 1.39 and 1.5. In 2012, there were five below 1.25, 136 between 1.25 and 1.39, and 720 between 1.39 and 1.5. Thus, the condition of the line deteriorated between 2005 and 2012. As discussed above, most of the metal loss was in proximity to GWs, which Spectra recognized as a specific threat for this particular segment in 2015, based on meeting documentation and interviews [Ref. 64].

6.2.2 Corrosion Growth Rates

DNV GL performed analyses to determine the corrosion growth rates (CGRs) for each external corrosion feature identified during the ILI tool runs, including the depth of the feature at the time of failure. The CGR, typically measured in mils per year (mpy), was determined by calculating the change in depth divided by the time interval between the two measurements.

6.2.2.1 Corrosion Growth Rates at the Failure Location

At the failure location, reported defect depths in 2005 ranged from 13% to 21% of the wall thickness (21% at the failure origin). In 2012, the reported depths ranged from 10% to 33% (25% at the failure origin). The change at the failure origin was only 4% of the wall thickness, which corresponds to a CGR of approximately 2 mpy. Therefore, the data, as called, do not indicate a high CGR at the failure origin.

Table 6 is a summary of the reported feature depths at the failure location (GW 2470) and the corresponding CGRs. As part of the metallurgical analysis following the failure, the depths of the feature associated with the failure origin and a second feature located at the 9:15 orientation were determined and are presented in the last column in Table 6. Assuming the 2012 inspection depths are accurate, for the feature that failed, the calculated CGR changed rather dramatically, from 2 mpy between 2005 and 2012 to 51 mpy between 2012 and 2016. Either the CGR accelerated rapidly, the ILI depths were not accurate, or both.

6.2.2.2 Corrosion Growth Rates Distributions

The CGR data were further analyzed to determine the likelihood of reaching values near 51 mpy. CGR distributions were determined using three (3) different datasets:

- 2012 ILI-2016 Field Measured Features
- 2005 ILI -2012 ILI Matched Features
- 2005 ILI -2012 ILI Unmatched Features

2012 ILI-2016 Field Measured Features

Following the April 29, 2016 failure, numerous digs were performed on the segment of Line 27 that contained the failure location (i.e. Isolated Segment). Digs on this line are ongoing, and the data used for this analysis are the findings from 154 digs that were performed between May 17, 2016 and August 20, 2016 [Ref. 11 and Ref. 117].

The results of these digs were compared to the 2012 ILI results, which were assumed to be accurate, to estimate CGRs for the identified features, and to compare those growth rates to those determined for features near GWs at and near the failure location. Figure 30 is a plot showing the measured depths of features, identified during the 2016 digs and metallurgical analyses at and near the failure location (GW 2470), vs. ILI log distance. The results show that the depth of the feature at the failure (red circle) is higher than any of the measured depths for the 2016 digs considered. Two methodologies were utilized during the field activities to measure and document the corrosion geometries. These included laser scanning and a pit-depth gauge with a bridging bar, each of which is identified in Figure 30. The results indicate that there is not a preferential bias in the depth of either methodology as the data have similar distributions for each.

Figure 31 and Figure 32 contain a plot of corrosion growth rates vs. ILI log distance and a histogram of CGRs, respectively, for the 2016 dig features and the failure location. Again, the results show that the CGR at the flaw that failed is much higher (approximately 60% higher) than the next highest CGR determined for the 2016 digs on Delmont Section 1.

2005 ILI -2012 ILI Matched & Unmatched Features

The 2005 ILI -2012 ILI datasets for the matched and unmatched features were consolidated in one distribution called ILI-ILI Master. The methodology used to combine the datasets is provided in Appendix C. The resulting ILI-ILI Master CGR distribution is shown in Figure 33 and is discussed below.

6.2.2.3 Statistical CGR Analysis

The CGR distributions discussed above were each fit with a 3-parameter Lognormal distribution to determine if there was a statistical shift in the corrosion growth rate distributions before and after 2012. The resulting curves for the Field Measured and the ILI-ILI Master distributions are shown in Figure 34 and Figure 35, respectively, while a consolidated plot showing both distributions is presented in Figure 36. In both CGR databases, the lognormal distribution fits the data well. Visually it can be seen that the field measured distribution has a longer tail. Larger CGRs are more likely for the 2016 Field Measured distribution based on this visual comparison.

Descriptive sample statistics for each distribution are shown in Table 7. The first and second columns in the table identify the dataset considered and the number of measurements in each dataset, respectively. Columns 3 – 6 provide the average CGR, standard deviation, minimum CGR, and maximum measured CGR (excluding the failure location) for each dataset, respectively. The table shows that the average CGR calculated

based on comparison of the 2012 ILI data to the 2016 dig data is 8.5 mpy, with CGRs ranging between 0.1 mpy and 31 mpy. The average CGR for the dataset that compared the 2005 ILI data to the 2012 ILI is 4 mpy, with CGRs ranging between 0 mpy and 24 mpy. Thus, the CGRs increased and exhibited more variability between 2012 and 2016 than before.

Appendix C provides inferential[9] statistical details to support the findings presented in this paragraph. Statistical hypothesis tests were performed to compare the population means, medians, and standard deviations of the two CGR populations. Whereas Table 7 is purely a descriptive summary of the data, the hypothesis tests assess if the true unknown population means, medians, and standard deviations are significantly different. For all three, a p-value is rounded to 0.000 (thus the value is < 0.001) implying that, with at least 99.9 confidence, all three population parameters are significantly different between the two databases. The mean, median, and standard distribution of the CGRs after 2012 are higher than before 2012.

6.2.2.4 Combined CGR and ILI Tolerance Analysis

A statistical analysis was performed to determine the probability (P1) of having a corrosion growth rate of a given value, binned in 1 mpy increments. Using the lognormal distribution for the 2016 Field to the 2012 ILI shown in Figure 34, the analysis was performed for a variety of CGR values. The corresponding probability is shown in Table 8; Column 3. The resulting probabilities are also presented graphically in Figure 37. The data show a decreasing probability as the CGR is increased, which is as expected based on the shape of the Lognormal distribution.

In addition, a statistical analysis was then performed to determine the probability (P2) that the 2012 ILI tool either undercalled or overcalled the origin feature on 2012. For each given CGR shown in Table 8, a feature of an assumed depth of 0.101 mils (or 25% of a 0.404 wall thickness), which is equal to the depth of the origin feature that was called in 2012, was grown over a 4 year period (2012-2016 – Failure). Column 4 represents the resulting depth of the feature in 2016. Based on the metallurgical examination, the origin feature was 0.303 mils deep or 75% of the wall thickness at the time of failure. Column 5 represents the difference between the 75% feature that failed and the calculated depth for a given CGR in 2016. In other words, this would be the necessary undercall or overcall in 2012 to achieve a depth of 75% in 2016.

9 Hypothesis testing in statistics where you go from the sample population to the larger population.

Using the vendor specifications that 80% of the ILI calls will be within ±10% wall thickness of the field depth, the probability that each undercall or overcall was near 75% (75±5%) was determined. The resulting probability (P2) for each CGR is provided in Column 6 in Table 8 and graphically in Figure 37.

The combined probability (P1*P2) or likelihood for a given growth rate and corresponding undercall or overcall to achieve a depth near 75% wall thickness in 2016 is provided in Columns 7 and 8 in Table 8 and graphically in Figure 37. The analysis indicates that the highest probability occurs at a CGR of 45 mpy and a corresponding ILI undercall of 5.4%. That is, the most likely scenario is that the anomaly was 5.4% undercalled in 2012 (actual depth of 30.4% versus the reported depth of 25%) and grew at an average growth rate of 45 mpy between 2012 and the failure. This finding is based on the growth rate distribution determined from digs conducted after the 2016 failure and the assumed ILI accuracy.

These analyses suggest an increasing corrosion growth rate played a larger part in the failure as opposed to errors in the ILI sizing.

6.2.3 Application of ASME B31.8S-2004 Figure 4

As previously mentioned, Spectra utilizes ASME B31.8S Figure 4 to determine a “due date” for each reported anomaly. The procedure is based on a tolerance-corrected failure pressure ratio, where the tolerance-corrected failure pressure ratio equals the predicted failure pressure of a defect that is 10% deeper than reported divided by the maximum allowable operating pressure. From the due date, one can calculate a CGR as a function of the geometry and properties of the pipe being considered. The CGR implicit in ASME B31.8S Figure 4 for the failure location (30-inch diameter 0.404-inch wall thickness X65 pipe material) is up to 8 mpy.

The analyses presented above indicate that the CGR of the feature that failed was approximately 45 mpy between 2012 and 2016. This rate is much higher than the rate implicit in Figure 4 of ASME B31.8S-2004 and, therefore, Figure 4 overstated the remaining life of the feature that failed by a factor of five or more. As a consequence, the feature that failed was not prioritized for remediation.

The ILI response for the failure location was governed by the most severe nearby defect, which was reported to be 33% deep and 5.31 in long.[10] The due date for this GW (#2470) is May 21, 2029, which is approximately 17 years after the 2012 ILI. Assuming evaluation and remediation is based on the due date, nearly 800 girth weld locations were prioritized before the location that failed.

10 The defect that failed was reported as 25% deep and 4.84 in long.

DNL GL examined the CGR distribution based on the 2005-2012 ILI-ILI Master data (see Figure 35) to determine if a CGR of 45 mpy was foreseeable based on information available to Spectra before the failure. The 90, 95, and 99 percentile CGRs based on the 2005-2012 data are 8, 9, and 14 mpy. A rate 45 mpy is at the 99.9996 percentile of the 2005-2012 CGR distribution (a probability of 4×10^{-6}). That is, it is unlikely Spectra would have identified the rate associated with the failure.

As stated in ASME B31.8S, Figure 4 is applicable for "reasonably anticipated or scientifically proven rate of corrosion" and is routinely used for the general threat of external corrosion. Once a threat with an accelerated corrosion rate, such as disbonded coating combined with wet dry cycling, is identified, an alternative threat assessment should be performed to handle the specific threat.

7.0 SUMMARY AND CONCLUSIONS

The results of the metallurgical analysis indicate that the immediate metallurgical cause for the Line 27 failure was wall thinning from external corrosion that ultimately failed by ductile overload at the operating pressure [Ref 2]. Supplemental analyses identified evidence of wet-dry cycling that contributed to the observed external corrosion.

The results of the root cause analysis presented below are based on the provided documentation referenced in Appendix A. DNV GL reserves the right to modify or supplement these conclusions should new information become available. The root causes are associated with the occurrence or absence of actions / decisions that either resulted in or worsened the failure. DNV GL identified two technical root causes of the failure:

1. ***Selection and use of tape coatings at girth welds did not mitigate external corrosion at the failure location.***

   Basis:

   Based on the presence of external corrosion at the failure location, the polyethylene tape coating was compromised. The tape coating failed to prevent moisture from reaching the pipe steel, allowing the external corrosion process to occur. The cathodic protection was also not beneficial in mitigating corrosion at the failure location.

   The external corrosion was exacerbated by

   - The mode of coating failure
   - The occurrence of wet/dry cycling

Additional possible contributing factors include (1) the operating temperature of the line and (2) the possibility of elevated chloride levels.

2. ***The high corrosion growth rate of the feature that failed was not recognized based on the available information. Thus, the use of applicable regulatory and industry standards (ASME B31.8S), and the implicit corrosion growth rate therein, resulted in a non-conservative estimate of the remaining life of the feature. Accordingly, the feature that failed was not prioritized for remediation.***

   Basis:

   - The most likely corrosion growth rate associated with the feature that failed was approximately 45 mpy.
   - The corrosion growth rate associated with the feature that failed was much higher (five or more times higher) than the rate implicit in ASME B31.8S Figure 4, which was used by Spectra to determine remediation priorities. Thus, the failure location was not prioritized for remediation.
   - It is unlikely that Spectra could have identified the rate associated with the failure based on available data and information before the failure.

8.0 LESSONS LEARNED

The RCFA identified improvements (Lessons learned) that could be made within the integrity management program. These observations are given below.

1. For new construction and field repairs, avoid the use of wraps/coatings that can disbond and shield CP.
2. Improve understanding and recognition of mechanisms and conditions under which extreme damage rates can occur
   - Investigating locations where corrosion is occurring under disbonded GW coating may provide insights needed to identify extreme value corrosion growth rates. Although data existed in 2012 indicating corrosion under GW coatings was not being controlled by CP, additional investigative efforts were not triggered. However, using only the 2012 ILI results and Figure 4 in ASME B31.8S, approximately 800 locations were prioritized for remediation before the failure location.
3. As stated in ASME B31.8S, Figure 4 is applicable for a “reasonably anticipated or scientifically proven rate of corrosion” and is routinely used for the general threat of external corrosion. Once a threat with an accelerated corrosion rate, such as

disbonded coating combined with wet dry cycling, is identified, an alternative threat assessment should be performed to handle the specific threat.

4. Enhance review, interpretation, and comparison of in-line inspection results to better identify areas with high growth rates or the possibility for high growth rates.
5. Incorporate lessons learned within the integrity management plan and risk models to improve identification of unusual integrity threats on pipelines.
    - Treat specific damage mechanisms (e.g., corrosion under disbonded coatings at girth welds) not addressed by general categories (e.g., external corrosion) as separate threats to be managed within an integrity management program.
    - Consider the distribution of damage rates (including extreme values) instead of average or typical rates for a mechanism.
    - Integrate data from corrosion, inspection, and risk management programs and combine knowledge of subject matter experts in these disciplines.

Table 1. Summary of dimensional analyses performed on areas of external corrosion on Line 27 GWs 2440 – 2520 in the vicinity of the failure.

Girth Weld Identification	**Axial Length** [1] (in)	**Circumferential Length** [1] (in)	**Maximum Depth** (in)	**Maximum Wall Loss** (%)	**Orientation**
2440	6.5	34.9	0.148	37	1:52 – 6:18
2450	7.0	32.4	0.217	54	4:11 – 8:17
2460 [2]	5.2	32.6	0.099	24	3:44 – 7:55
2470 (Failure Location)	12.0	55.0	0.303	75	3:22 – 10:22
2480 a [2, 3]	7.2	21.1	0.174	43	1:37 – 4:19
2480 b [2, 3]	6.3	18.4	0.104	26	7:10 – 9:30
2490	1.8	6.1	0.101	25	12:15 – 1:12
2500	3.5	19.0	< 0.0505	< 12.5	3:03 – 5:27
2510	–	–	–	–	–
2520	2.3	12.1	< 0.0505	< 12.5	5:25 – 6:57

1 Measurements obtained using a tape measure.
2 Measurements reported in DNV GL's metallurgical report for the failure [Ref. 2].
3 Two discrete areas of external corrosion were identified adjacent to GW 2480.

Table 2. Results of compound analyses, using X-ray diffraction, performed on representative corrosion products removed from GWs on Line 27 in the vicinity of the failure.

Compound	Composition (~ wt %)			
	GW 2420	**GW 2440**	**GW 2450**	**GW 2500**
Goethite – α FeO(OH)	45	55	50	5
Magnetite – Fe_3O_4	40	40	45	90
Lepidocrocite – ɣ FeO(OH)	–	5	5	–
Siderite – $FeCO_3$	15	–	–	5

Table 3. Results of elemental analyses, using EDS, performed on external corrosion deposits removed from GWs on Line 27, in the vicinity of the failure.

Element		Average Composition (wt %)						
		GW 2420	GW 2440	GW 2450	GW 2490	GW 2500	GW 2510	GW 2520
C	(Carbon)	19.54	17.8	11.93	19.50	64.17	22.54	18.33
O	(Oxygen)	19.27	18.63	22.73	27.65	8.03	26.65	18.20
Na	(Sodium)	ND	ND	0.03	0.43	1.07	1.01	0.40
Mg	(Magnesium)	0.04	ND	0.17	0.77	0.27	0.42	ND
Al	(Aluminum)	0.49	0.03	1.87	5.84	ND	5.23	ND
Si	(Silicon)	1.40	0.13	3.70	10.40	0.07	10.06	ND
P	(Phosphorous)	0.08	ND	0.07	0.07	ND	ND	ND
S	(Sulfur)	0.22	0.38	0.10	0.14	0.60	0.27	ND
Cr	(Chromium)	0.08	ND	ND	ND	ND	ND	0.03
Cl	(Chlorine)	ND	0.70	1.70	0.85	3.33	0.75	ND
K	(Potassium)	0.06	ND	0.37	2.47	0.07	1.53	ND
Ca	(Calcium)	0.05	ND	0.23	0.10	0.07	0.15	ND
Ti	(Titanium)	ND	ND	0.07	0.50	ND	0.70	ND
V	(Vanadium)	0.08	ND	ND	ND	ND	ND	ND
Mn	(Manganese)	0.50	0.40	1.63	0.34	0.40	0.40	0.47
Fe	(Iron)	58.18	61.60	55.40	32.95	21.87	30.78	62.20
Ni	(Nickel)	ND	0.28	ND	ND	ND	ND	0.10
Cu	(Copper)	ND	0.05	ND	ND	ND	ND	ND

Table 4. Summary of results of analyses performed on soil samples removed along Line 27 after the failure and analyzed by DNV GL.[11]

Line 27 Field ID	Soluble Anions, mg/L							Total Acidity mg/L	Total Alkalinity mg/L $CaCO_3$	pH	Saturated Resistivity Ω-cm	As Received Resistivity Ω-cm
	NO_2^-	NO_3^-	Cl^-	SO_4^{2-}	S^{2-}	CO_3^{2-}	HCO_3^-					
2410	< 0.3	0.9	9.3	40.2	<0.6	<12.4	<12.4	<61.8	<12.4	5.79	5550	4800
2420	< 0.3	1.3	12.9	51.0	<0.7	<12.9	13.6	64.6	13.6	5.03	6625	5125
2430	< 60.0	2.4	21.6	61.2	<0.6	<12	45.6	<60	45.6	5.52	7750	5250
2460	<63.8	<63.8	30.6	ND	<0.6	<12.8	14.7	<63.8	14.7	5.71	4400	2600
2470	<57.2	<57.2	<5.7	50.9	<0.6	<11.4	12.0	<57.2	12.0	5.34	9300	50000
2530	ND	0.39	1.7	11.7	<0.6	<12	25.8	<60	25.8	6.17	3825	3825
Ground water samples												
2420	<0.05	1.5	52.1	12.3	< 0.1	< 2	3.0	< 10	3.0	5		
2430	<0.05	2.8	108	20.1	< 0.1	< 2	3.8	< 10	3.8	5		

ND = not detected

11 Values with a < sign were not detected during the analysis. Values reported are based on the detection limit multiplied by the dilution factor.

Table 5. Summary of risk rankings[1], performed by Spectra, between 2011 and 2015 for a portion of the Isolated Segment that contained the Failure.

Threat	Year				
	2011 [2, 3]	2012 [3]	2013 [3]	2014 [4]	2015 [4]
Third Party Damage	3	4	4	4	4
External Corrosion	1	1	2	2	2
Internal Corrosion	6	5	6	5	5
Stress Corrosion Cracking	–	–	–	–	–
Manufacturing	–	–	–	–	–
Construction	5	6	5	–	–
Equipment	–	–	–	–	–
Outside Force	2	2	1	1	1
Incorrect Operation	4	3	3	3	3

1 The highest ranking corresponds to a value of 1.
2 Threat weightings were different in 2011 than in 2012 - 2015.
3 125.53 foot section from between Chainage 10810.00 and 10935.528.
4 99.39 foot section from between Chainage 10810.00 and 10909.386.

Table 6. Summary of the ILI as-called depths and measured feature depths associated with the failure location.

Feature	2005 ILI, % wall	2005 – 2012 Growth Rate (range accounting for ±10% tool accuracy), mpy	2012 ILI, % wall	2012 – 2016 Growth Rate (range accounting for ±10% tool accuracy), mpy	2016 Field Measure-ment, % wall
Feature at 5:30 (Origin)	21%	2 (0-14)	25%	51 (40-61)	75%
Feature at 9:15	13%	12 (0-23)	33%	21 (11-31)	54%

Table 7. Summary of statistical parameters associated with the corrosion growth rate distributions determined from the ILI datasets and Field-measured dataset. Data shown in Figure 36.

Dataset	Number of Measurements (N)	Corrosion Growth Rate (mpy)			
		Average (Mean)	Standard Deviation	Minimum Measured	Maximum Measured
CGR (2012 ILI - 2016 Field Data)	106	8.5	7.4	0.1	31
CGR (2005 ILI - 2012 ILI)	3742	4	2.8	0.0	24

Table 8. Summary of probability calculations based on an initial feature depth of 0.101 mils or 25% wall thickness.

Corrosion Growth Rate mpy	Corrosion Growth Rate % wall (0.404 in)/y	Probability of Equaling Value, 1 mpy bin (P1)	Estimated Field in 2016	Undercall or Overcall % needed to hit 75%	Probability of Undercall or Overcall within 75% ± 5% using vendor spec (P2)	P = P1*P2	Normalized Likelihood
5	1.24%	8.35E-02	30.0%	45.0%	1.46E-07	1.22E-08	0.00%
10	2.48%	3.81E-02	34.9%	40.1%	3.00E-06	1.33E-07	0.01%
15	3.71%	1.84E-02	39.9%	35.1%	5.60E-05	1.04E-06	0.07%
20	4.95%	9.70E-03	44.8%	30.2%	6.24E-04	6.06E-06	0.38%
25	6.19%	5.50E-03	49.8%	25.2%	4.71E-03	2.60E-05	1.64%
30	7.43%	3.30E-03	54.7%	20.3%	2.45E-02	8.16E-05	5.14%
35	8.66%	2.10E-03	59.7%	15.3%	8.80E-02	1.85E-04	11.7%
40	9.90%	1.40E-03	64.6%	10.4%	2.20E-01	3.04E-04	19.2%
45	11.14%	9.00E-04	69.6%	5.4%	3.87E-01	3.62E-04	22.8%
50	12.38%	7.00E-04	74.5%	0.5%	4.77E-01	3.10E-04	19.5%
55	13.61%	5.00E-04	79.5%	-4.5%	4.15E-01	1.92E-04	12.1%
60	14.85%	3.00E-04	84.4%	-9.4%	2.54E-01	8.53E-05	5.37%
65	16.09%	2.00E-04	89.4%	-14.4%	1.09E-01	2.70E-05	1.70%
70	17.33%	2.00E-04	94.3%	-19.3%	3.26E-02	6.06E-06	0.38%

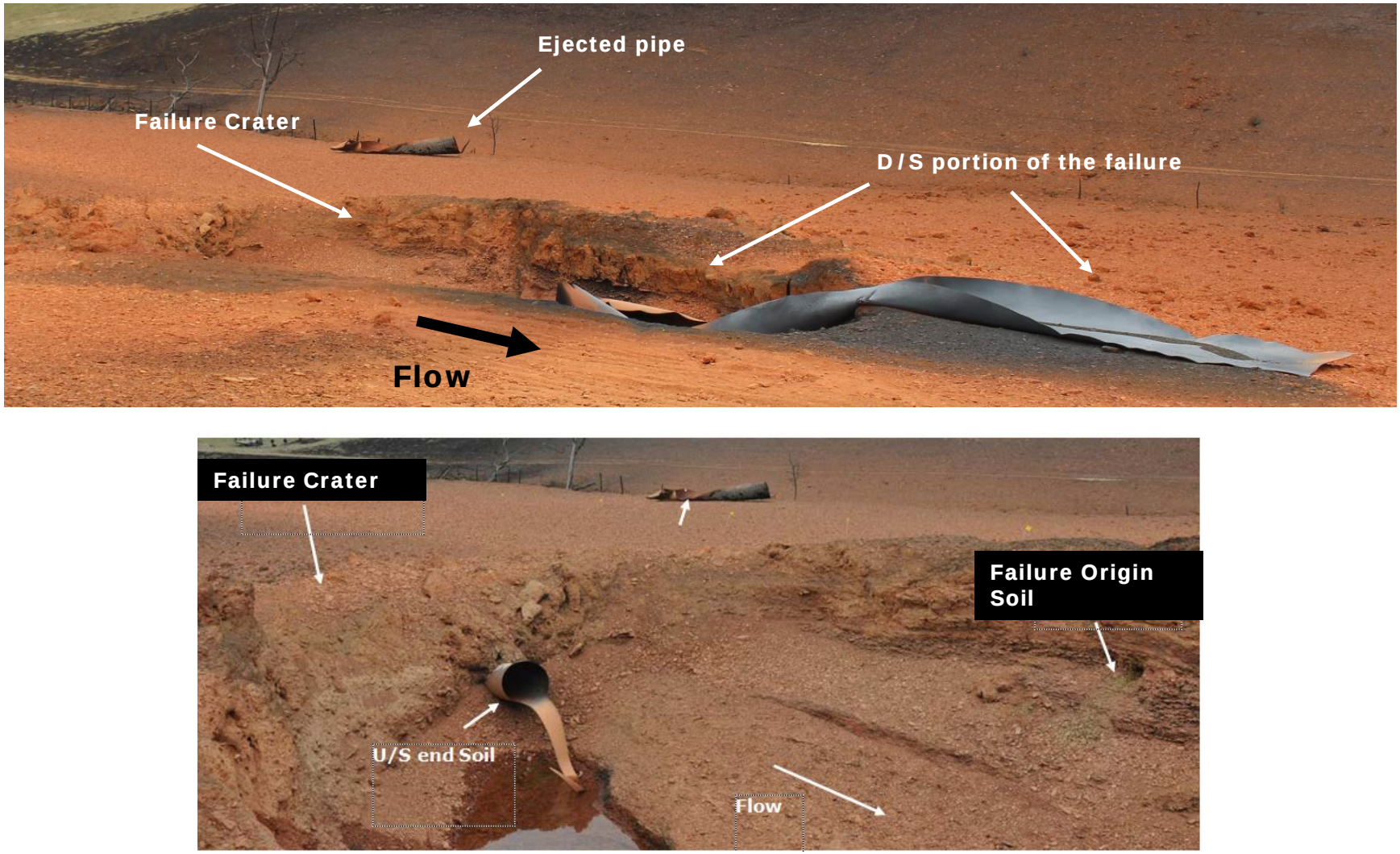

Figure 1. Photographs of the Failure Site showing the failure crater, the ejected pipe section, the U/S and D/S termini of the failure, and the locations where soil samples were collected.

Photograph looking west

Photograph looking south

Figure 2. Field photographs showing the topography in the vicinity of the Failure Site.

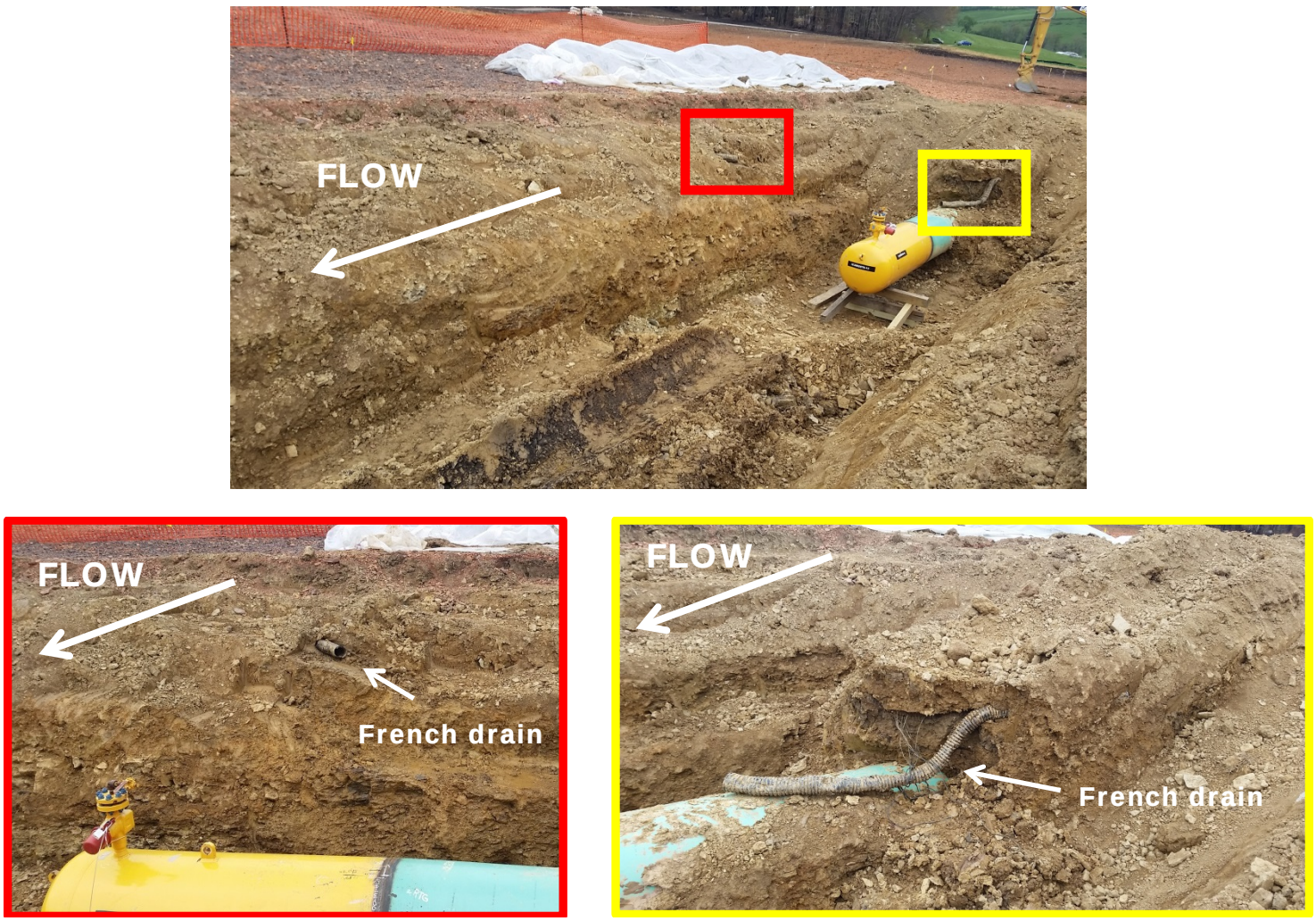

Figure 3. Photographs showing the ends of a French drain within the excavation site near the Failure.

Figure 4. Drawing (Left) and satellite imagery (Right) showing locations of French drains relative to the Failure Site. The blue lines on the drawing (Left) correspond to locations of French drains. The white and red dots identified in the satellite imagery (Right) correspond to GPS coordinates obtained for French drains and the failure crater, respectively. The red line corresponds to the location of Line 27 and the yellow star corresponds to the failure origin in the satellite imagery.

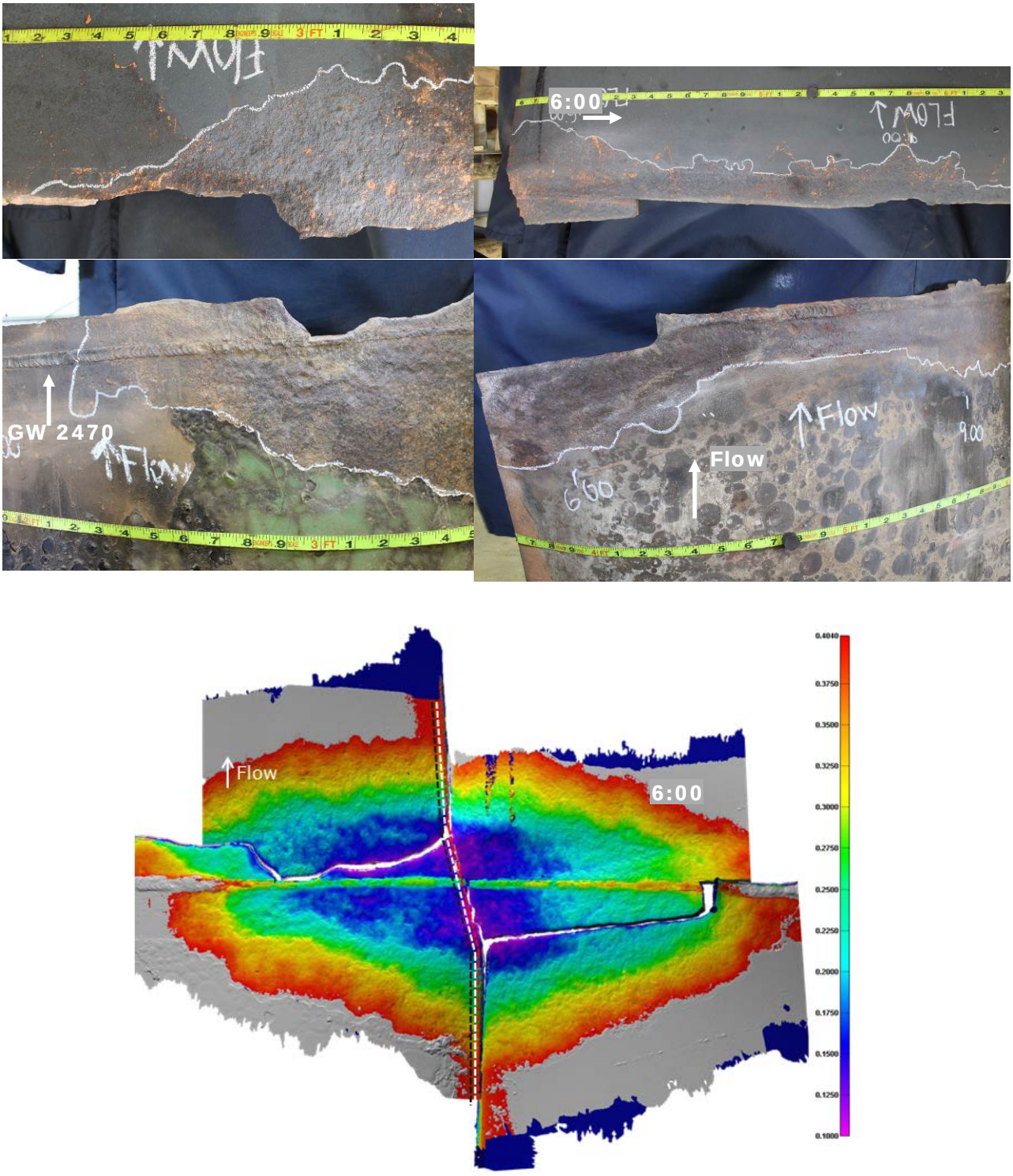

Figure 5. Photographs (top) and color map from laser scanning (bottom) showing region of external wall loss at the failure origin following cleaning the pipe with a solvent. The tape measure indicates distance CW from the 12:00 o'clock orientation at GW 2470.

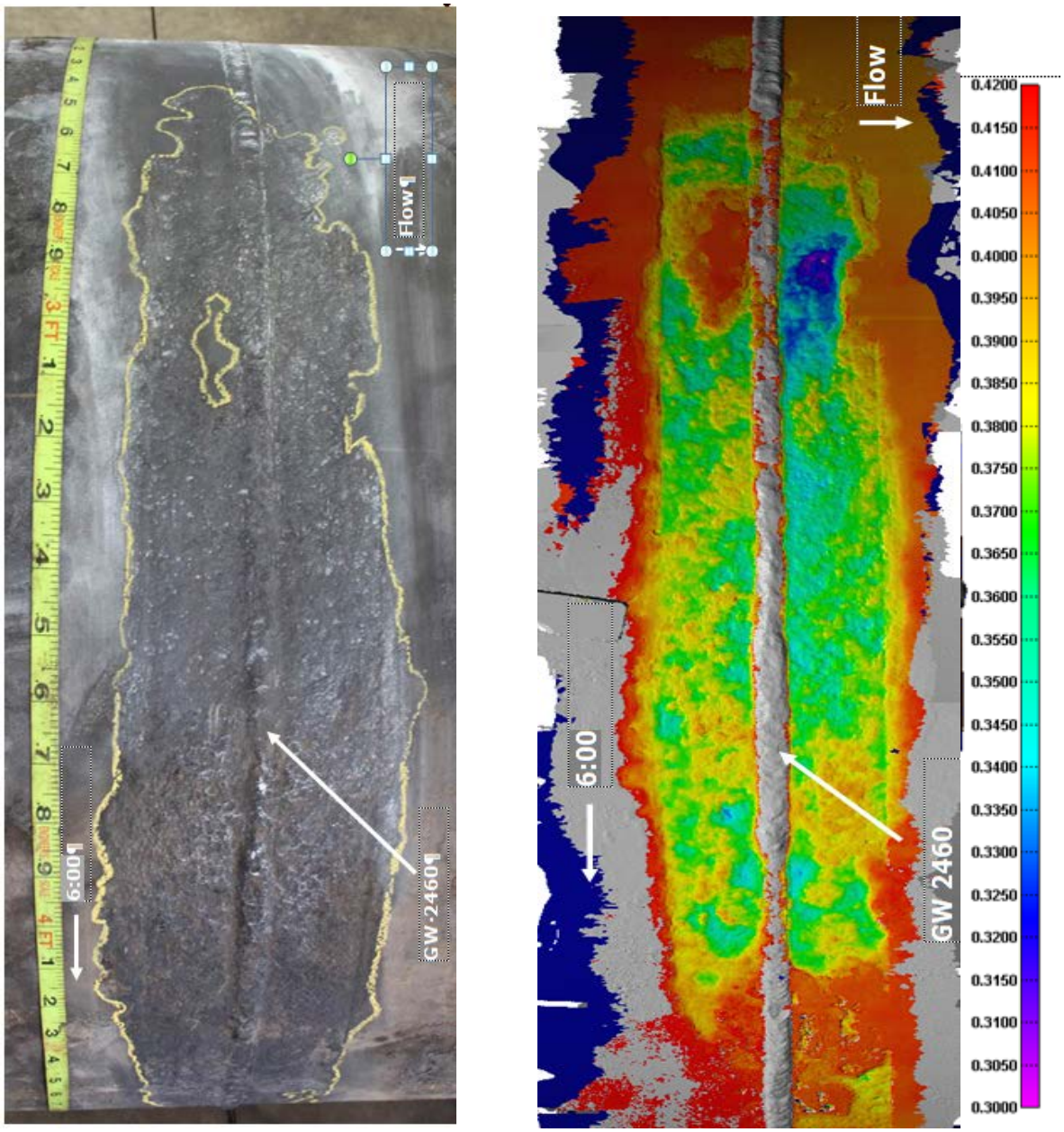

Figure 6. Photograph showing the region of external wall loss at GW 2460 (Left) and color map showing the remaining wall thickness (viewed from the OD surface) from laser scan data (Right). The tape measure indicates distance CW from the 12:00 o'clock orientation at GW 2460.

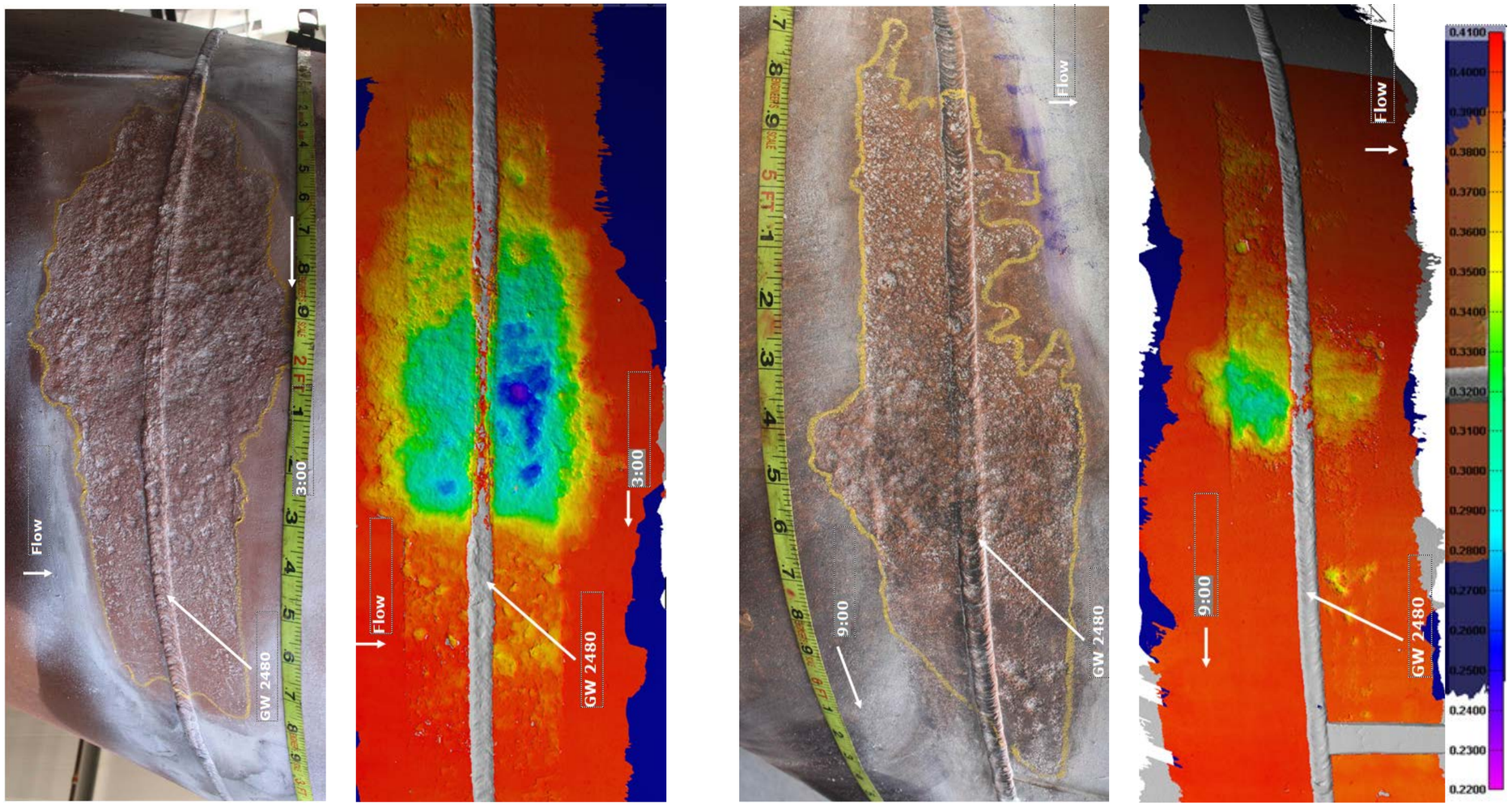

Figure 7. Photographs showing the regions of external wall loss at GW 2480 and color maps showing the remaining wall thickness (viewed from the OD surface) from laser scan data: wall loss region near 3:00 o'clock orientation (Left) and wall loss region near 9:00 o'clock orientation (Right). The tape measure indicates distance CW from the 12:00 o'clock orientation at GW 2460.

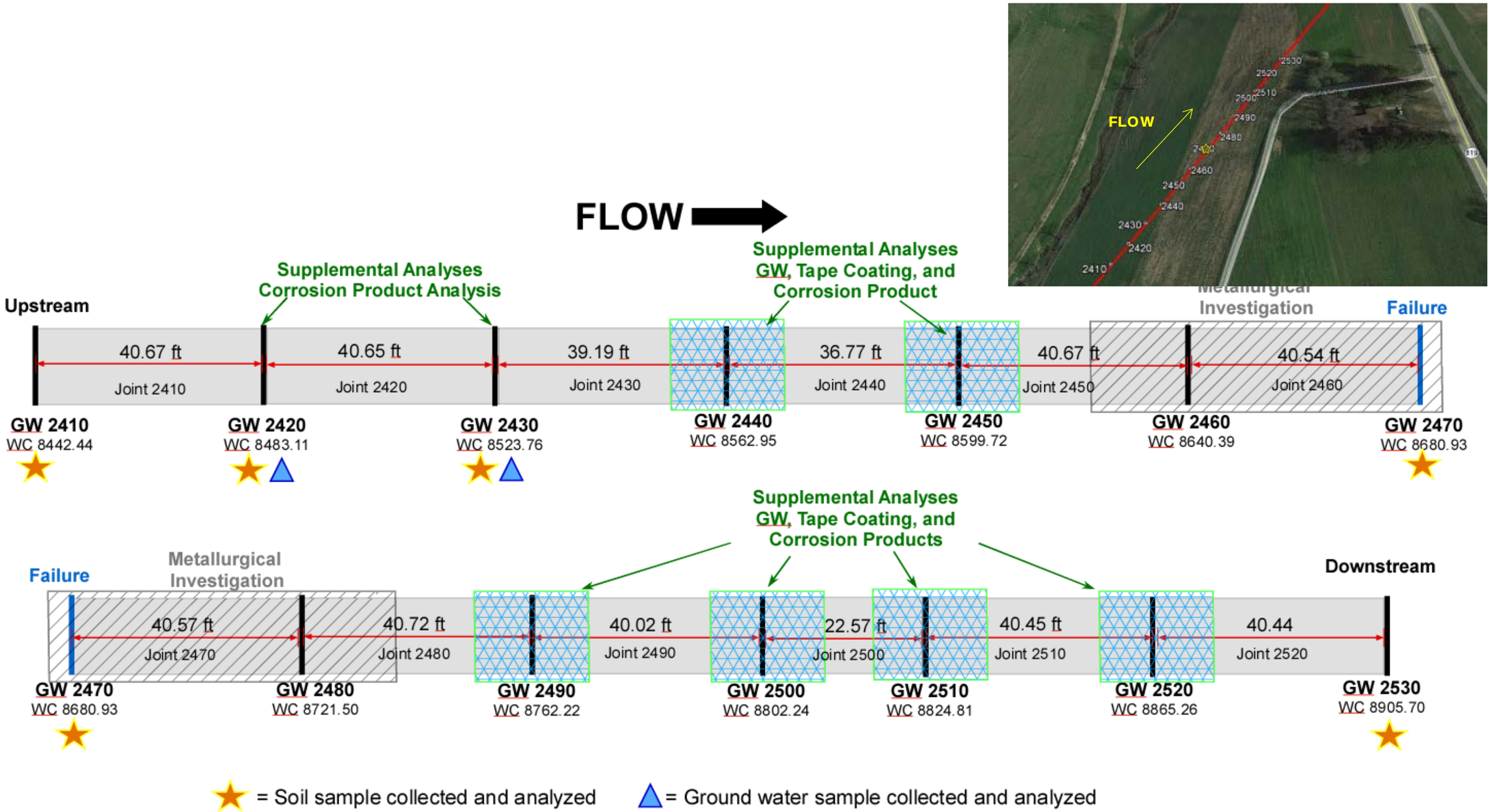

Figure 8. Schematic and a google map image showing girth welds on Line 27 in the vicinity of the failure. The locations where metallurgical, tape coating, corrosion deposit, soil, and ground water samples were taken for various analyses are identified on the schematic.

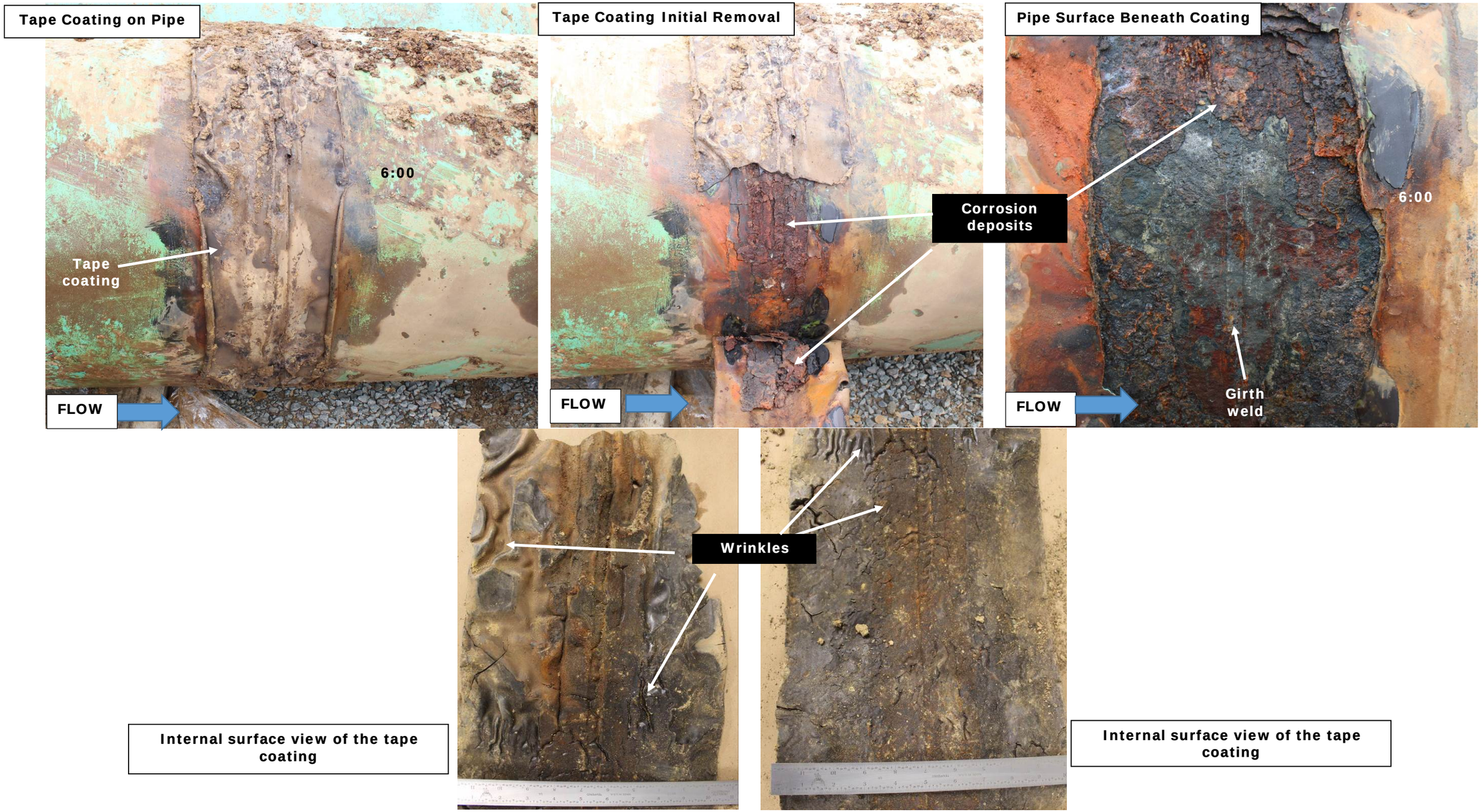

Figure 9. Photographs showing the tape coating and the pipe surface at GW 2450 before and after removal of the tape from the pipe.

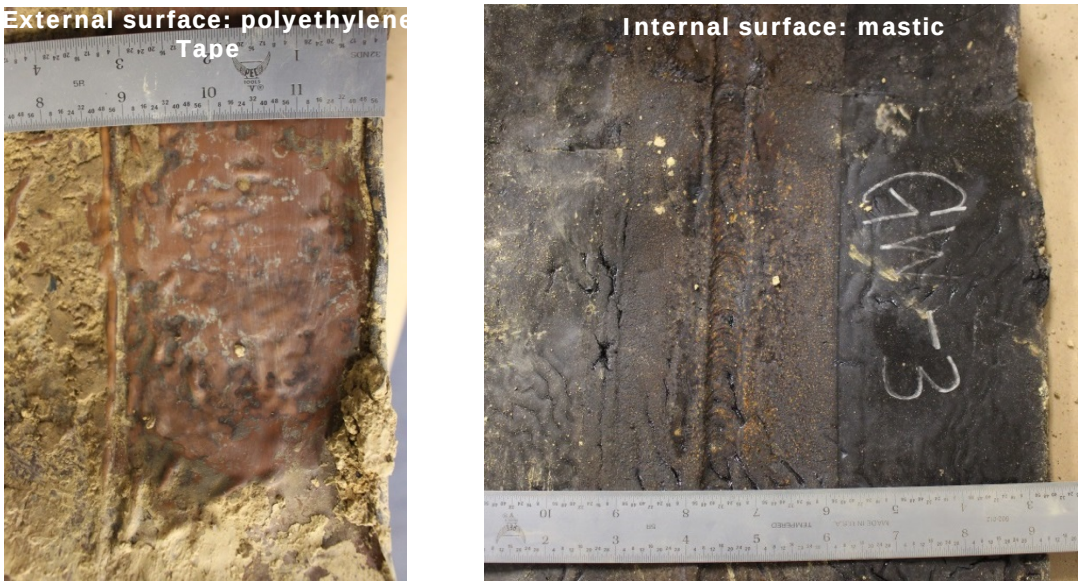

Photographs of tape coating from GW 2440

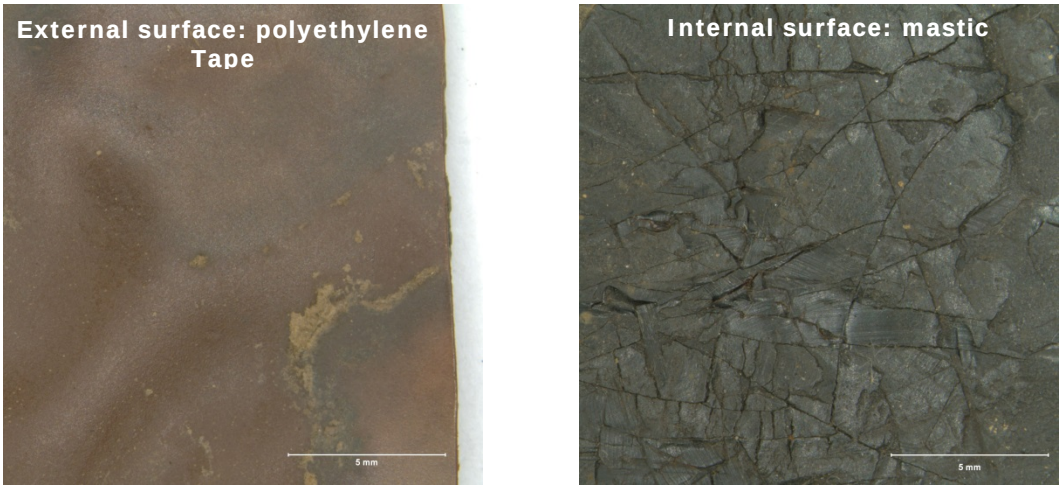

Light photomicrographs of tape coating from GW 2450

Figure 10. Photographs (Top) and light photomicrographs (Bottom) showing the polyethylene tape and mastic surfaces of tape coatings from GW 2440 and GW 2450.

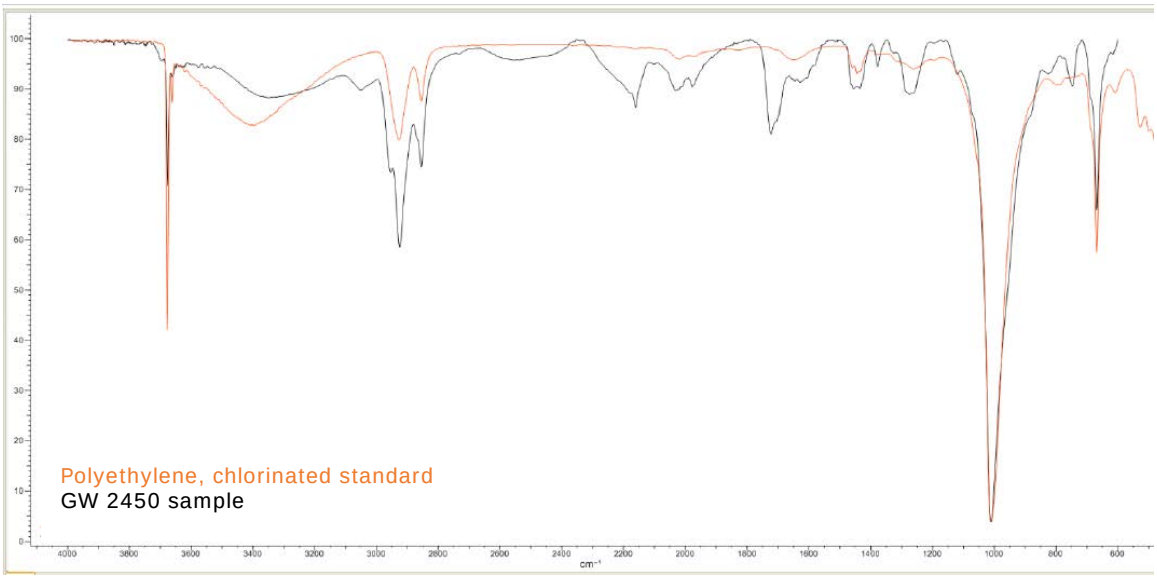

Figure 11. FTIR spectral comparison of representative tape sample removed from GW 2450 to a standard spectrum for chlorinated polyethylene.

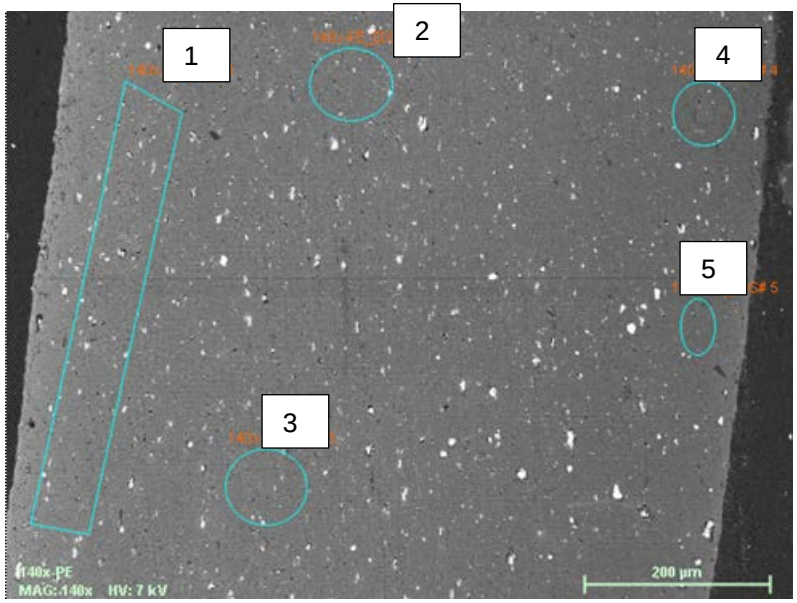

Chlorinated Polyethylene tape only

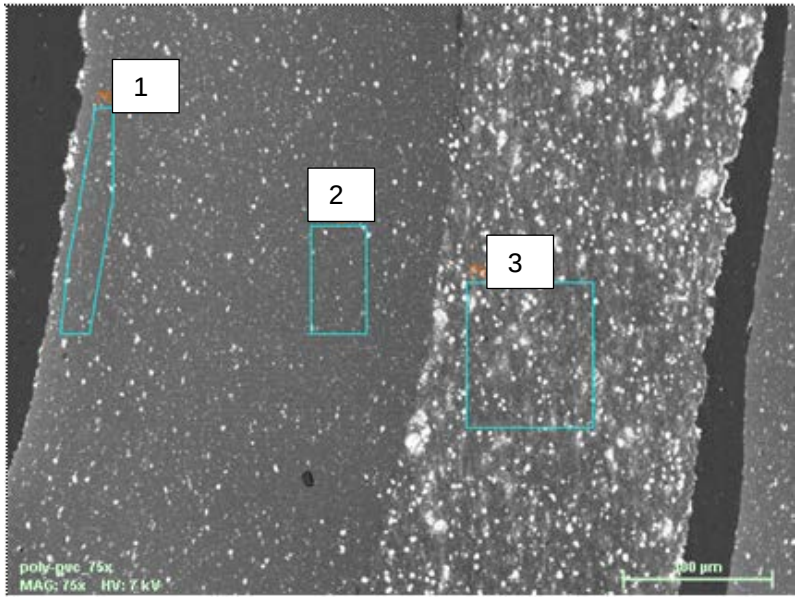

Chlorinated Polyethylene **Mastic**

Spectrum	C	O	Mg	Si	S	Cl	Ca
140x-PE_EDS# 1	84.6	8.5	0.1	0.2	0.7	4.6	1.3
140x-PE_EDS# 2	85.7	7.0	–	0.1	0.8	5.5	0.8
140x-PE_EDS# 3	85.9	6.8	0.0	0.2	0.8	5.5	0.8
140x-PE_EDS# 4	86.5	8.9	–	0.2	0.8	3.1	0.5
140x-PE_EDS# 5	85.3	9.5	–	0.1	0.7	3.9	0.5

Spectrum	C	O	Mg	Al	Si	S	Cl	Ca
75x_# 1	78.5	13.1	0.1	0.2	0.8	0.5	5.6	1.1
75x_# 2	83.0	9.7	–	–	0.6	0.8	5.3	0.5
75x_# 3	73.4	14.7	1.3	–	7.0	0.6	3.0	–

Figure 12. EDS data collected from a representative cross sectional mount of the tape coating from GW 2520. Numbers in photographs indicate locations of analyses.

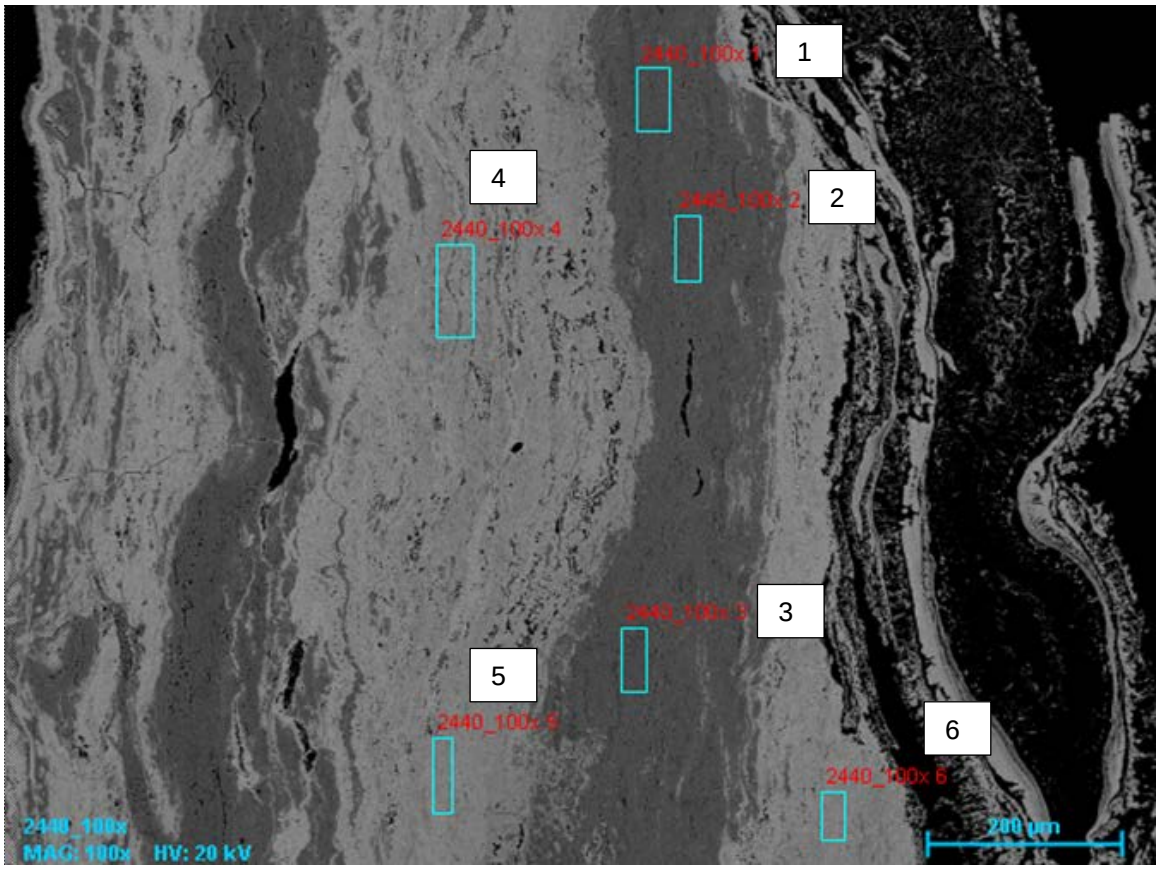

Spectrum	O	Si	S	Cl	V	Cr	Mn	Fe	Ni
2440_100x 1	30.4	0.2	0.3	–	0.1	0.1	0.8	68.1	0.1
2440_100x 2	32.8	0.1	0.3	0.1	–	–	0.5	66.3	–
2440_100x 3	31.1	0.2	0.3	–	0.1	0.1	0.8	67.4	–
2440_100x 4	24.8	0.3	0.1	–	–	0.1	0.4	74.3	–
2440_100x 5	25.1	0.2	0.1	–	–	0.1	0.3	74.1	–
2440_100x 6	24.5	0.2	0.1	–	–	0.0	0.1	75.0	–

Figure 13. EDS data collected from a representative cross sectional mount of corrosion products from GW 2440 (100X magnification). Numbers in photographs indicate locations of analyses.

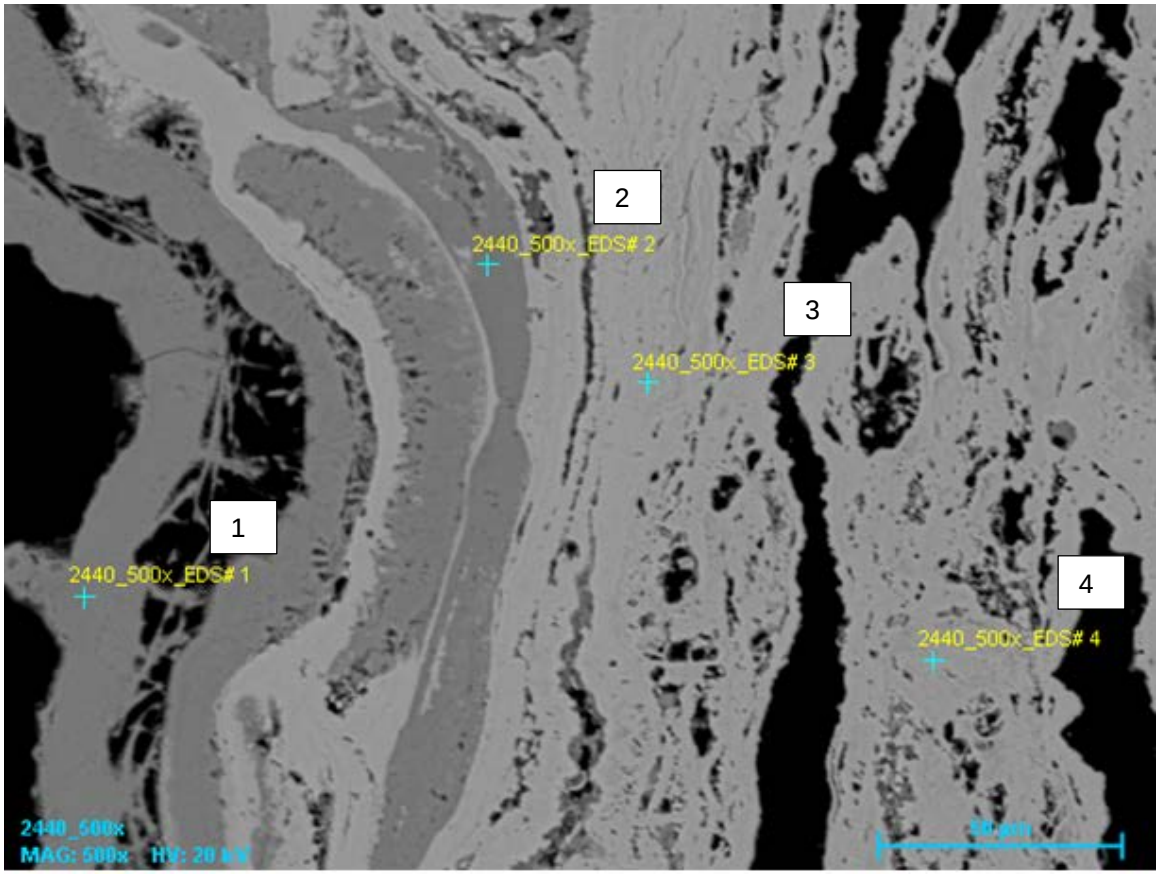

Spectrum	O	Si	S	Mn	Fe
2440_500x_EDS# 1	31.9	0.2	0.1	2.6	65.2
2440_500x_EDS# 2	33.9	0.2	0.0	0.6	65.3
2440_500x_EDS# 3	28.8	0.2	–	0.1	70.9
2440_500x_EDS# 4	29.2	0.4	–	0.1	70.3

Figure 14. EDS data collected from a representative cross sectional mount of corrosion products from GW 2440 (500X magnification). Numbers in photographs indicate locations of analyses.

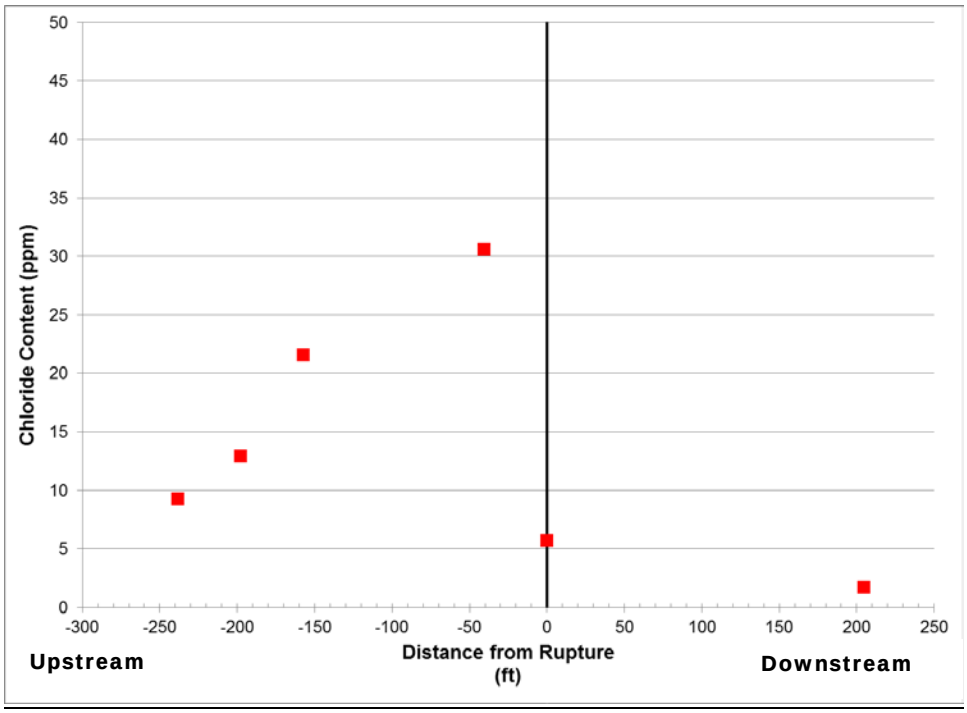

Figure 15. Plot showing chloride content (ppm) identified in soil samples collected along the Isolated Segment in the vicinity of the Failure.

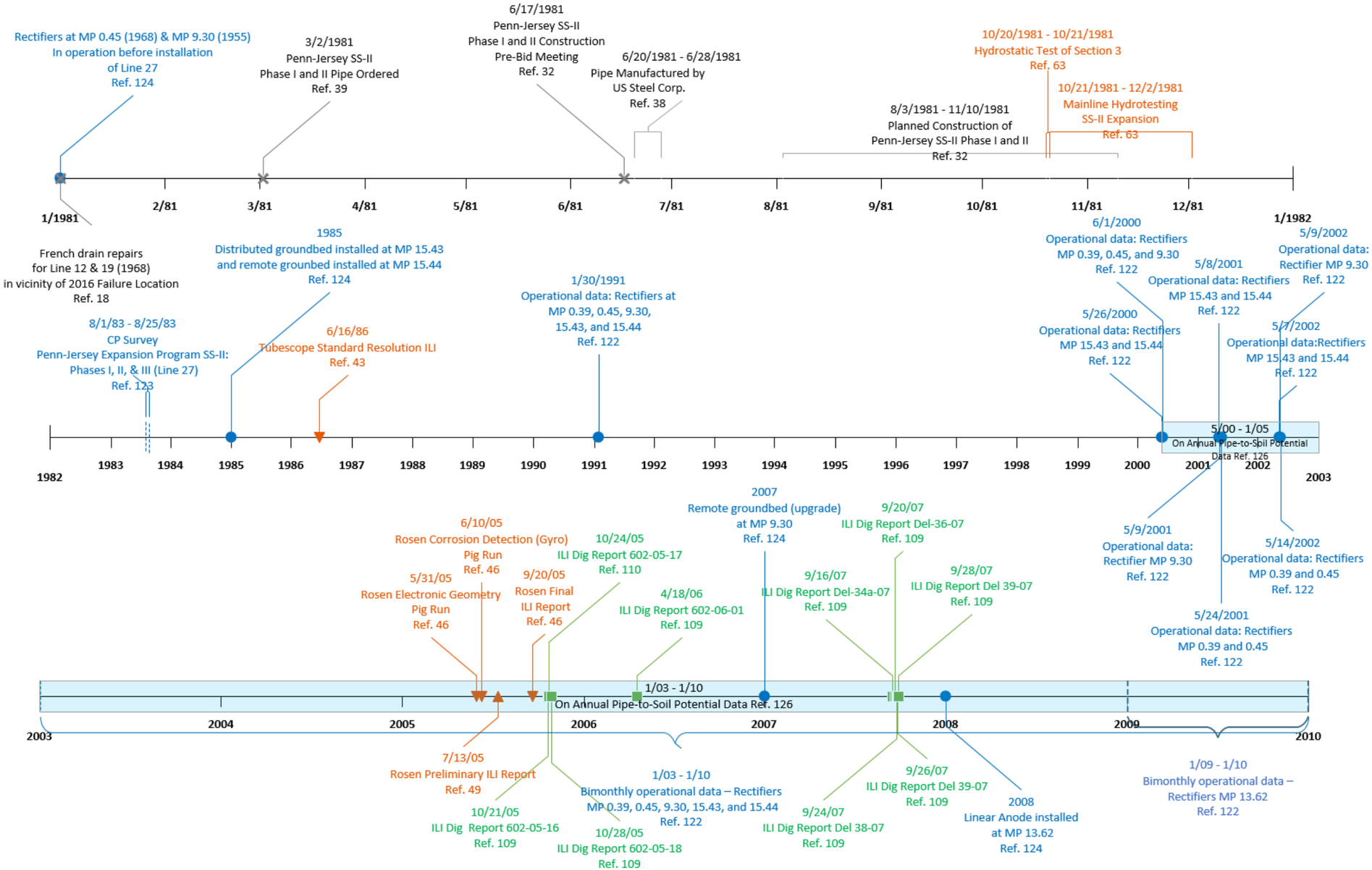

Figure 16. Timeline showing key events for Line 27 (Isolated Segment only) from the time of construction January 1, 2010. The timeline includes dates for (1) construction (Black x and brackets), (2) CP related activities (blue circles, brackets, and blocks), (3) integrity related assessments (orange triangles and brackets), and (4) ILI related digs (Green squares).

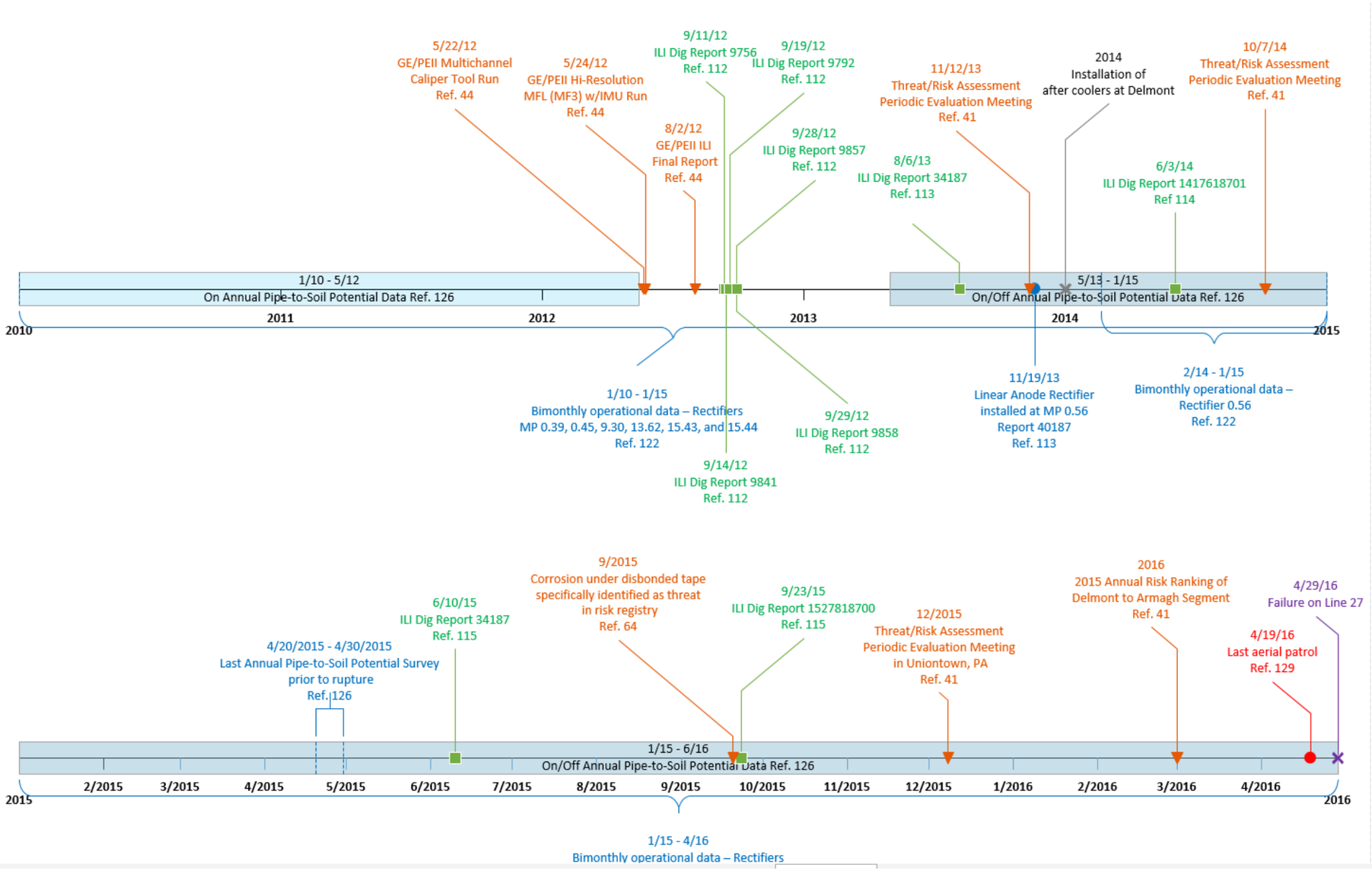

Figure 17. Timeline showing key events for Line 27 (Isolated Segment only) from January 1, 2010 until the failure on April 29, 2016. The timeline includes dates for (1) construction (Black x), (2) CP related activities (blue circles, brackets, and blocks), (3) integrity related assessments (orange triangles), (4) ILI related digs (Green squares), (5) aerial patrol (red circles), and (6) the April 29, 2016 failure (purple X).

4/1994 **4/2016**

Figure 18. Satellite imagery showing the failure site coincident with an area of probable high moisture content: Imagery from 4/1994 (Left) and 4/2016 (Right). Red dotted lines identify the perimeter of the failure crater and yellow arrows point to high moisture areas.

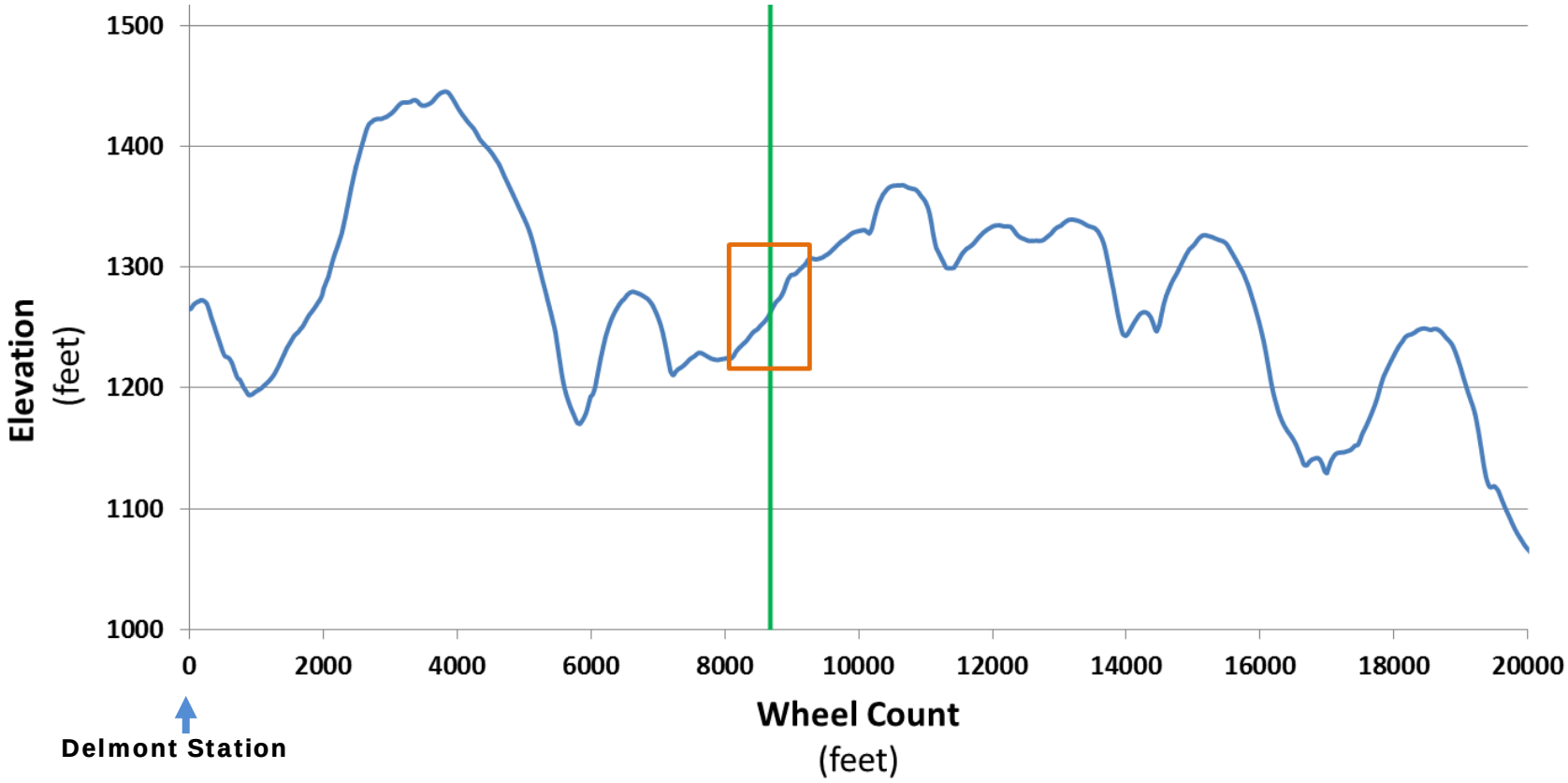

Figure 19. Plot showing the elevation profile for Line 27 in the vicinity of the Failure. The vertical green line on the plot identifies the location of the April 29, 2016 failure.

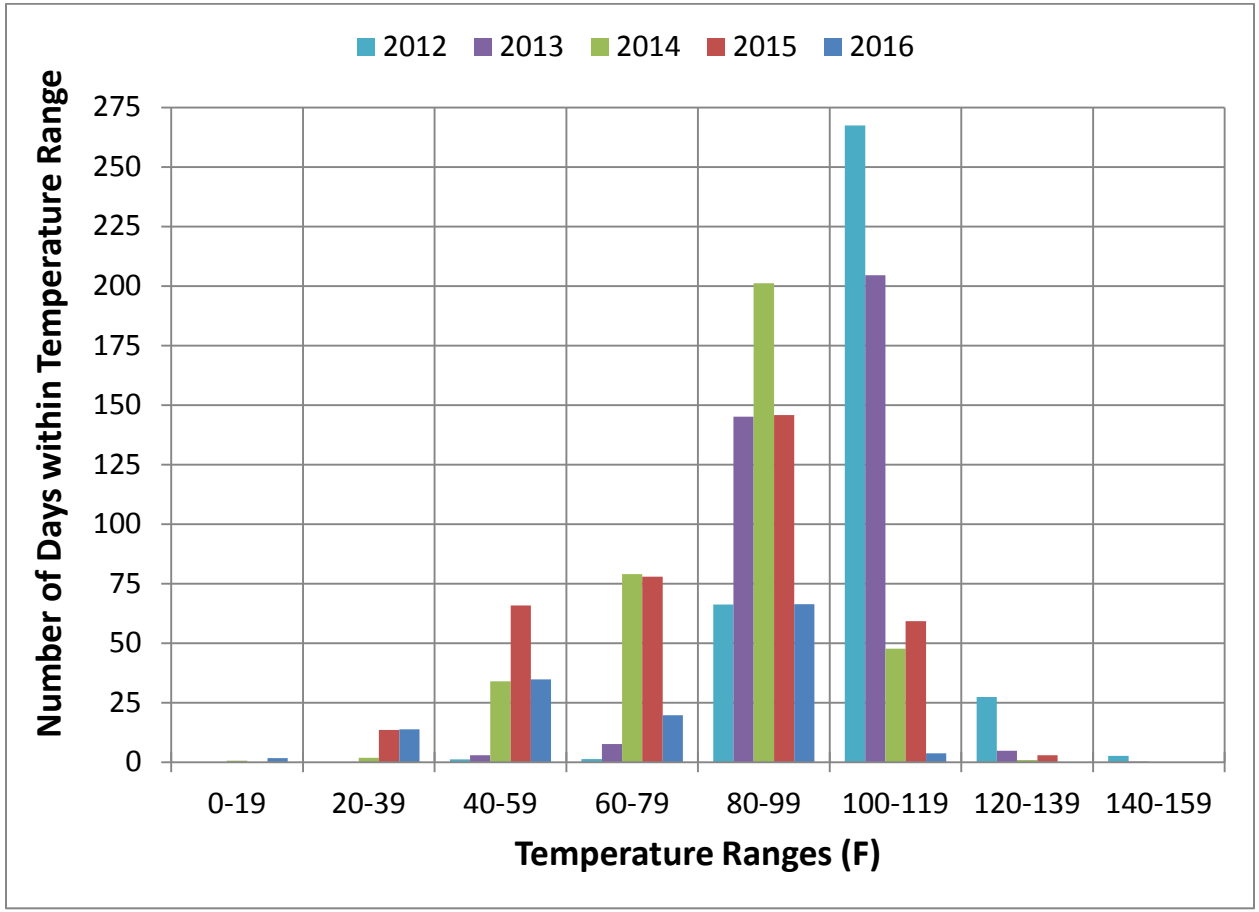

Figure 20. Plot showing Delmont discharge temperatures between 2012 and 2016.

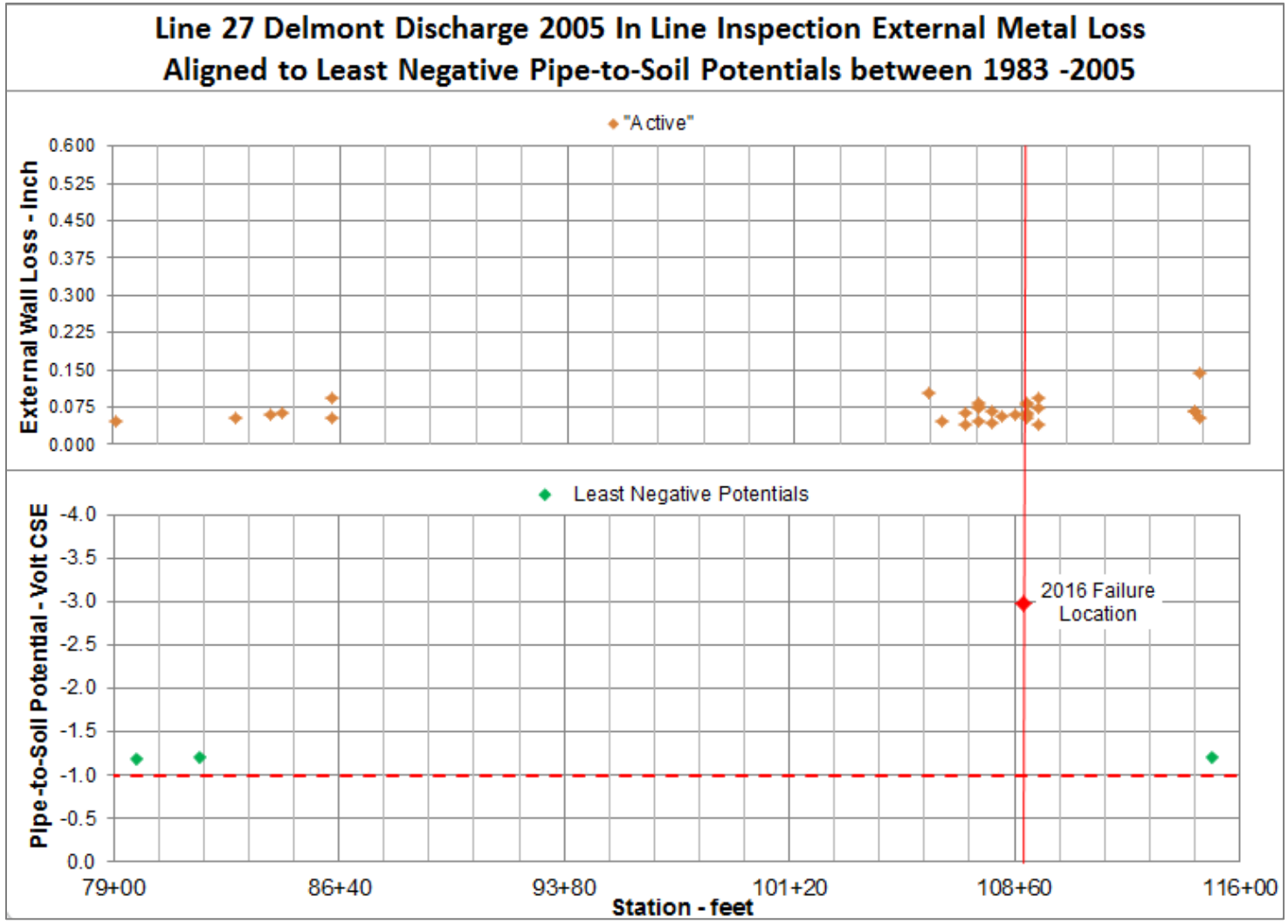

Figure 21. Line 27 Delmont discharge in the vicinity of the failure: External metal loss depths reported in 2005 In-Line inspection report aligned to least negative pipe-to-soil potentials between 1983 and 2005.

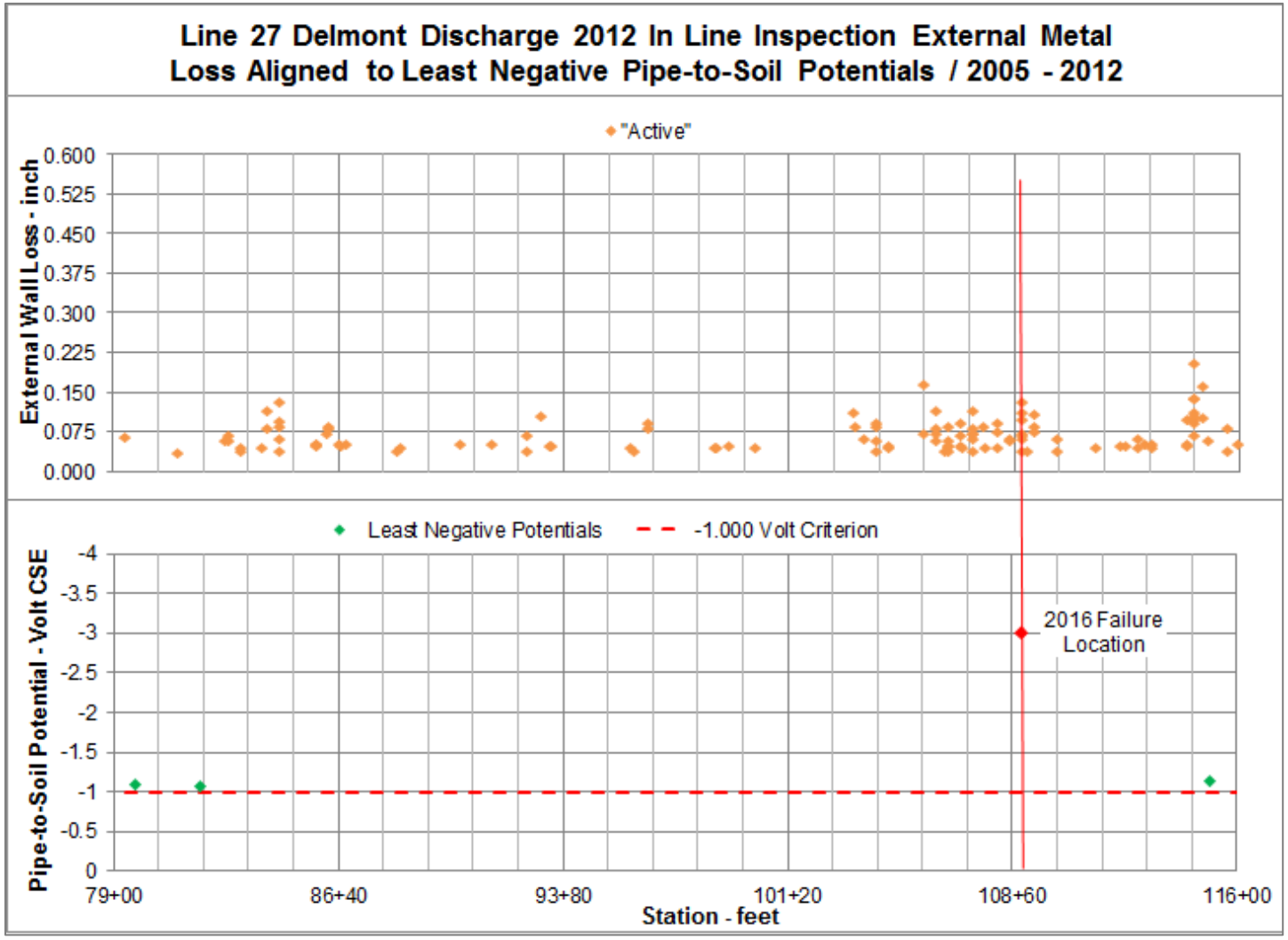

Figure 22. Line 27 Delmont discharge in the vicinity of the failure: External metal loss depths reported in 2012 In-Line inspection report aligned to least negative pipe-to-soil potentials between 2005 and 2012.

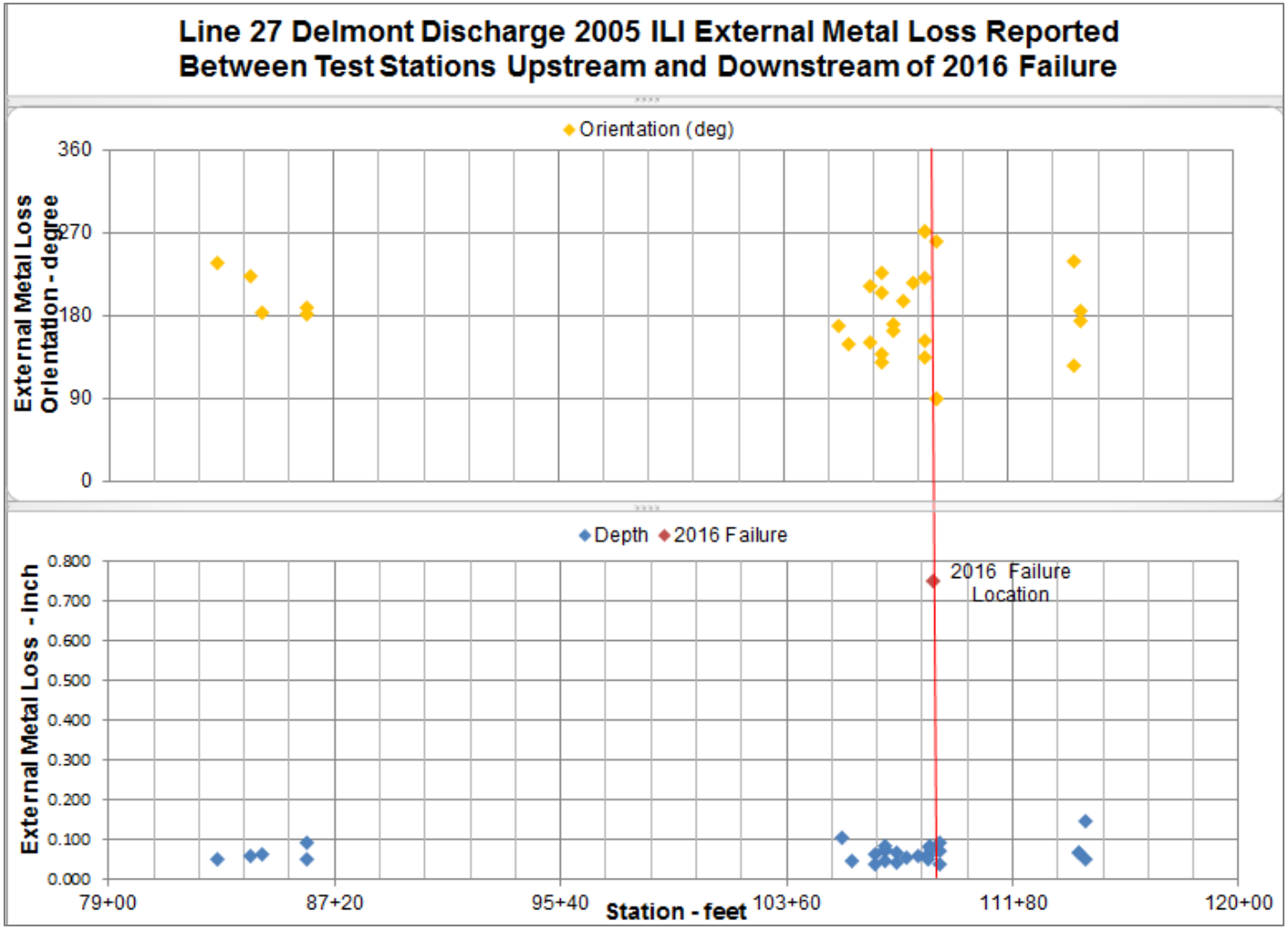

Figure 23. Line 27 Delmont discharge in the vicinity of the failure: External metal loss (orientations and depths) reported in 2005 In-Line inspection report between test stations located upstream and downstream of the 2016 failure. (Figure 7)

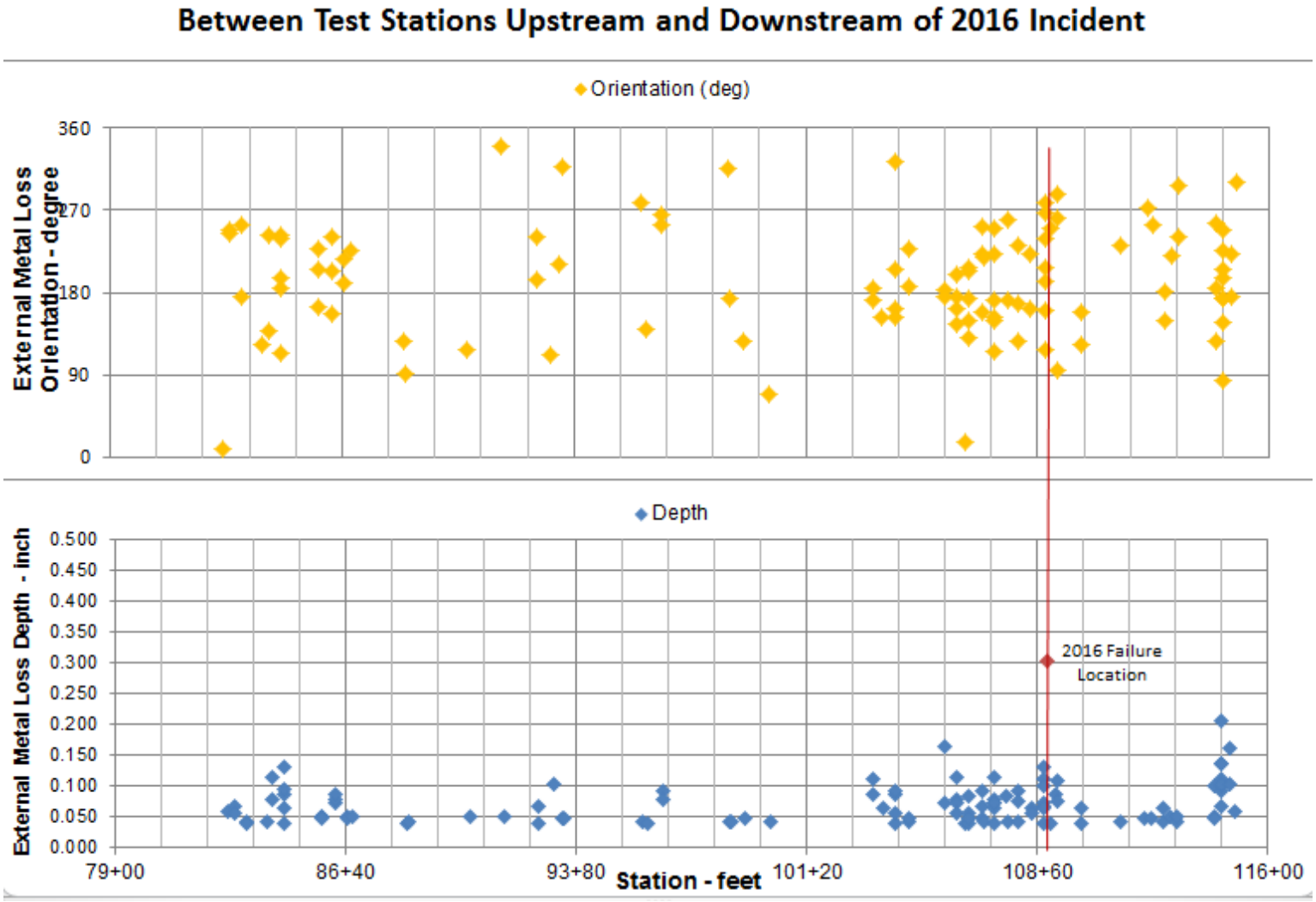

Figure 24. Line 27 Delmont discharge in the vicinity of the failure: External metal loss (orientations and depths) reported in 2012 In-Line inspection report between test stations located upstream and downstream of the 2016 failure.

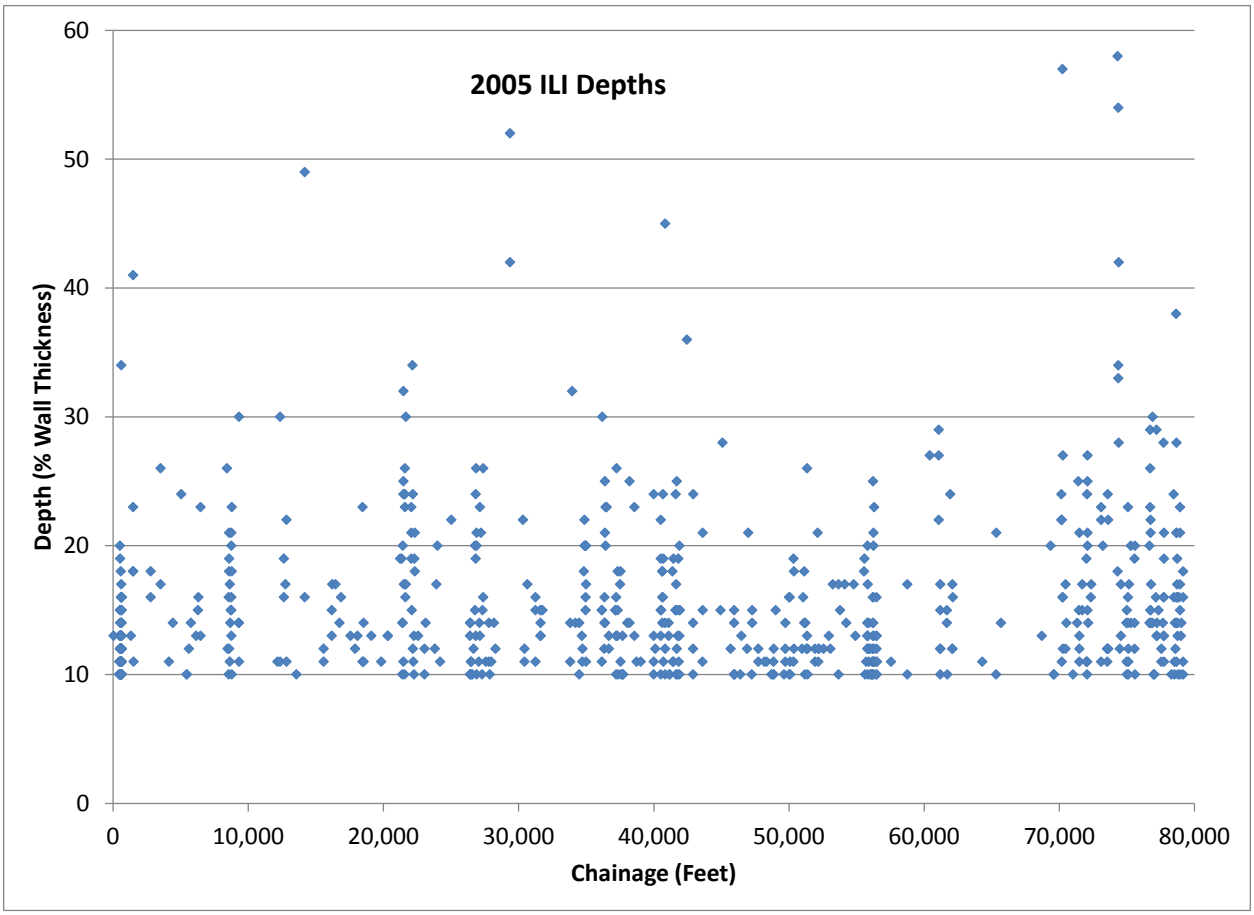

Figure 25. 2005 ILI results (depths) versus distance downstream of Delmont Compressor Station.

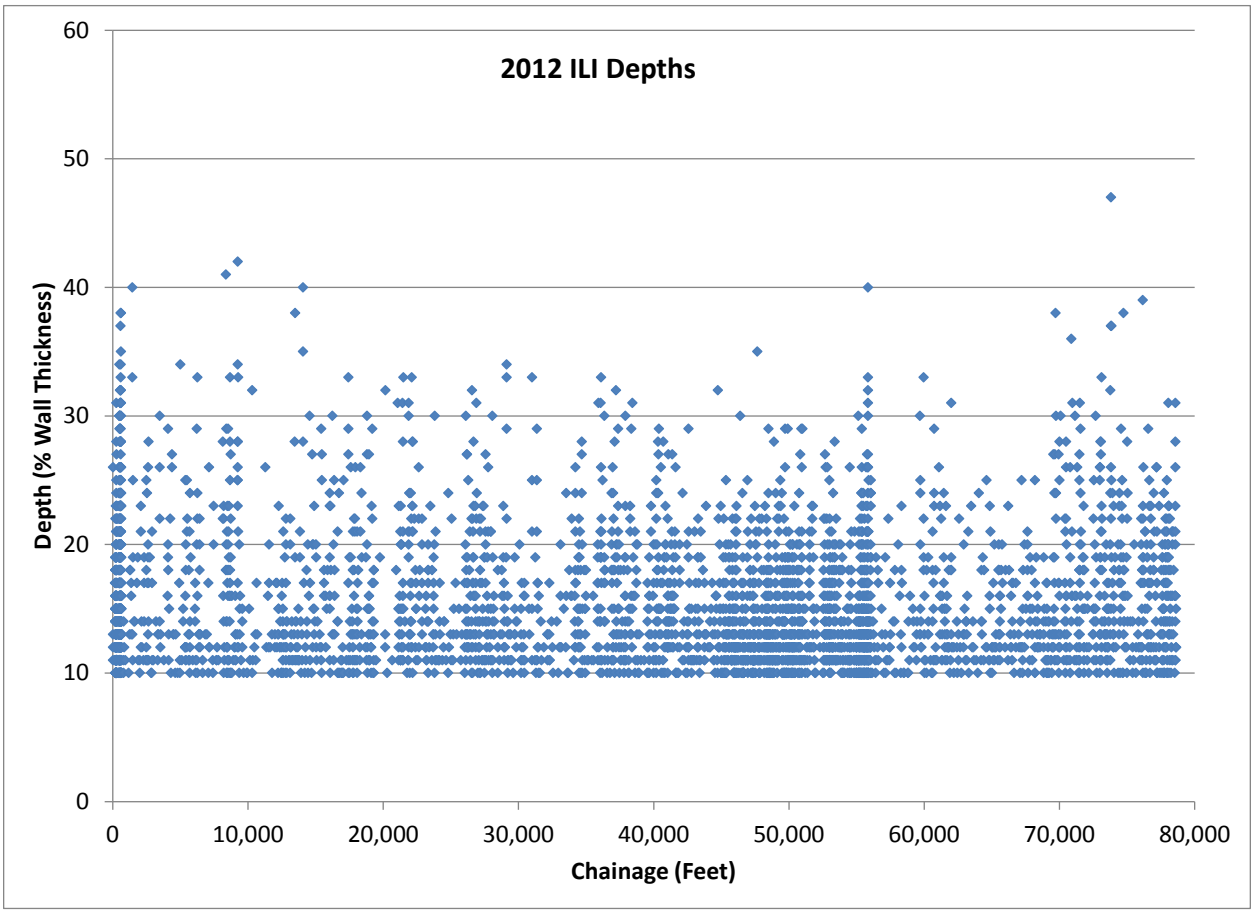

Figure 26. 2012 ILI results (depths) versus distance downstream of Delmont Compressor Station.

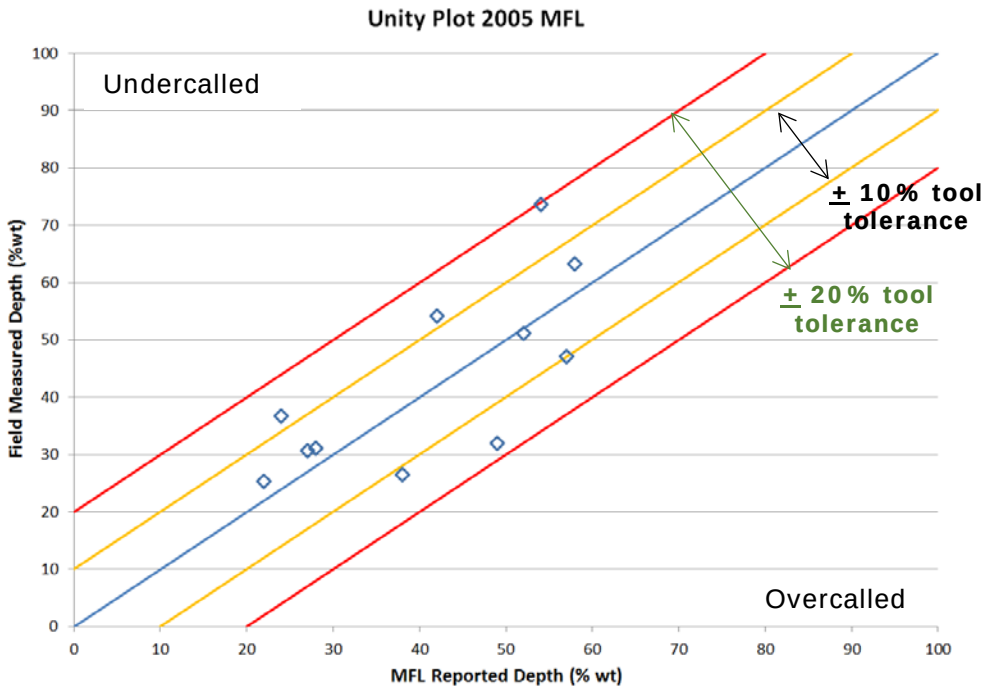

Figure 27. Metal loss depth unity plot from digs following 2005 ILI run. Data provided by Spectra [Ref. 57].

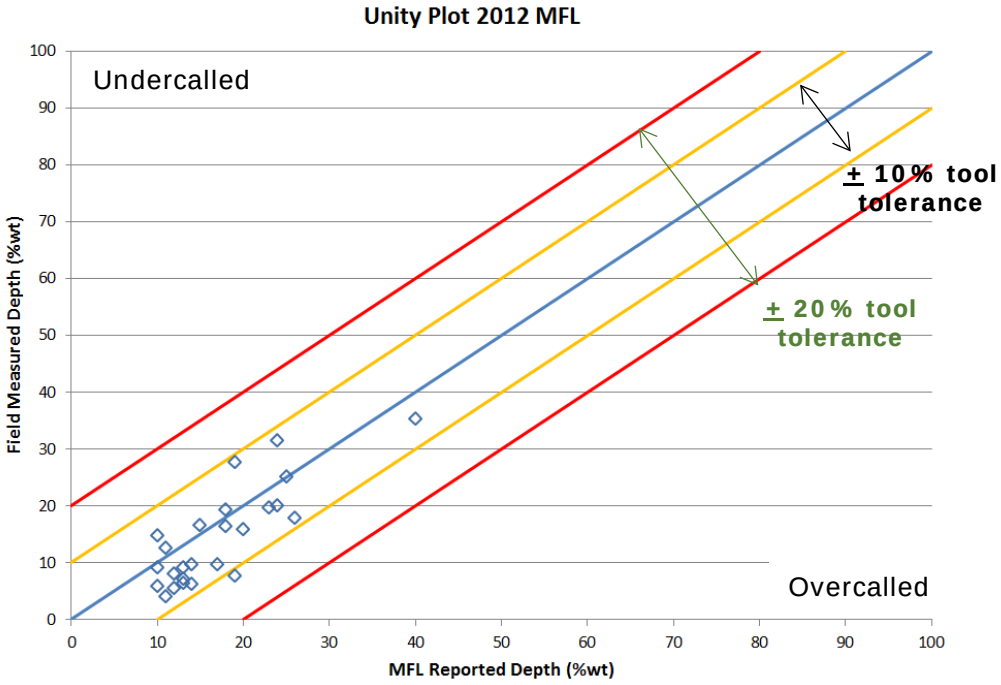

Figure 28. Metal loss depth unity plot from 2012 - 2015 digs following 2012 ILI run. Data provided by Spectra [Ref. 57].

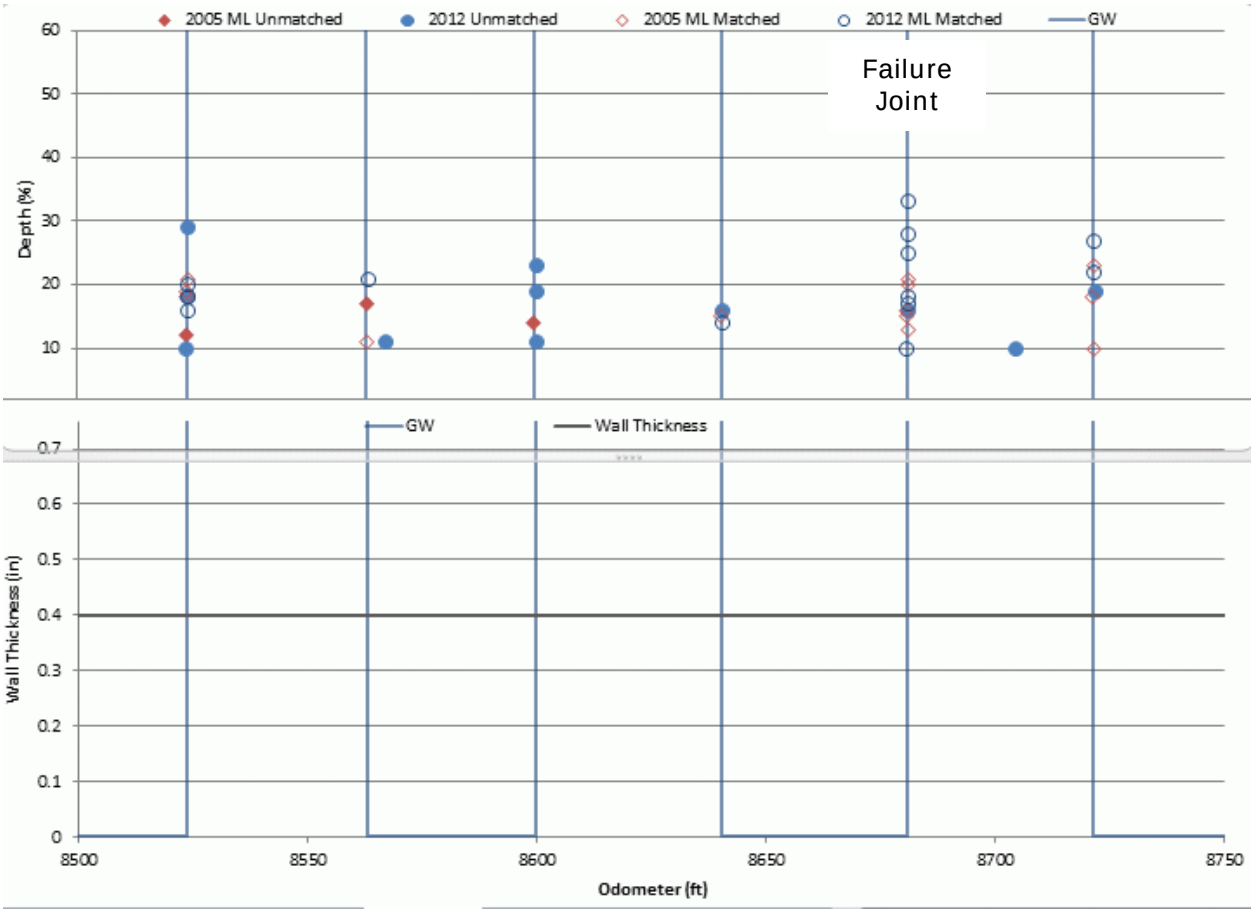

Figure 29. External ILI calls from the 2005 and 2012 ILI runs showing a strong correlation with girth weld locations (vertical lines).

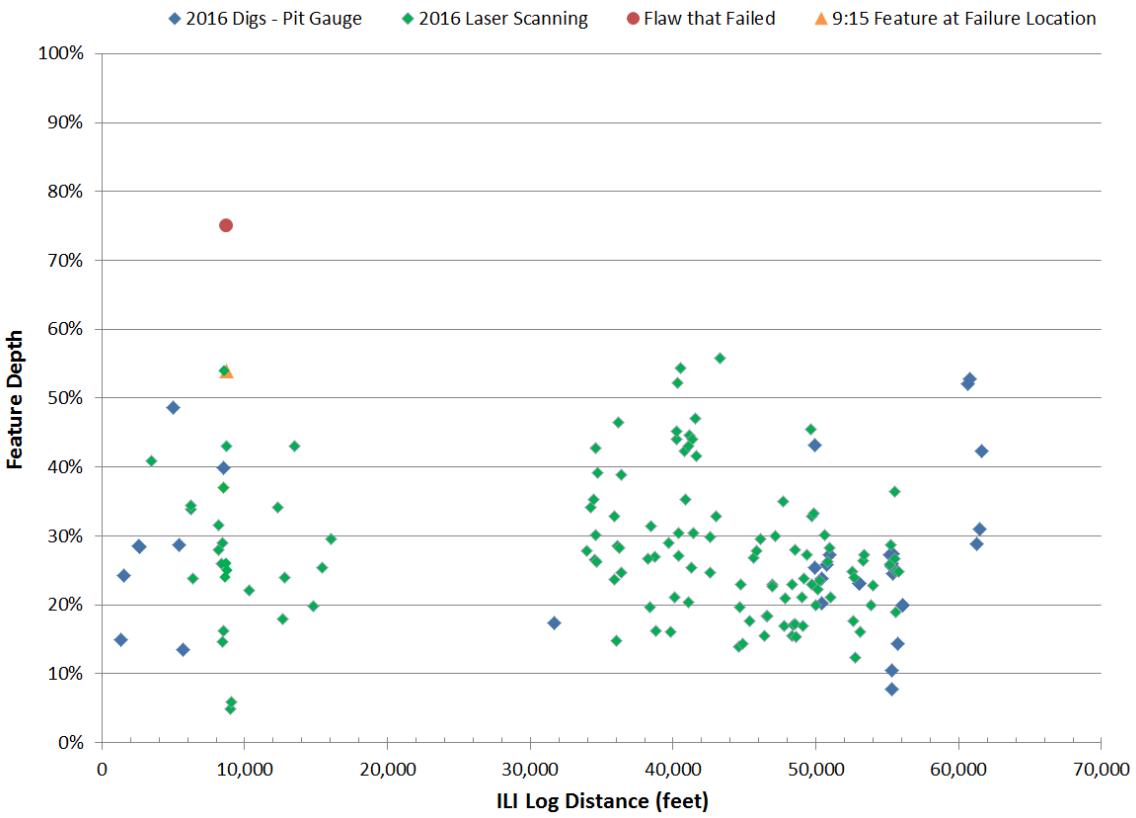

Figure 30. Distribution of feature depths determined from 2016 digs performed between May 17, 2016 and August 20, 2016 on the Isolated Segment and the depths determined for features near GWs at and near the failure location vs. ILI log distance.

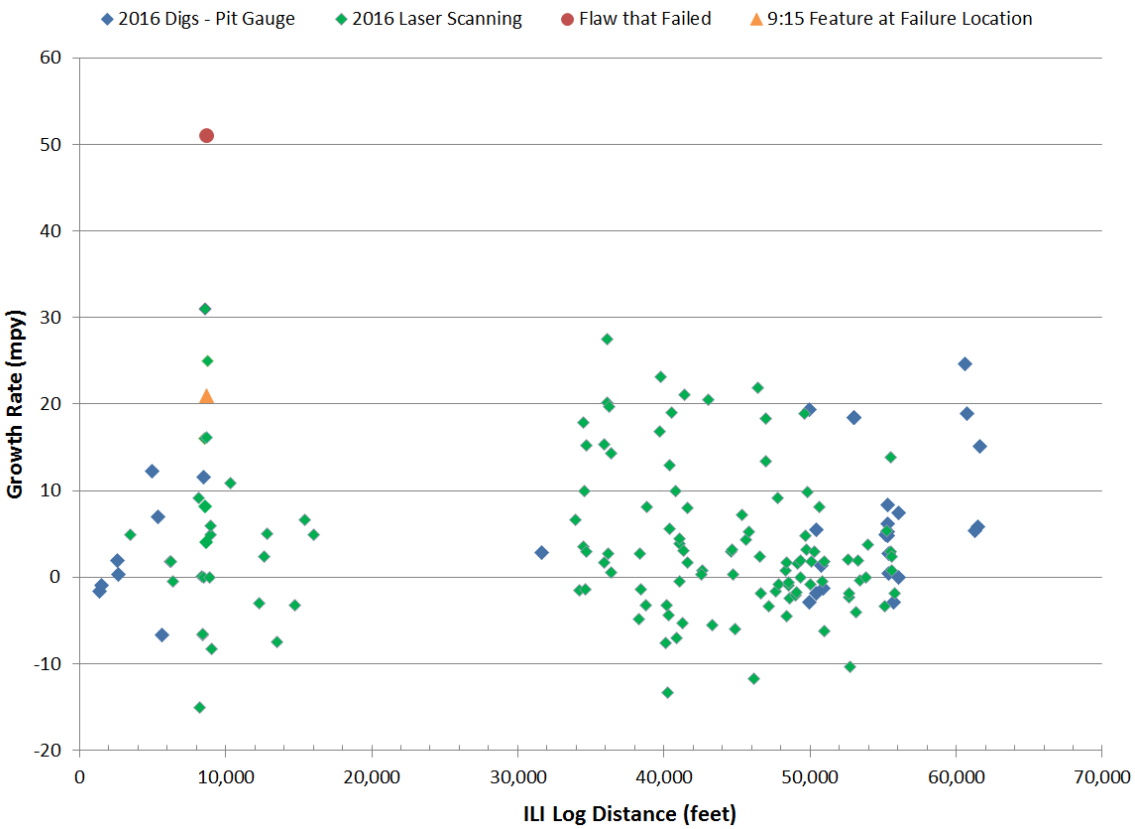

Figure 31. Distribution of corrosion rates determined from 2016 digs performed between May 17, 2016 and August 20, 2016 on the Isolated Segment and the corrosion rates determined for features on GWs at and near the failure location vs. ILI log distance. Corrosion rates determined based on comparison to 2012 ILI results.

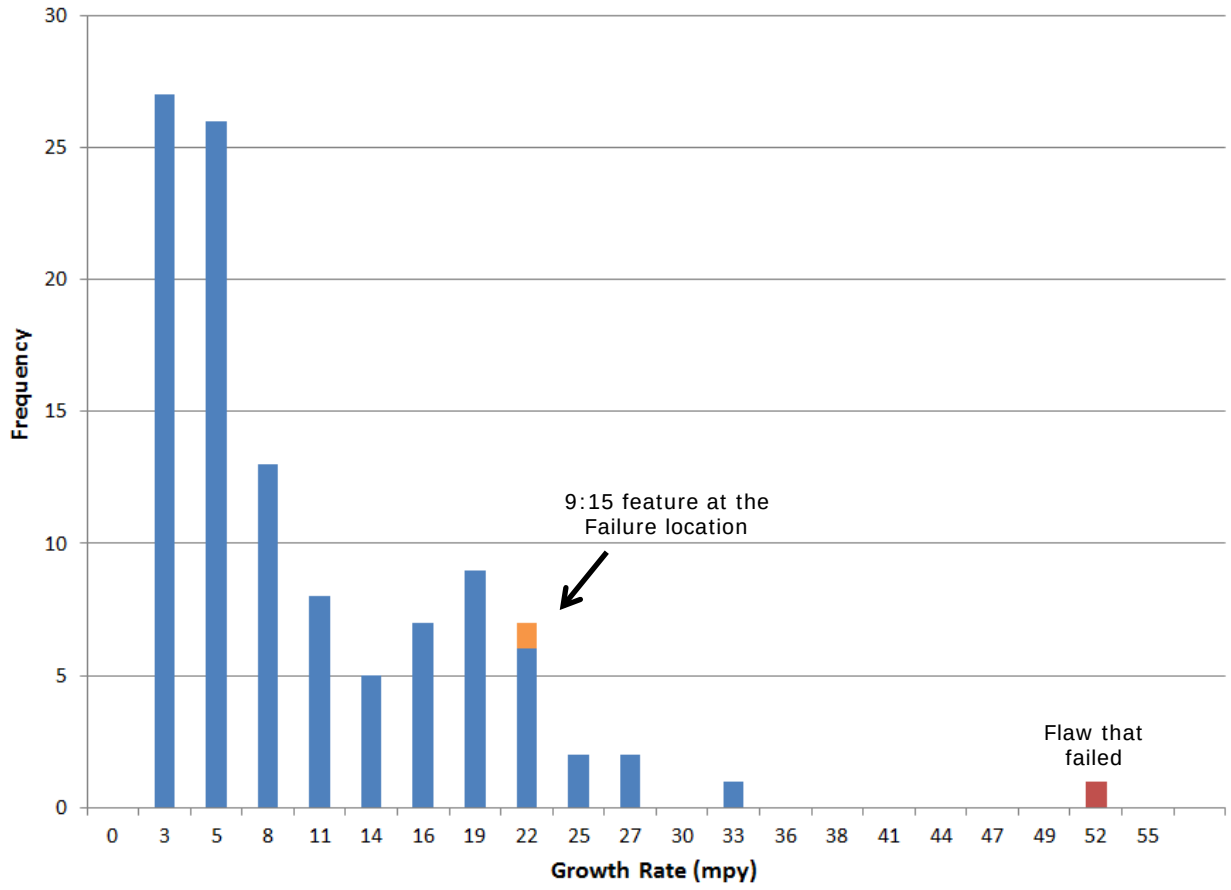

Figure 32. Histogram showing the distribution of corrosion rates determined from 2016 digs performed between May 17, 2016 and August 20, 2016 on the Isolated Segment and the corrosion rates determined for features on GWs at and near the failure location. Corrosion rates determined based on comparison to 2012 ILI results.

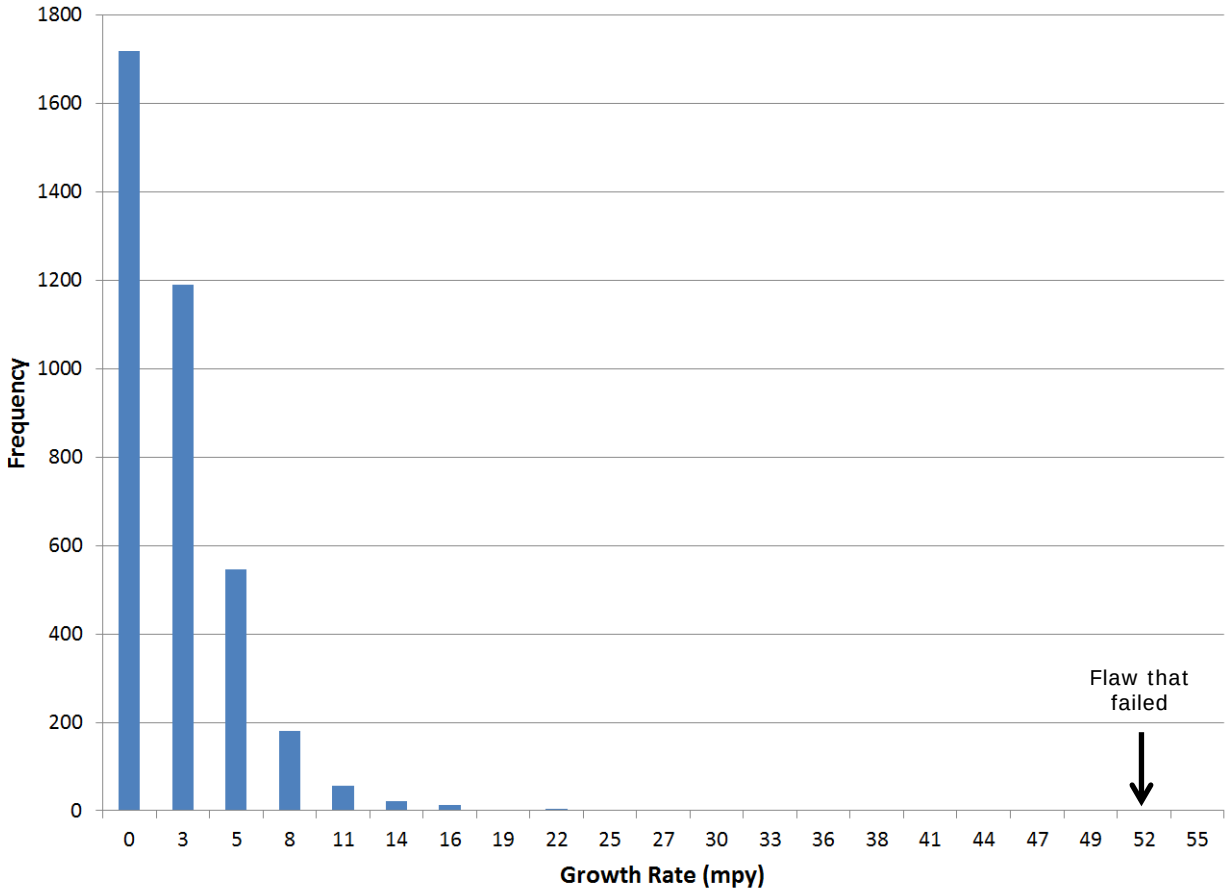

Figure 33. Histogram showing the distribution of corrosion rates determined from the ILI-ILI Master dataset. Corrosion rates determined based on comparison of the 2005 ILI data to the 2012 ILI data.

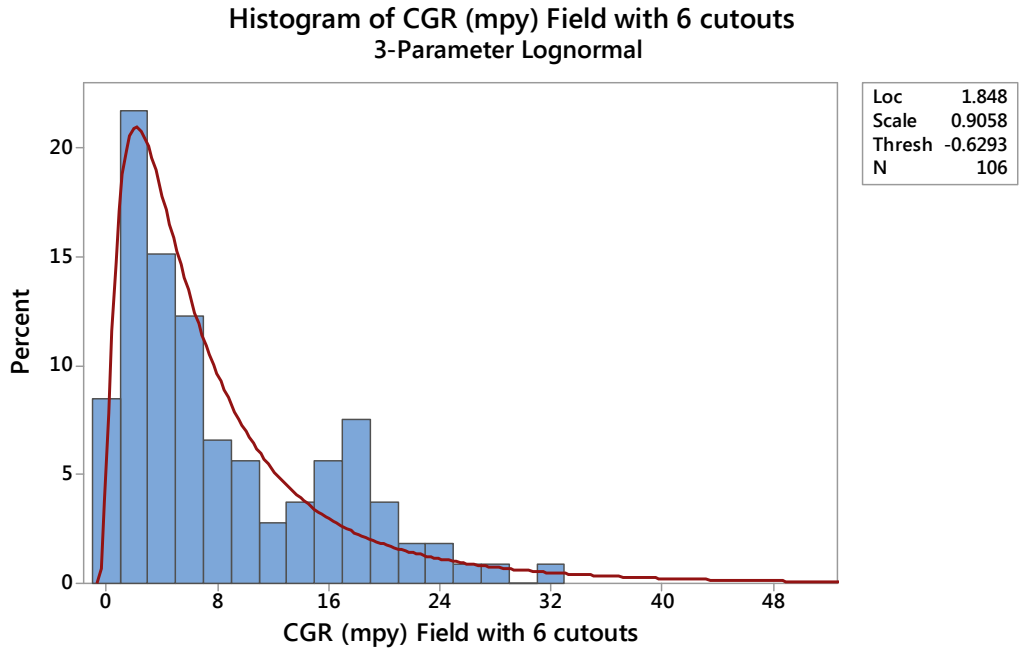

Figure 34. Distribution fit of a 3-Parameter Lognormal to the corrosion growth rates determined from the comparison of the 2016 Field measurements and 2012 ILI data.

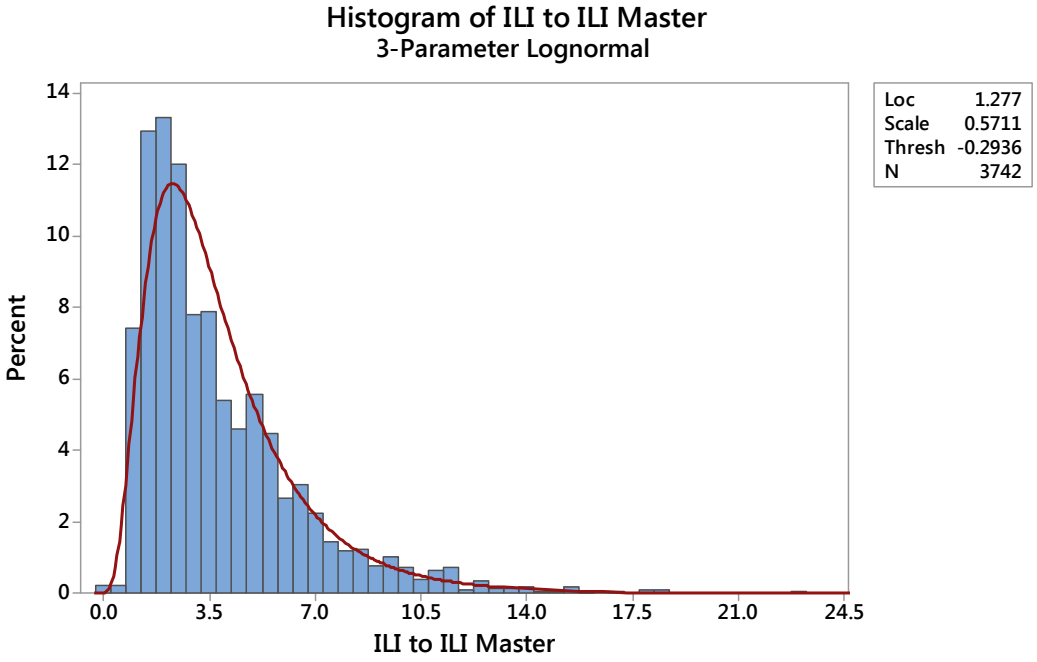

Figure 35. Distribution fit of a 3-Parameter Lognormal to the corrosion growth rates determined from the comparison of the 2005 and 2012 ILI data.

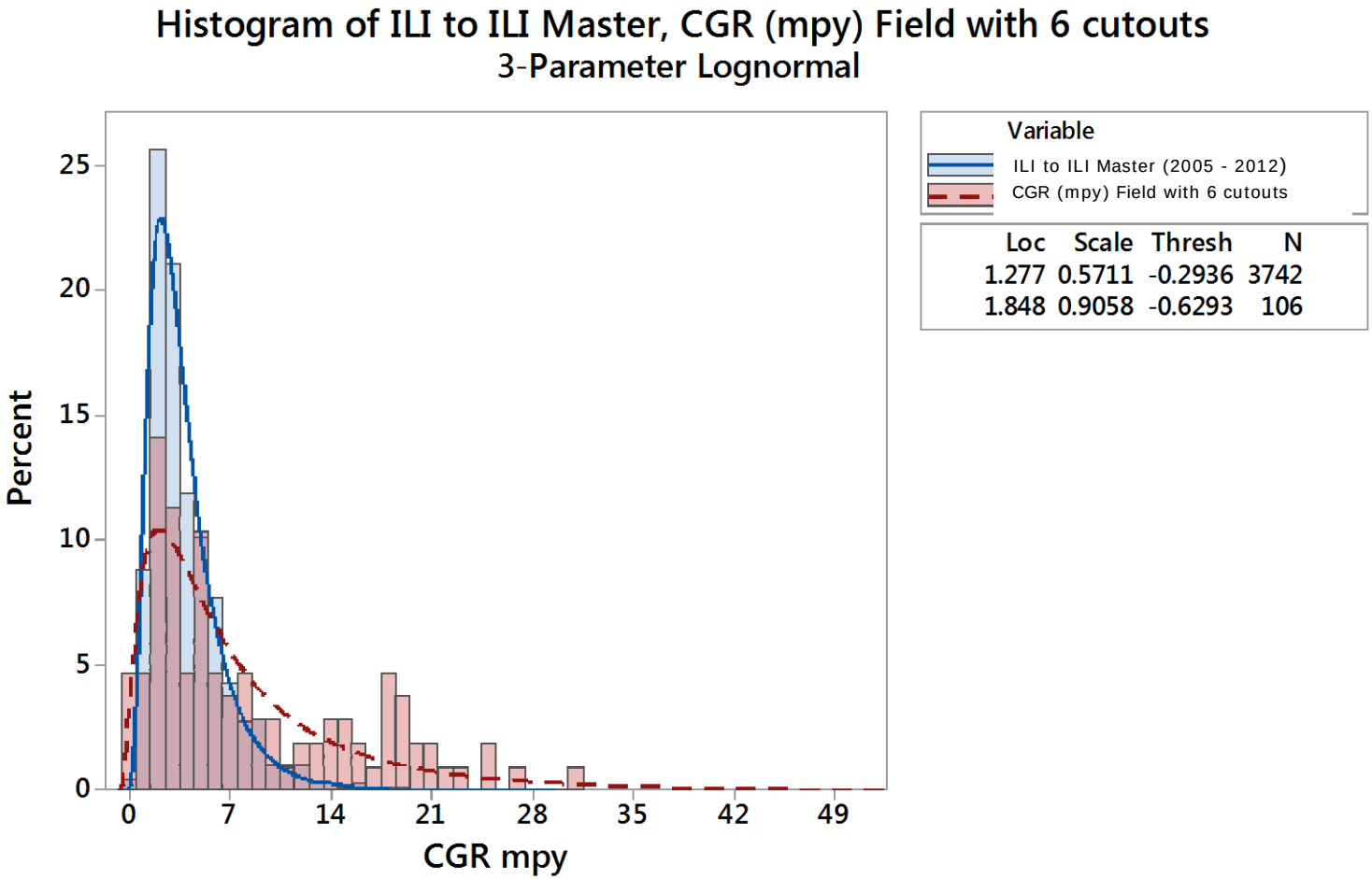

Figure 36. Combined histogram showing the previous two figures overlaid onto each other (i.e. 2005 - 2012 ILI data distribution overlaid with 2012 ILI data – 2016 Field measurement distribution.

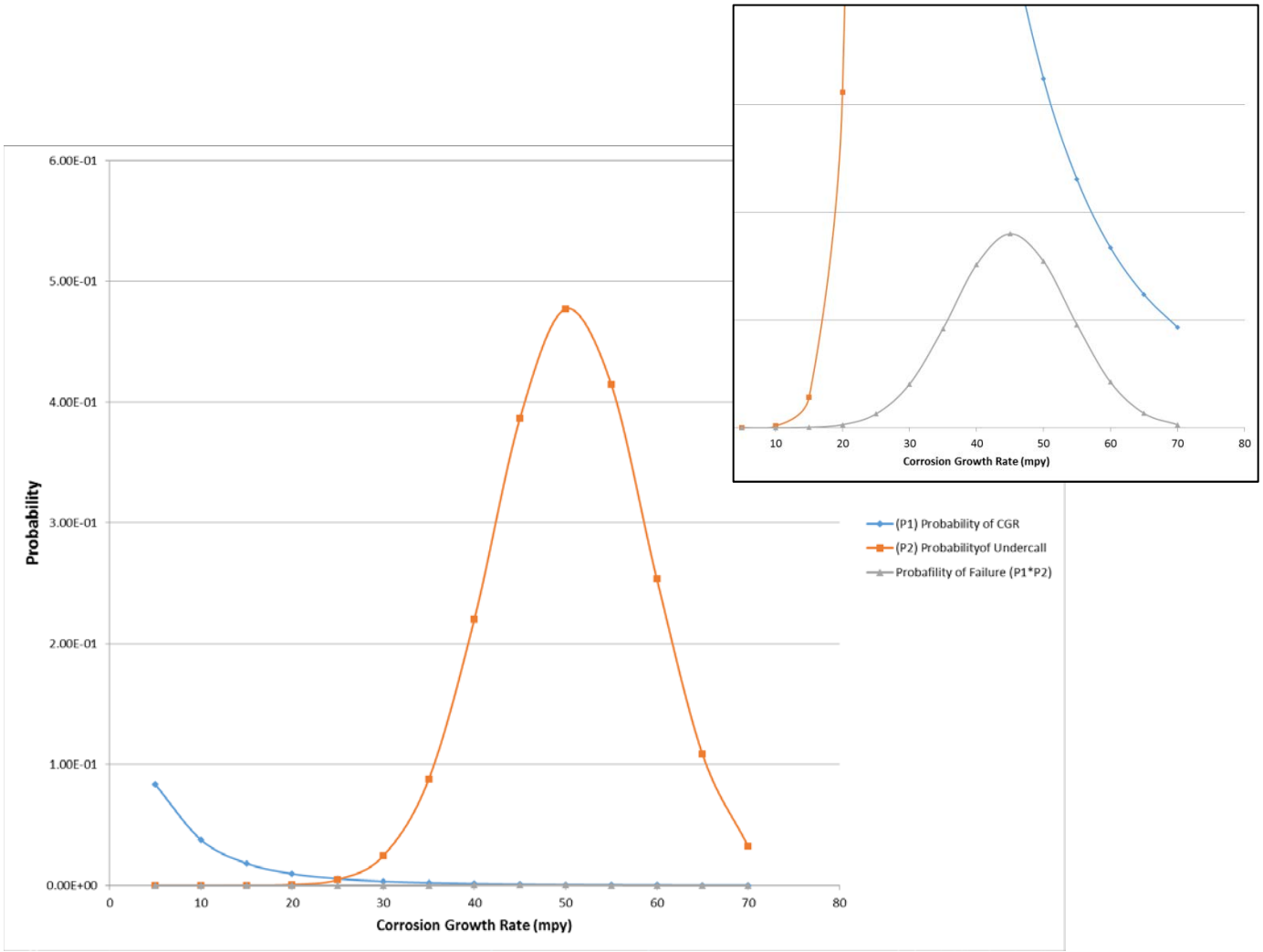

Figure 37. Plot showing the probability of a given CGR, the corresponding probability for an undercall, and the combined probability.

APPENDIX A

References

The following is a list of references that were used for the RCFA. The reference numbers listed below are used throughout this report to identify the source of information.

Reference Number	Document Name
Incident Related Documents	
1.	Spectra_ACAO_CPF_No_1_2016_1004H.pdf
2.	Spectra Energy Partners, LP Delmont Rupture Final Report (PP15 7718) July 5.pdf
3.	Delmont Incident - PHMSA Request 05-01-16.pdf
4.	1a-b - TETLP Delmont Line 27 Incident Report 042916.pdf
5.	1c Delmont NRC Report Data.pdf
6.	Delmont Timeline-Ln27 Rupture 4-29-16.pdf
7.	GasControlLog-DELMONT.pdf
8.	Scott Hill April 29 Line 27 Rupture Review.docx
9.	Tom Panico April 29 Line 27 Rupture Review.docx
10.	1dv - Delmont Line 27 HCA Analysis.pdf
11.	**Photographs provided by Spectra. File names:** 20160430_151627.jpg, 20160430_151631.jpg, 20160430_153701.jpg, 20160430_153704.jpg, 20160430_153713.jpg, 20160430_153956.jpg, 20160430_154001.jpg, 20160430_154006.jpg, 20160430_154014.jpg, 20160430_154237.jpg, 20160430_154249.jpg, 20160430_154326.jpg, 20160430_154358.jpg, 20160430_154416.jpg, 20160430_154624.jpg, 20160430_154629.jpg, 20160430_154650.jpg, 20160430_154958.jpg, 20160430_155112.jpg, 20160430_155117.jpg, 20160430_190624.jpg, 20160430_190630.jpg, 20160430_204935.jpg, 20160430_204939.jpg, 20160430_205103.jpg, 20160501_094515.jpg, 20160501_094519.jpg, 20160501_115108.jpg, 20160501_115124.jpg, 20160501_115321.jpg, 20160501_152502.jpg, 20160501_152511.jpg, 20160501_190823.jpg, 20160501_190831.jpg, 20160501_190845.jpg, 20160501_190858.jpg,

Reference Number	Document Name
	20160501_191438.jpg, 20160501_191446.jpg, 20160502_082849.jpg, 20160502_082854.jpg, 20160502_082903.jpg 20160502_082937.jpg, 20160502_083203.jpg, 20160502_083208.jpg, 20160502_084518.jpg, 20160502_084523.jpg, 20160502_085333.jpg, 20160503_100112.jpg, 20160503_100250.jpg, 20160503_100311.jpg, 20160503_100313.jpg, 20160503_101336.jpg, 20160503_101345.jpg 20160503_101351.jpg, 20160503_102728.jpg, 20160503_103156.jpg, 20160503_111145.jpg, 20160503_111147.jpg, 20160503_120558.jpg, 20160503_140932.jpg, 20160503_140934.jpg, 20160503_141038.jpg, 20160503_141051.jpg, 20160503_185411.jpg, 20160503_185428.jpg, 20160503_185431.jpg, 20160503_185444.jpg, 20160504_103343.jpg, 20160504_103346.jpg, 20160504_103349.jpg, 20160504_103456.jpg 20160504_103500.jpg, 20160504_103506.jpg, 20160504_103540.jpg, 20160504_104111.jpg, 20160504_104118.jpg, 20160504_104119.jpg, 20160504_104127.jpg, 20160504_104221.jpg, 20160504_104230.jpg, 20160504_104247.jpg, 20160504_104252.jpg, 20160504_105409.jpg, 20160504_105410.jpg, 20160504_105430.jpg, 20160504_105433.jpg, 20160504_110034.jpg, 20160504_110313.jpg, 20160504_110319.jpg, 20160504_111245.jpg, 20160504_111259.jpg, 20160504_111903.jpg, 20160504_111933.jpg, 20160504_112650.jpg, 20160504_112653.jpg, 20160504_112707.jpg, 20160504_112727.jpg, 20160504_112753.jpg, 20160504_112830.jpg, 20160504_112833.jpg, 20160504_113121.jpg, 20160504_113126.jpg, 20160504_113259.jpg, 20160504_113324.jpg, 20160504_152951.jpg, 20160504_152954.jpg, 20160504_153008.jpg, 20160504_153014.jpg, 20160504_153655.jpg, 20160504_171659.jpg, 20160504_171701.jpg, 20160504_175426.jpg, 20160504_175432.jpg, 20160504_175441.jpg, 20160504_181334.jpg, 20160504_181346.jpg, 20160504_181454.jpg, 20160504_181501.jpg, SAM_0599.jpg, SAM_0600.jpg, SAM_0601.jpg
12.	**Satellite and aerial views provided by Spectra. File names:** Capture04192014.JPG, Capture05122007.JPG, Capture2007.JPG, Capture2fromEdge2016.JPG, CapturefromEDGE2016.JPG
13.	**Maps and alignment sheets for Line 12. Files Designated:** DELM-ARMA_12.Operations.001.pdf, DELM-ARMA_12.Operations.002.pdf, DELM-ARMA_12.Operations.003.pdf, DELM-ARMA_12.Operations.004.pdf, DELM-ARMA_12.Operations.005.pdf, DELM-ARMA_12.Operations.006.pdf, DELM-ARMA_12.Operations.007.pdf, DELM-ARMA_12.Operations.008.pdf, DELM-ARMA_12.Operations.009.pdf, DELM-ARMA_12.Operations.010.pdf, DELM-ARMA_12.Operations.011.pdf, DELM-ARMA_12.Operations.012.pdf, DELM-ARMA_12.Operations.013.pdf, DELM-ARMA_12.Operations.014.pdf, DELM-ARMA_12.Operations.015.pdf, DELM-ARMA_12.Operations.016.pdf, DELM-ARMA_12.Operations.017.pdf, DELM-ARMA_12.Operations.018.pdf
14.	**Maps and alignment sheets for Line 19. Files Designated:** DELM-ARMA_19-AUX-1.Operations.011.pdf, DELM-ARMA_19.Operations.001.pdf, DELM-ARMA_19.Operations.002.pdf, DELM-ARMA_19.Operations.003.pdf, DELM-ARMA_19.Operations.004.pdf,

Reference Number	Document Name
	DELM-ARMA_19.Operations.005.pdf, DELM-ARMA_19.Operations.006.pdf, DELM-ARMA_19.Operations.007.pdf, DELM-ARMA_19.Operations.008.pdf, DELM-ARMA_19.Operations.009.pdf, DELM-ARMA_19.Operations.010.pdf, DELM-ARMA_19.Operations.011.pdf, DELM-ARMA_19.Operations.012.pdf, DELM-ARMA_19.Operations.013.pdf, DELM-ARMA_19.Operations.014.pdf, DELM-ARMA_19.Operations.015.pdf, DELM-ARMA_19.Operations.016.pdf, DELM-ARMA_19.Operations.017.pdf, DELM-ARMA_19.Operations.018.pdf
15.	**Maps and alignment sheets for Line 27. Files Designated:** DELM-ARMA_27-AUX-1.Operations.011.pdf, DELM-ARMA_27.Operations.001.pdf, DELM-ARMA_27.Operations.002.pdf, DELM-ARMA_27.Operations.003.pdf, DELM-ARMA_27.Operations.004.pdf, DELM-ARMA_27.Operations.005.pdf, DELM-ARMA_27.Operations.006.pdf, DELM-ARMA_27.Operations.007.pdf, DELM-ARMA_27.Operations.008.pdf, DELM-ARMA_27.Operations.009.pdf, DELM-ARMA_27.Operations.010.pdf, DELM-ARMA_27.Operations.011.pdf, DELM-ARMA_27.Operations.012.pdf, DELM-ARMA_27.Operations.013.pdf, DELM-ARMA_27.Operations.014.pdf, DELM-ARMA_27.Operations.015.pdf, DELM-ARMA_27.Operations.016.pdf, DELM-ARMA_27.Operations.017.pdf, DELM-ARMA_27.Operations.018.pdf
16.	**Maps and alignment sheets for Line 28. Files Designated:** DELM-ARMA_28.Operations.001.pdf, DELM-ARMA_28.Operations.002.pdf, DELM-ARMA_28.Operations.003.pdf, DELM-ARMA_28.Operations.004.pdf, DELM-ARMA_28.Operations.005.pdf
17.	**Soil analysis reports from Spectra. Files Designated:** LN 12 WC 10043 10083 10123-05192016-COC42700.pdf, LN 12 WC 9600-05192016-COC42706.pdf LN 12 WC 9620 9659 9692-05192016-COC42705.pdf LN 19 Disc Welds-05062016-COC42640.pdf LN 27 Incident - Saddle Stock Pile 1 and 2-05042016-COC42752.pdf LN 27 Incident - Saddle Stock Pile 1and 2-05042016-COC42753.pdf LN12-28DiscWeld-BellHole-05102016-COC42678.pdf North Soil Pile - 05022016-COC42748.pdf Pit 1-05022016-COC42750.pdf South Soil Pile - 05022016-COC42749.pdf
18.	**French drain locations. Files Designated:** 100.pdf, 1605017 Spectra Delmont Discharge-Incident-1-30.pdf, 160505 Spectra Delmont Line 27 Incident Field Points.xls, 160506 Spectra Delmont Discharge-Incident Soil Sample Plan.pdf, 160506 Spectra Delmont Discharge-Incident-1=100-Aerial-Contours.pdf, 160506 Spectra Delmont Discharge-Incident.pdf 160513 Spectra Delmont Discharge-Incident-1-30-Aerial-Contours.pdf 160513 Spectra Delmont Discharge-Incident-1-30.pdf 160513 Spectra Delmont Discharge-Incident-1=100-Aerial-Contours.pdf 160513 Spectra Delmont Discharge-Incident-1=100.pdf 160513 Spectra Delmont Line 27 Incident Field Points.xls 160516 Spectra Delmont Line 27 Incident Field Points.xls 160517 Spectra Delmont Discharge-Incident-1=100.pdf

Reference Number	Document Name
	Daily Rpt WO 0176_1968_ Ln 12 and 19_ Drain Tile Repairs.pdf Ln 28 Survey Notes_WO 110119_1994_Drain Tile Xing.pdf
19.	100-Aerial-Contours.pdf
20.	1605017 Spectra Delmont Discharge-Incident-1-30-Aerial-Contours.pdf
21.	160516 Spectra Delmont Line 27 Incident Field Points.xls
22.	160517 Spectra Delmont Discharge-Incident-1=100-Aerial-Contours.pdf
23.	DELMONT 4 LINES.pdf
24.	GW summary.docx
25.	weldseamsketch.JPG
Design and Construction Related Documents	
26.	2 - Delmont Line 27 - Historical Information Summary.pdf
27.	2a-iii - FIELD JOINT CTG.pdf
28.	2a-iii - FIELD JOINT CTG_Daily Report.pdf
29.	2a-iii - FUSED EPOXY POWDER EXT COATING.pdf
30.	2a-iii - Pipe and Ctg Matl Inv_WO 5986.pdf
31.	2a-v - INDEX TO SPECIAL PROVISIONS.pdf
32.	2a-v - PRE-BID MINUTES.pdf
33.	2a-v - SPECIFICATION INDEX.pdf

Reference Number	Document Name
34.	2a-v - STANDARDS.pdf
35.	2a-vi - DOUBLE SUBMERGED ARC.pdf
36.	2a-vi - WELD TEST REPORTS.pdf
37.	2a_iv - JOINT TALLY SURVEY NOTES.pdf
38.	2d - QUALITEST PIPE MILL INSP RPT.pdf
39.	2d - WO 5986_PURCHASE ORDER_USS_3156R.pdf
Integrity Related Documents	
40.	Integrity Management Program (IMP) Manual 09-0000.doc
41.	Integrity Managment White paper Line 27 Incident.pdf
42.	DELM_27 SEC1 Delmont, PA to Armagh, PA (120230_30I) InspReport.pdf
43.	ILI History - DELM_27_Sec_1.docx
44.	DELM_27 SEC1 Delmont, PA to Armagh, PA (120230_30I) Pipeline Lis.xlsx
45.	ILI 2005 30IN Line 27 - Delm to Cone River.xls
46.	ILI 2005: Sect 00-05.pdf
47.	ILI 2005: Sect 06.pdf
48.	ILI 2005: Sect 07.pdf
49.	ILI 2005: Sect 08.pdf

Reference Number	Document Name
50.	ILI 2005: Sect 09.pdf
51.	ILI 2005: Sect 10.pdf
52.	2005 ILI raw data files
53.	2012 ILI raw data files
54.	2005 DELM_27_SEC1 7T-281.pdf
55.	2012 DELM_27_SEC1 7T-281.pdf
56.	SOP Volume 9 - Pipeline Integrity: In-line Tool Pipeline Inspection 9_2010.doc
57.	DELM 27 Unity Plots.xlsx
58.	SOP Volume 9 - Pipeline Integrity: Response to In-line Tool Inspection 9_3010.doc
59.	DELM_27_SEC1 2005 Line Listing.xlsx
60.	DELM_27_SEC1 2012 Line Listing.xlsx
61.	2005 DELM_27_SEC1 7T-288.pdf
62.	2012 DELM_27_SEC1 7T-288.pdf
63.	3d - HYDROTEST JOB 1 (Test Section 3).pdf
64.	**Integrity Related Responses. File Designations:** Integrity Related Question 1.docx, Integrity Related Question 3.docx, Integrity Related Question 4.docx, Integrity Related Question 5.docx, DELM-ARMA_27_RunID 121 (2011).pdf, DELM-ARMA_27_RunID 171 (2012).pdf, Integrity Related Question 7.docx, Integrity Related Question 8.docx, Integrity Related Question 9.docx, Integrity Related Question 10.docx, Integrity Related Question 11.docx, Integrity Related Question 12.docx, Integrity Related Question 13.docx, Risk Algorithm Spectra_revised_March_27_2014 (3).pdf

Reference Number	Document Name
65.	SOP Volume 2 - Corrosion: Table of Contents corr_toc-1.pdf
66.	Threat Response Guidance Document - External Corrosion IMP_410.docx
67.	SOP Volume 2 - Corrosion: Action Item Summary Sheet 2_1010.doc
68.	SOP Volume 2 - Corrosion: Glossary 2_1020.doc
69.	SOP Volume 2 - Corrosion: Tables and Formulae 2_1030.doc
70.	SOP Volume 2 - Corrosion: Structure-to-Electrolyte Potential Measurement 2_2010.doc
71.	SOP Volume 2 - Corrosion: Line Current Flow Measurement 2_2020.doc
72.	SOP Volume 2 - Corrosion: Soil Resistivity Measurement 2_2040.doc
73.	SOP Volume 2 - Corrosion: Rectifier Inspection and Maintenance 2_2070.doc
74.	SOP Volume 2 - Corrosion: Groundbed Specifications and Inspection 2_2080.doc
75.	SOP Volume 2 - Corrosion: Close Interval Survey 2_2130.doc
76.	SOP Volume 2 - Corrosion: Current Requirement Testing 2_2140.doc
77.	SOP Volume 2 - Corrosion: Coating Systems for Buried or Submerged Piping 2_2160.doc
78.	SOP Volume 2 - Corrosion: Annual Corrosion Control Surveys 2_2180.doc
79.	SOP Volume 2 - Corrosion: Application of Cathodic Protection Criteria 2_2200.doc
80.	SOP Volume 2 - Corrosion: Cathodic Protection System Design 2_2230.doc
81.	SOP Volume 2 - Corrosion: Coating Fault Detection Surveys 2_2240.doc

Reference Number	Document Name
82.	SOP Volume 2 - Corrosion: Coating Resistance Measurement 2_2260.doc
83.	SOP Volume 2 - Corrosion: Evaluation of Remaining Strength of Pipe with Metal Loss 2_4020.doc
84.	SOP Volume 2 - Corrosion: Buried Pipe Inspections 2_4040.doc
85.	SOP Volume 2 - Corrosion: Corrosion Control Remedial Action 2_4080.doc
86.	SOP Volume 2 - Corrosion: Evaluation of Remaining Strength of Pipe with Metal Loss 2_4020.doc
87.	ILI Data 2005 and 2012 in Proximity to Failure.pptx
88.	BERV_27 Bernville to Bechtelsville (439189_30C) RunCom_Report_Issue1_Rev.pdf and .xlsx
89.	BERV_BECH_19 RunCom Report.pdf
90.	DELM_ARMA_12 Delmont to Lilly (438327_24I) RunCom Report Issue1 Rev1.pdf & .xlsx
91.	ENTR_PERU_19 Entriken to Shermans Dale (438327_30M)_RunCom_Report_Rev2.pdf and .xlsx
92.	GRAN 27 Runcom Report.pdf
93.	GRAN_BERV_12 Grantville to Bechtelsville (437613_24F)_RunCom_Report_Issue1_Rev1.pdf and .xlsx
94.	ILI and RunCom Analysis 2011 BERV-BECH-LAMB_2011 - ILI Ran v0.9.9.7.xlsm
95.	ILI and RunCom Analysis 2012 GRAN-BERV_27 - Run Com Ran v0.9.9.7.xlsm
96.	LILL_ENTR_12 Lilly to Perulack (438327_24H) RunCom Report Issue1 Rev1.pdf and .xlsx
97.	RunCom Analysis for 10 Line Segments.xlsx

Reference Number	Document Name
98.	RunCom Excerpts September 1 2016 (2).docx
99.	SHER_GRAN_19 Shermans Dale to Bernville (437613_30U) RunCom Report_Issue1_Rev1.pdf and .xlsx
Dig and Repair Historical Documents	
100.	1417618701 AI_2014_DELM-ARMA_30_Ln27_WC54508.3_GW_14920_ILI2012 With Attachments .pdf
101.	1520618700 AI_2015_DELM-ARMA_30_Ln27_VS02_WC56052.6_GW15610_ILI2012 With Attachments.pdf
102.	1527818700 AI_2015_DELM-ARMA_30_Ln27_VS04_WC6023_GW1710_ILI2012 With Attachments.pdf
103.	SOP Volume 9 - Pipeline Integrity: Defect Assessment and Repair Options for Internal Corrosion 9_4010.doc
104.	SOP Volume 9 - Pipeline Integrity: Defect Assessment & Repair Options for External Corrosion 9_4020.doc
105.	SOP Volume 9 - Pipeline Integrity: Direct Examination & Repair Options for Stress Corrosion Cracking 9_4030.doc
106.	SOP Volume 9 - Defect Assessment & Repair Options for Dents and Mechanical Damage 9_4040.doc
107.	SOP Volume 9 - Pipeline Integrity: Defect Assessment and Repair Options for Miscellaneous Defects 9_4050.doc
108.	SOP Volume 9 - Pipeline Repair Procedures 9_5010.doc
109.	DELM_27_SEC-1 Anomaly Dig List Summary.pdf
110.	DELM_27_SEC-2 Anomaly Dig List Summary.pdf
111.	**2005 Dig Reports. File Designations:** CONE-ARMA_27_602-05-17.pdf
112.	**2012 Dig Reports. File Designations:** 9756_DELM-ARMA_Ln27_WC46657.8.pdf, 9792_DELM-ARMA_Ln27_WC 29124.pdf, 9841_DELM-ARMA_Ln27_WC56564.5.pdf,

Reference Number	Document Name
	9857_DELM-ARMA_Ln27_WC2766.2.pdf, 9858_DELM-ARMA_Ln27_WC3351.9.pdf, 9756 Line 27 WC 46657.8, 2012 With Attachment.pdf, 9792 Line 27 WC29124.pdf, 9841 Line 27 WC56564.5, 2012 With Attachment.pdf, 9857 Line 27 WC2766.2, 2012 With Attachment.pdf, 9858 Line 27 WC3351.9 With Attachment.pdf
113.	**2013 Dig Reports. File Designations:** 34187_DELM-ARMA_Ln27_WC55839.4.pdf 40187_DELM-ARMA_Ln27.pdf 34187 Line 27 WC55839.4 with Attachments.pdf, 40187 Line 27 Crooked Run Rd Neg With Attachment.pdf
114.	**2014 Dig Reports. File Designations:** 1417618701_DELM-ARMA_Ln27_WC54508.3.pdf
115.	**2015 Dig Reports. File Designations:** 1520618700_DELM-ARMA_Ln27_WC56052.6.pdf, 1527818700_DELM-ARMA_Ln27_WC6023.pdf 1528220603_DELM-ARMA_Ln27.pdf
116.	**2016 Dig Reports. File Designations:** 1614645802_DELM-ARMA_Ln27_WC1374.2.pdf, 1616144202_DELM-ARMA_Ln27_WC1494.pdf, 1615647800_DELM-ARMA_Ln27_WC8135.8.pdf, 1616144203_DELM-ARMA_Ln27_WC5002.pdf, 1616145801_DELM-ARMA_Ln27_WC31660.7.pdf, 1616544200_DELM-ARMA_Ln27_WC13488.pdf, 1616644200_DELM-ARMA_Ln27_WC3476.pdf, 1620434000_DELM-ARMA_Ln27_WC49917.pdf, 1620434002_DELM-ARMA_Ln27_WC49992.pdf, 1622349215_DELM-ARMA_Ln27_WC52591.pdf, 1622349218_DELM-ARMA_Ln27_WC52714.pdf, 1622349219_DELM-ARMA_Ln27_WC52999.pdf, 1622349220_DELM-ARMA_Ln27_WC53152.pdf, 1622349220_DELM-ARMA_Ln27_WC53152.pdf, 1622349221_DELM-ARMA_Ln27_WC53273.pdf, 1622349223_DELM-ARMA_Ln27_WC53831.pdf, 1604120600_DELM-ARMA_Ln27.pdf, 1611844204_DELM-ARMA_Ln27_WC55788.4.pdf, 1612418700_DELM-ARMA_Ln27_WC8524.pdf, 1614944200_DELM-ARMA_Ln27_WC1374.2.pdf, 1615547800_DELM-ARMA_Ln27_WC8208.pdf, 1615947800_DELM-ARMA_Ln27_WC8905.pdf, 1616047800_DELM-ARMA_Ln27_WC8946.pdf, 1616144200_DELM-ARMA_Ln27_WC2608.pdf, 1616144201_DELM-ARMA_Ln27_WC2643.pdf, 1616144204_DELM-ARMA_Ln27_WC5403.pdf,

Reference Number	Document Name
	1616144205_DELM-ARMA_Ln27_WC8363.pdf, 1616144206_DELM-ARMA_Ln27_WC8404.pdf, 1616144207_DELM-ARMA_Ln27_WC8442.pdf, 1616144208_DELM-ARMA_Ln27_WC8483.pdf, 1616147800_DELM-ARMA_Ln27_WC8986.pdf, 1616147801_DELM-ARMA_Ln27_WC9027.pdf, 1616844200_DELM-ARMA_Ln27_WC12617.pdf, 1616844201_DELM-ARMA_Ln27_WC12272.pdf, 1616844202_DELM-ARMA_Ln27_WC14749.pdf, 1616844203_DELM-ARMA_Ln27_WC15418.pdf, 1616844204_DELM-ARMA_Ln27_WC6220.pdf, 1616844205_DELM-ARMA_Ln27_WC6259.pdf, 1616844206_DELM-ARMA_Ln27_WC16054.pdf 1616848900_DELM-ARMA_Ln27_WC6421.pdf 1616944207_DELM-ARMA_Ln27_WC12814.pdf, 1618044200_DELM-ARMA_Ln27_WC33931.pdf, 1618049000_DELM-ARMA_Ln27_WC34213.pdf, 1618149000_DELM-ARMA_Ln27_WC34445.pdf, 1618149001_DELM-ARMA_Ln27_WC34480.pdf, 1618149002_DELM-ARMA_Ln27_WC34556.pdf 1618149003_DELM-ARMA_Ln27_WC34597.pdf, 1618149004_DELM-ARMA_Ln27_WC34677.pdf, 1618149005_DELM-ARMA_Ln27_WC34710.pdf, 1618149007_DELM-ARMA_Ln27_WC35874.pdf, 1618149009_DELM-ARMA_Ln27_WC36107.pdf, 1618149011_DELM-ARMA_Ln27_WC36072.pdf, 1618149012_DELM-ARMA_Ln27_WC36228.pdf, 1618149013_DELM-ARMA_Ln27_WC36347.pdf, 1618149025_DELM-ARMA_Ln27_WC38269.pdf, 1618149026_DELM-ARMA_Ln27_WC38350.pdf, 1618149027_DELM-ARMA_Ln27_WC38425.pdf, 1618149028_DELM-ARMA_Ln27_WC38725.pdf, 1618149029_DELM-ARMA_Ln27_WC38805.pdf, 1618149030_DELM-ARMA_Ln27_WC39680.pdf, 1618149031_DELM-ARMA_Ln27_WC39799.pdf, 1618149032_DELM-ARMA_Ln27_WC40119.pdf, 1618149033_DELM-ARMA_Ln27_WC40200.pdf, 1618149034_DELM-ARMA_Ln27_WC40241.pdf, 1618149035_DELM-ARMA_Ln27_WC40319.pdf, 1618149036_DELM-ARMA_Ln27_WC40356.pdf, 1618149037_DELM-ARMA_Ln27_WC40394.pdf, 1618149037_DELM-ARMA_Ln27_WC40394.pdf, 1618149038_DELM-ARMA_Ln27_WC40525.pdf, 1618149040_DELM-ARMA_Ln27_WC40787.pdf, 1618149041_DELM-ARMA_Ln27_WC40869.pdf, 1618149042_DELM-ARMA_Ln27_WC41031.pdf,

Reference Number	Document Name
	1618149043_DELM-ARMA_Ln27_WC41052.pdf, 1618149044_DELM-ARMA_Ln27_WC41092.pdf, 1618149046_DELM-ARMA_Ln27_WC41335.pdf, 1618149047_DELM-ARMA_Ln27_WC41376.pdf, 1618249000_DELM-ARMA_Ln27_WC41573.pdf, 1618249001_DELM-ARMA_Ln27_WC41613.pdf, 1618249003_DELM-ARMA_Ln27_WC42572.pdf, 1618249004_DELM-ARMA_Ln27_WC42596.pdf, 1618249005_DELM-ARMA_Ln27_WC43034.pdf, 1618249006_DELM-ARMA_Ln27_WC43293.pdf, 1618249008_DELM-ARMA_Ln27_WC44593.pdf, 1618249009_DELM-ARMA_Ln27_WC44634.pdf, 1618249011_DELM-ARMA_Ln27_WC44873.pdf, 1618249012_DELM-ARMA_Ln27_WC45348.pdf, 1618249013_DELM-ARMA_Ln27_WC45601.pdf, 1618249014_DELM-ARMA_Ln27_WC45835.pdf, 1618249015_DELM-ARMA_Ln27_WC46129.pdf, 1618249016_DELM-ARMA_Ln27_WC46393.pdf, 1619018700_DELM-ARMA_Ln27_WC5672.pdf, 1619834011_DELM-ARMA_Ln27_WC46594.pdf, 1619834013_DELM-ARMA_Ln27_WC46969.pdf, 1620134003_DELM-ARMA_Ln27_WC47666.pdf, 1620134004_DELM-ARMA_Ln27_WC47788.pdf, 1620144204_DELM-ARMA_Ln27_WC50593.pdf, 1620144205_DELM-ARMA_Ln27_WC50756.pdf, 1620144206_DELM-ARMA_Ln27_WC50834.pdf, 1620144207_DELM-ARMA_Ln27_WC50916.pdf 1620334000_DELM-ARMA_Ln27_WC47828.pdf, 1620334002_DELM-ARMA_Ln27_WC48376.pdf, 1620334003_DELM-ARMA_Ln27_WC48418.pdf, 1620334004_DELM-ARMA_Ln27_WC48497.pdf, 1620334005_DELM-ARMA_Ln27_WC48538.pdf, 1620334006_DELM-ARMA_Ln27_WC48618.pdf, 1620334007_DELM-ARMA_Ln27_WC49017.pdf, 1620334008_DELM-ARMA_Ln27_WC49057.pdf, 1620334009_DELM-ARMA_Ln27_WC49139.pdf, 1620334010_DELM-ARMA_Ln27_WC49360.pdf, 1620334011_DELM-ARMA_Ln27_WC49637.pdf, 1620334012_DELM-ARMA_Ln27_WC49678.pdf, 1620334013_DELM-ARMA_Ln27_WC49718.pdf, 1620836900_DELM-ARMA_Ln27.pdf, 1621018702_DELM-ARMA_Ln27.pdf, 1621018706_DELM-ARMA_Ln27.pdf, 1622349210_DELM-ARMA_Ln27_WC50955.pdf, 1622349211_DELM-ARMA_Ln27_WC50996.pdf, 1622449200_DELM-ARMA_Ln27_WC53951.pdf

Reference Number	Document Name
117.	20160822 Circumferential Anomaly Dig Status Worksheet Line 27.xlsx
118.	Circumferential Assessment Question Response (8-23-16).docx
119.	Circumferentially Oriented Corrosion Acceptance Criteria August 3 2016 Rev 5.pdf
Management of Change Documents	
120.	5a - Delmont Ln 27 - Changes in Operating Conditions.pdf
121.	5a - Delmont Ln 27 - Pipe Installed Since 2006.pdf
Cathodic Protection Records	
122.	DELM-ARMA Rectifier Data.xlsx
123.	Line 27 Initial CP Survey 1984.pdf
124.	6.b. Initial CP system type.docx
125.	6.c. Historical CP data.docx
126.	DELM-ARMA Line 27 Anuual Survey Data.xlsx
127.	**CP Related Responses. File Designations:** CP Related Question 1.docx, CP Related Question 2.docx, CP Related Question 3.docx, CP Related Question 4.docx, CP Related Question 7.docx
128.	IR Drop Line 27 - Spectra Energy Response (8-24-16).docx
Leak Detection Records	
129.	SAP 2012-2016 Delmont - Air Patrol Segment, Frequency, and Follow Up.xls
130.	Alarm Management SOP 8_2030.docx

Reference Number	Document Name
131.	Initial Notif SOP 8_2010.docx
132.	Incident Screen Shots.docx
133.	Performance Analysis.docx
134.	Delmont24HrData.xlsx
135.	7c - SET_External_Communication_Plan 8-20-15.pdf
136.	**Leak Survey Reports. File Designations:** 7T-0065 Leak Survey Apr 2014.pdf, 7T-0065 Leak Survey Aug 2010.pdf, 7T-0065 Leak Survey Aug 2012.pdf, 7T-0065 Leak Survey Feb 2010.pdf, 7T-0065 Leak Survey Feb 2012.pdf, 7T-0065 Leak Survey Jan 2011.pdf, 7T-0065 Leak Survey Jan 2013.pdf, 7T-0065 Leak Survey MR Sites Apr 2013.pdf, 7T-0065 Leak Survey MR Sites Jun 2010.pdf, 7T-0065 Leak Survey MR Sites May 2011.pdf, 7T-0065 Leak Survey MR Sites May 2012.pdf, 7T-0065 Leak Survey MR Sites May 2014.pdf, 7T-0065 Leak Survey Sep 2009.pdf, 7T-0065 Leak Survey Sep 2011.pdf, 7T-0065 Leak Survey Sep 2013.pdf,
137.	Air Patrol Segment, Frequency, and Follow Up.pdf
138.	Delmont Leakage Survey Line 27 - WO Detail report.xlsx
139.	Delmont Leakage Survey Line 27.xlsx
140.	Maximo 2008-2012 Air Patrol Segment, Frequency, and Follow Up.xls
141.	Maximo 2008-2012 Spectra_AirPatrol_SegmentAndFrequency_Audit-223310.xlsx
142.	Spectra_AirPatrol_Followup-3150.xlsx

Reference Number	Document Name
Operations Related Documents	
143.	OM_Plan.pdf
144.	DELMONT2013_2016_LN27_PRESS.xlsx
145.	DELMONT_PRESS_DETAIL_LN27.xlsx
146.	_20160510102700 pressure record LN27.csv
147.	DELMONT2013_2016_LN27_TEMP.xlsx
148.	DELMONT_TEMP_DETAIL_LN27.xlsx
149.	8c - 09-0000 IMP Manual.pdf
150.	8c - SOP 5_2030 Investigation of Failures.pdf
151.	**Delmont Discharge Temperature Data. File Designations:** Year 2012 TETCO North TPDISC Data.xlsx, Year 2013 TETCO North TPDISC Data.xlsx, Year 2014 TETCO North TPDISC Data.xlsx, Year 2015 TETCO North TPDISC Data.xlsx, Year 2016 TETCO North TPDISC Data (until May 20).xlsx
Other Documents	
152.	9b - SEP Org Chart - Delmont Incident - 6-14-16.pdf
153.	Delmont to Armagh Drawing (Uniontown Area) pld331a.pdf
154.	Delmont to Armagh Drawing (UNIONTOWN AREA AND CHAMBERSBURG AREA) pld331b.pdf
155.	NACE International Standard Practice SP0169-2013 “Control of External Corrosion on Underground or Submerged Metallic Piping Systems”.
Interviews	

Reference Number	Document Name
156.	Interview - Paul Sinclair on August 26, 2016
157.	Interview - Andy Drake on August 29, 2016
158.	Penn Jersey Regional Interviews on September 7, 2016
159.	Pipeline Integrity Interviews (Houston) on September 7, 2016
160.	Interview - Rod Rheaume on September 8, 2016

APPENDIX B

Additional Tape Coating Photographs

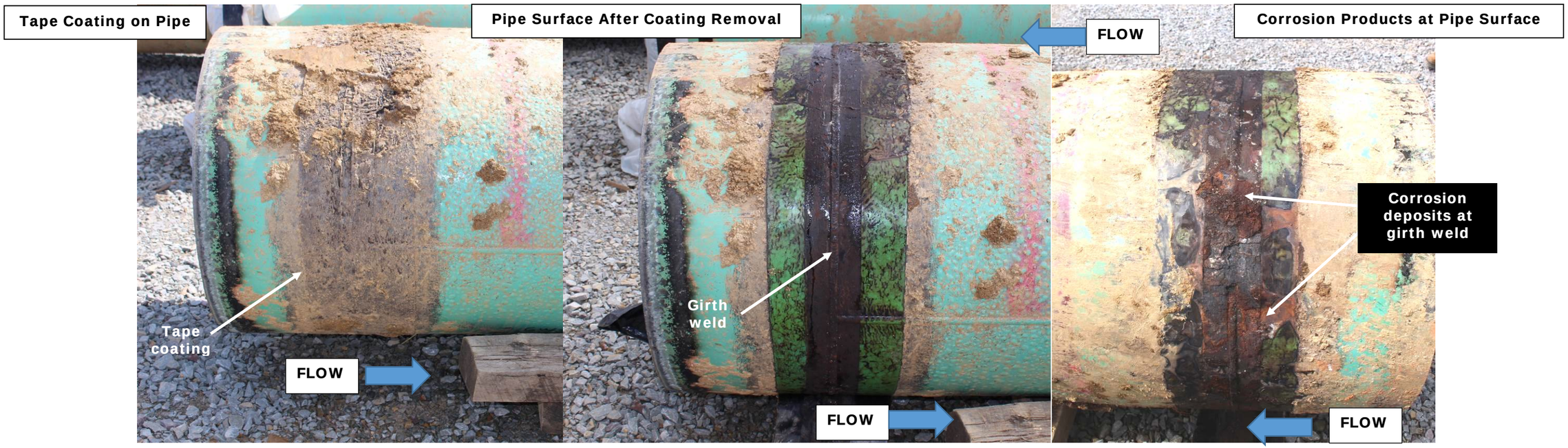

Figure B-1. Photographs showing the tape coating and the pipe surface at GW 2440 before and after removal of the tape from the pipe.

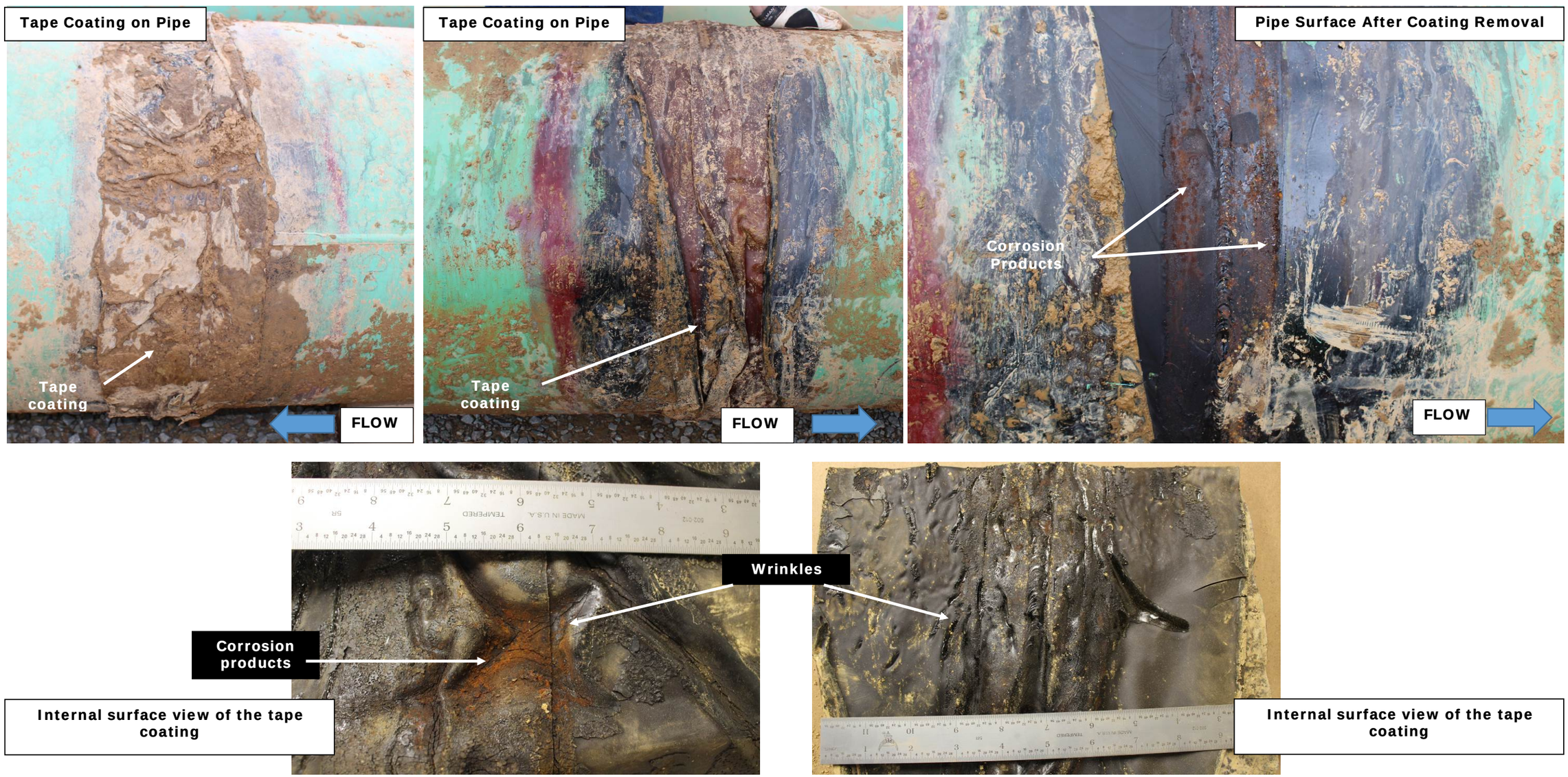

Figure B-2. Photographs showing the tape coating and the pipe surface at GW 2490 before and after removal of the tape from the pipe.

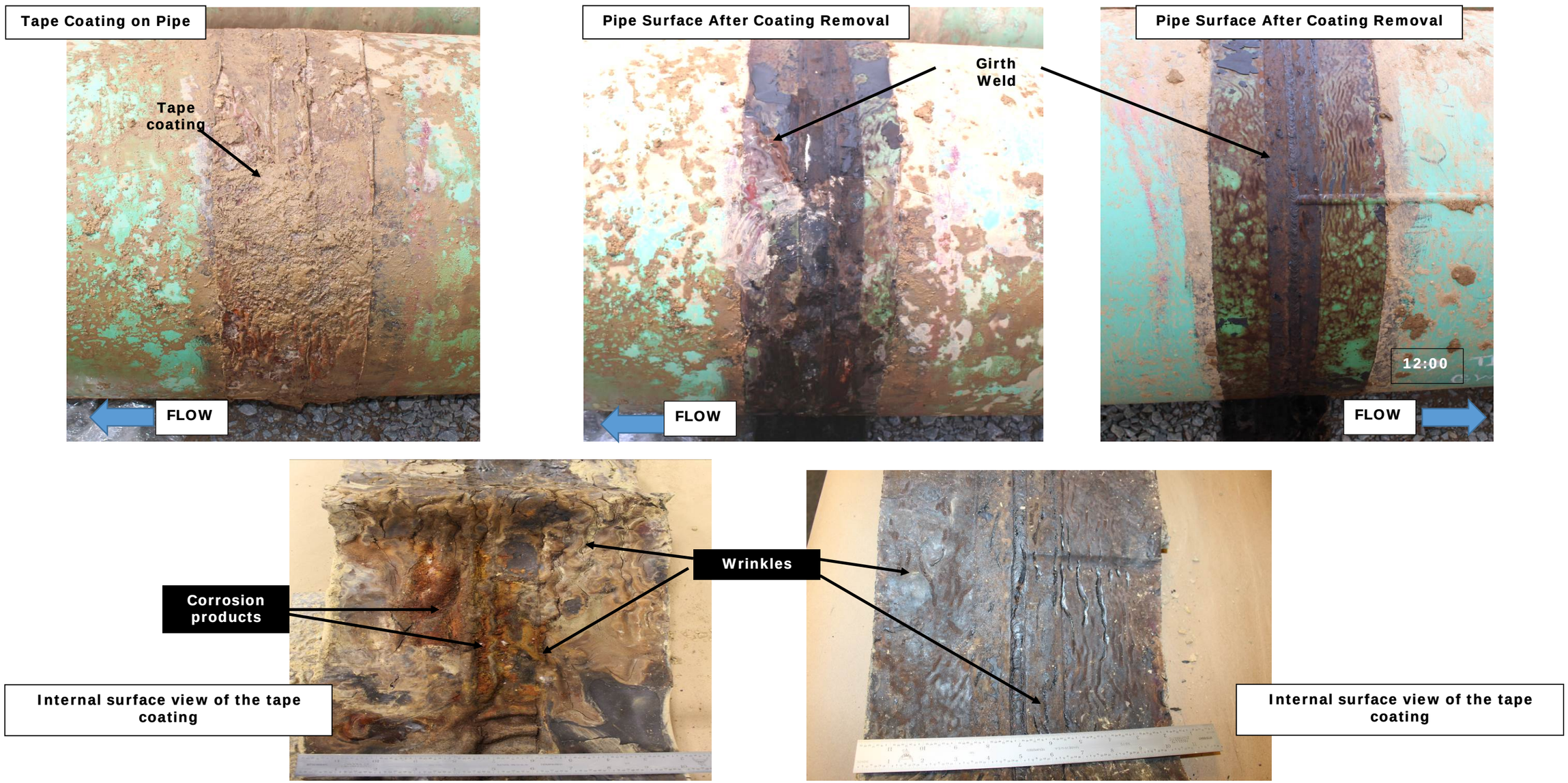

Figure B-3. Photographs showing the tape coating and the pipe surface at GW 2500 before and after removal of the tape from the pipe.

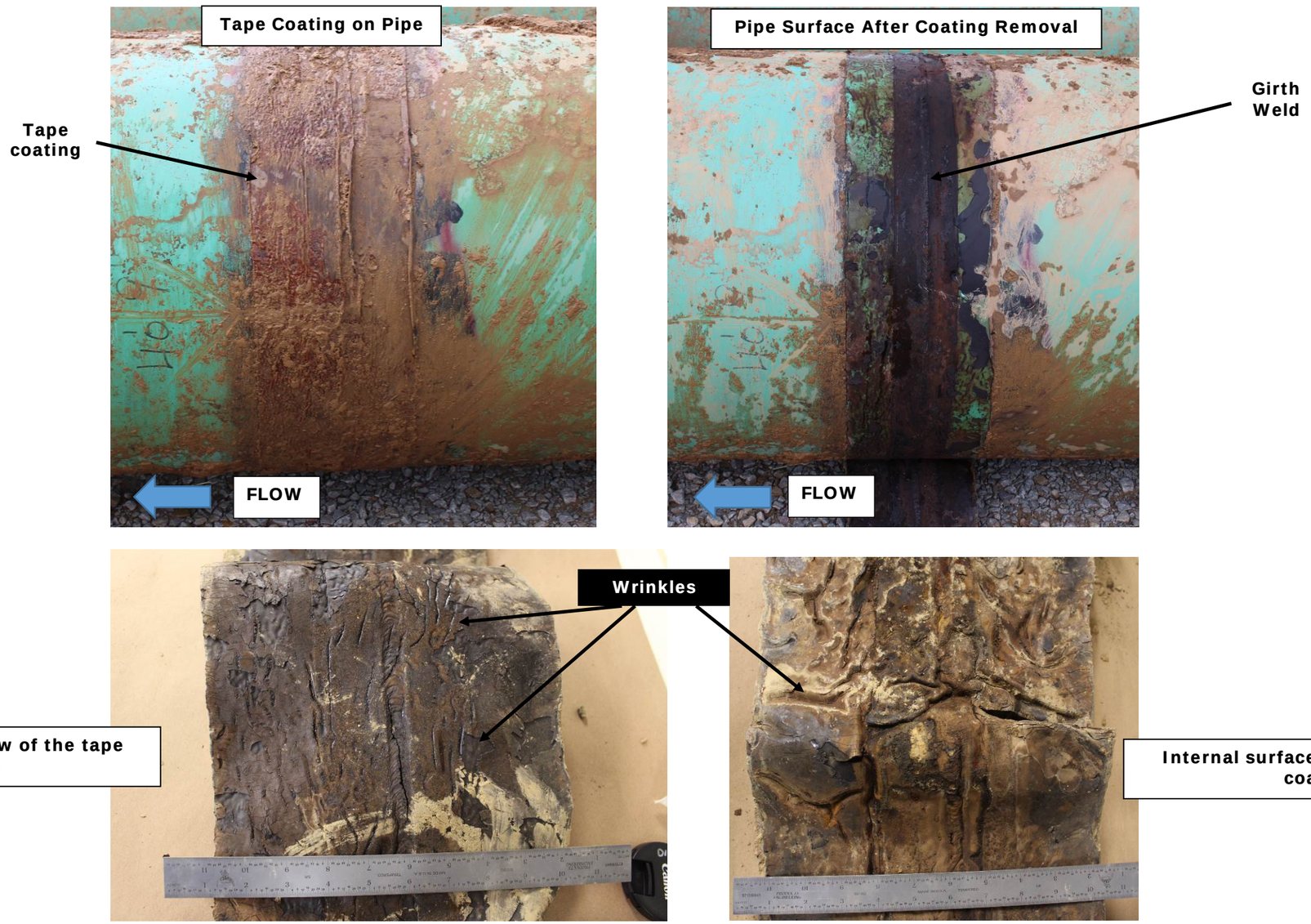

Figure B-4. Photographs showing the tape coating and the pipe surface at GW 2510 before and after removal of the tape from the pipe.

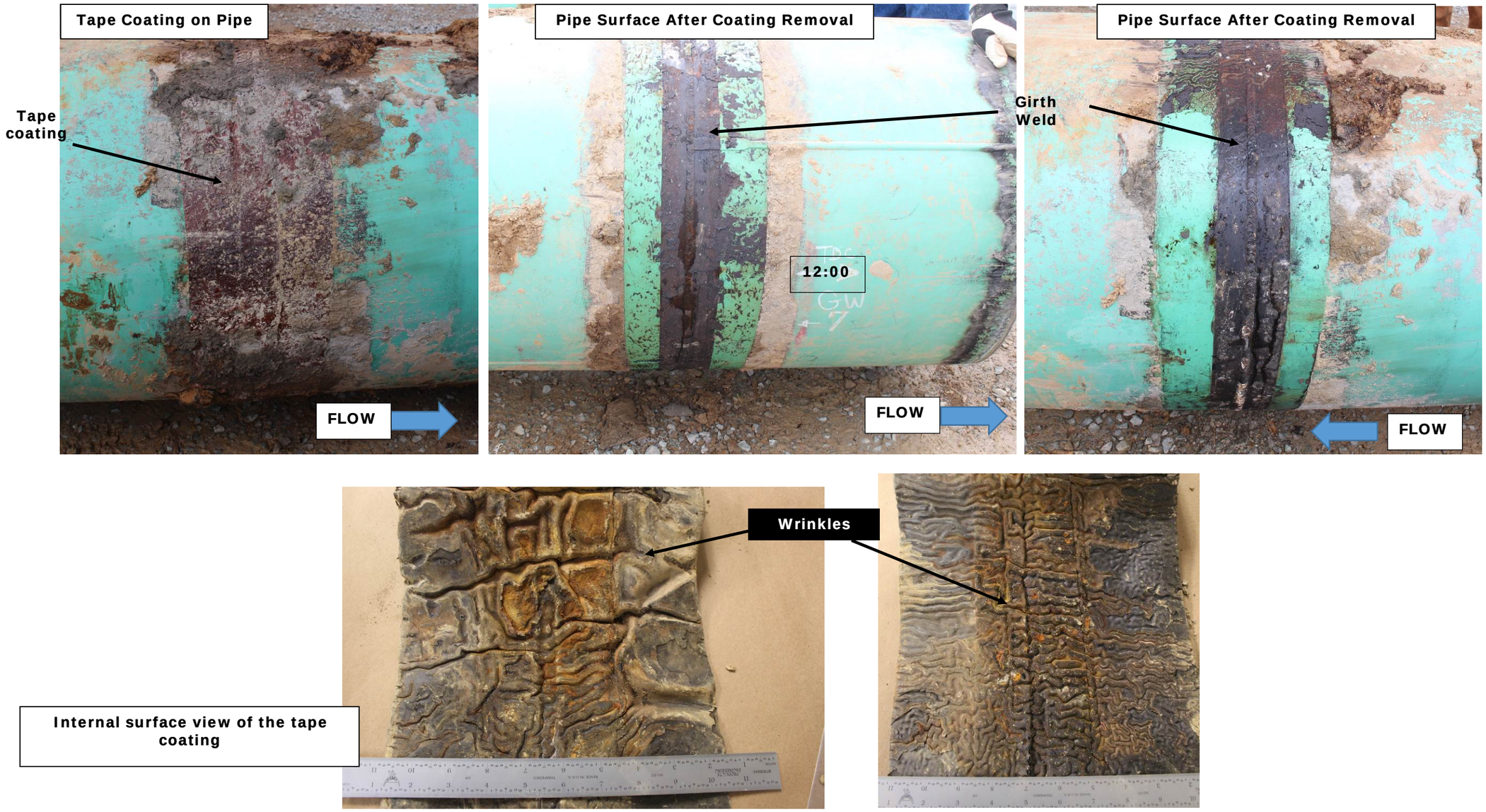

Figure B-5. Photographs showing the tape coating and the pipe surface at GW 2520 before and after removal of the tape from the pipe.

APPENDIX C

ILI-ILI Master Methodology

The distribution of the matched features between the 2005 and 2012 ILI datasets is shown in Figure C1. This distribution provides the most accurate representation of corrosion growth rates between 2005 and 2012. In order to attain a corrosion rate distribution from the 2012 ILI data for the unmatched pits, assumptions were made to the possible initial or starting depths that may not have been called in 2005. For example, a starting value of 0% would indicate that there was not a feature in 2005, while 10% would indicate that the feature was 10% of the wall thickness in 2005, but was not called. In looking at the signal data from the 2005 and 2012 ILI, it is apparent that many of the locations that were not call in 2005 did in fact exhibit a signal indicating corrosion. Therefore, a range of assumed starting values were used to determine the corrosion growth rate distribution for the unmatched feature. These include 0, 5, 7.5, and 10%. The resulting distributions are presented in Figure C2 through Figure C5, respectively. The distributions were then compared to the matched distribution in Figure C1. It is apparent that the distribution with an assumed starting size of 7.5% exhibited the best fit as compared to the matched distribution. Therefore these two datasets were combined to yield a Master ILI to ILI distribution for the 2005 to 2012 corrosion growth rate distributions. This distribution is presented in Figure C6.

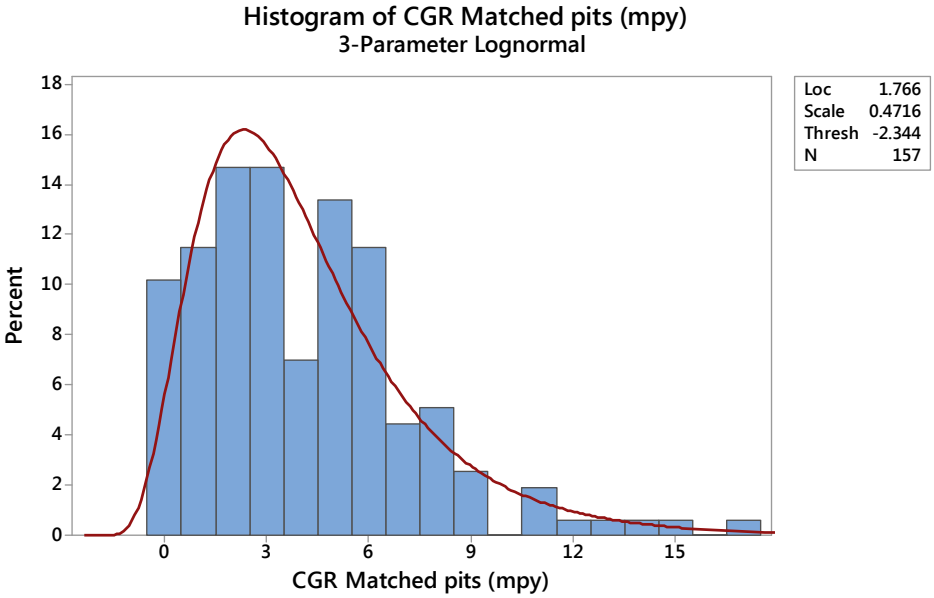

Figure C1. Distribution fit of a 3-Parameter Lognormal to the corrosion growth rates determined from the comparison of the 2005 to 2012 ILI data for matched features.

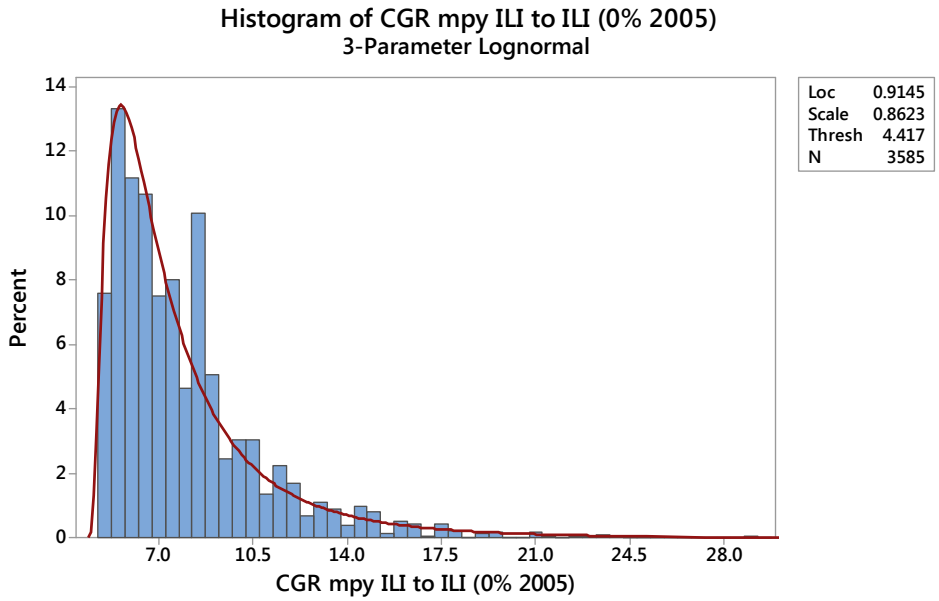

Figure C2. Distribution fit of a 3-Parameter Lognormal to the corrosion growth rates determined from the comparison of the 2005 and 2012 ILI data for unmatched features; assuming depth of 0% in 2005.

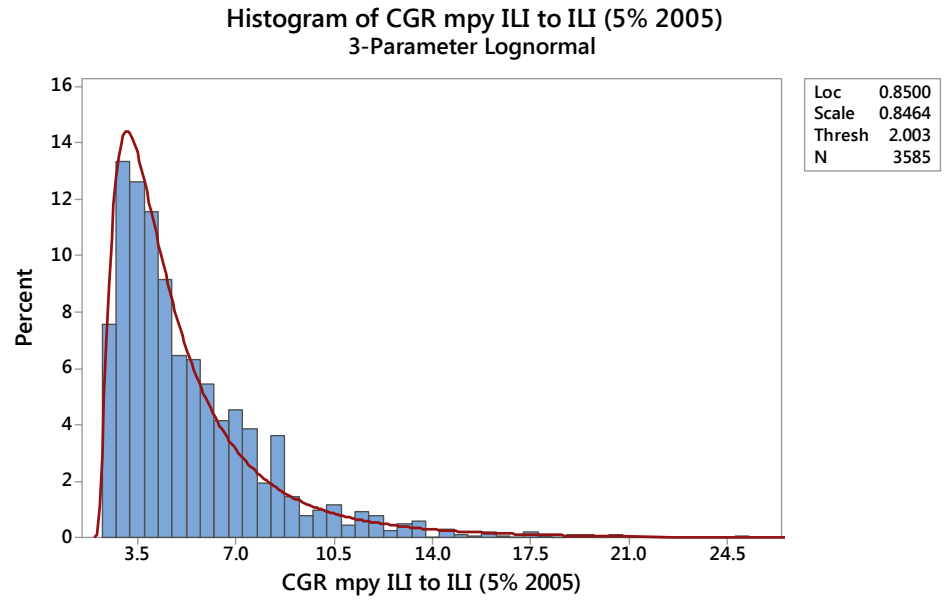

Figure C3. Distribution fit of a 3-Parameter Lognormal to the corrosion growth rates determined from the comparison of the 2005 and 2012 ILI data for unmatched features; assuming depth of 5% in 2005.

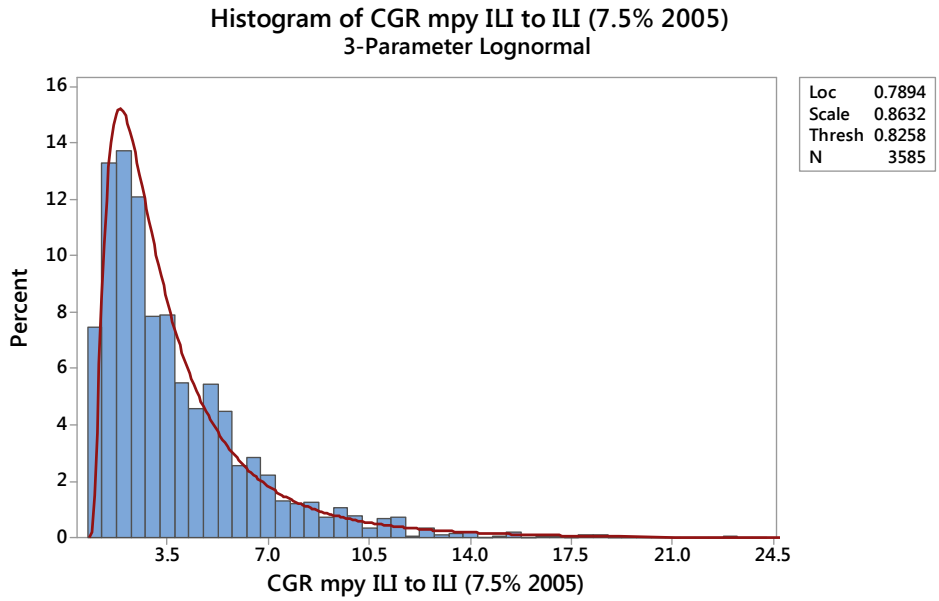

Figure C4. Distribution fit of a 3-Parameter Lognormal to the corrosion growth rates determined from the comparison of the 2005 and 2012 ILI data for unmatched features; assuming depth of 7.5% in 2005.

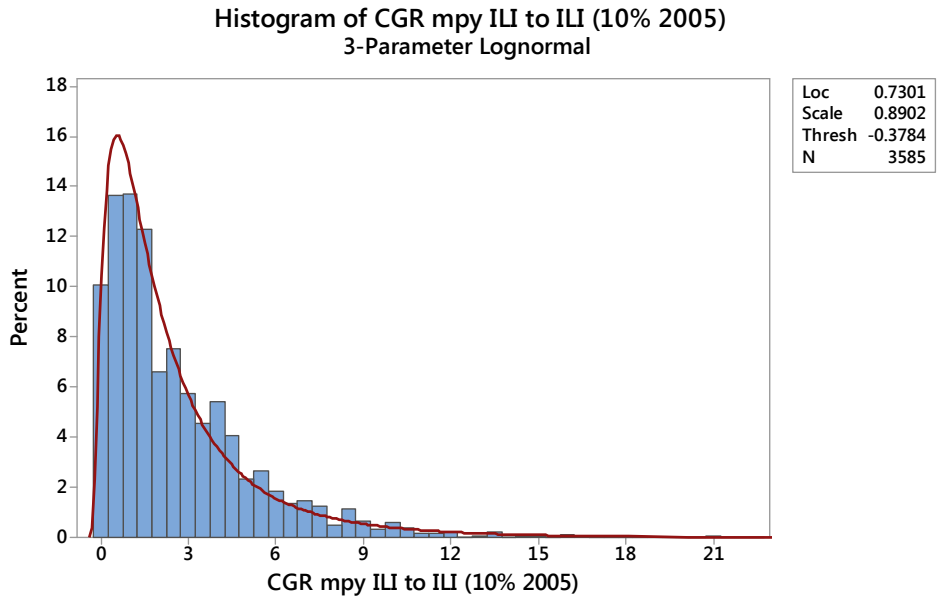

Figure C5. Distribution fit of a 3-Parameter Lognormal to the corrosion growth rates determined from the comparison of the 2005 and 2012 ILI data for unmatched features; assuming depth of 10% in 2005.

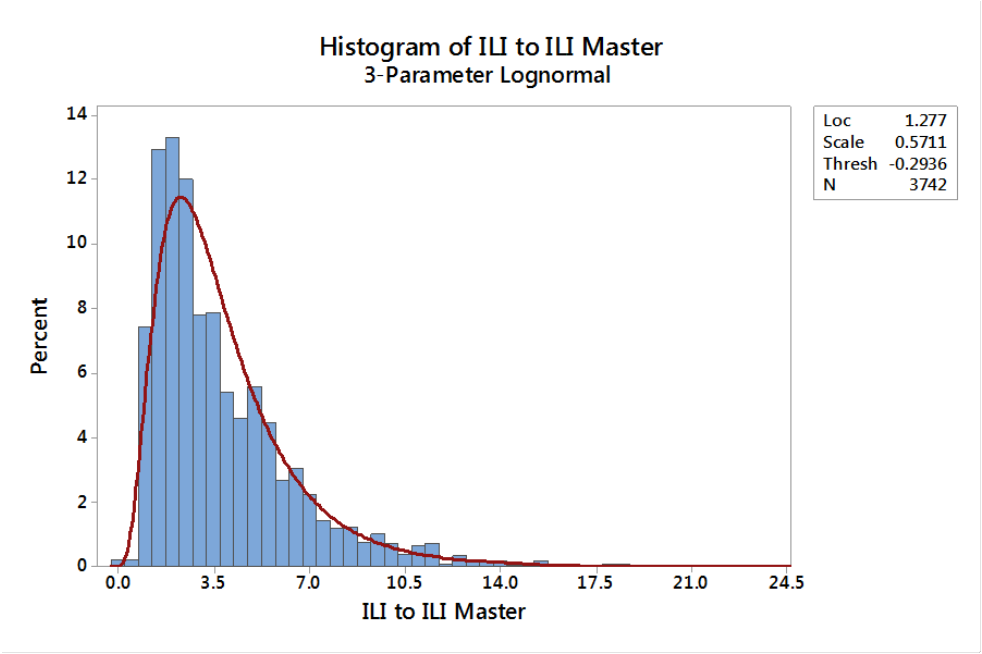

Figure C6. Distribution fit of a 3-Parameter Lognormal to the corrosion growth rates determined from consolidated 2005 to 2012 matched features and 2005 and 2012 ILI data for unmatched features with an assuming depth of 7.5% in 2005.

Inferential Statistical Details

Two-Sample T-Test and CI: CGR (mpy) Field with 6 cutouts, ILI to ILI Master

```
Two-sample T for CGR (mpy) Field with 6 cutouts vs ILI to ILI Master

                            N  Mean  StDev  SE Mean
CGR (mpy) Field with 6 c   106  8.49   7.36     0.72
ILI to ILI Master         3742  3.95   2.75    0.045


Difference = μ (CGR (mpy) Field with 6 cutouts) - μ (ILI to ILI Master)
Estimate for difference:  4.544
95% CI for difference:  (3.123, 5.966)
T-Test of difference = 0 (vs ≠): T-Value = 6.34  P-Value = 0.000  DF = 105
```

Descriptive Statistics: CGR (mpy) Field with 6 cutouts, ILI to ILI Master

```
Variable                    N    Mean   StDev  Minimum      Q1  Median      Q3
Maximum
CGR (mpy) Field with 6 c   106   8.495   7.365    0.130   2.724   5.455  13.965
31.000
ILI to ILI Master         3742  3.9502  2.7509   0.0000  2.1857  3.1571  5.1000
24.1500
```

Mann-Whitney Test and CI: CGR (mpy) Field with 6 cutouts, ILI to ILI Master

```
                                 N  Median
CGR (mpy) Field with 6 cutouts   106   5.455
ILI to ILI Master               3742   3.157


Point estimate for η1 - η2 is 2.018
95.0 Percent CI for η1 - η2 is (1.441,3.265)
W = 272460.0
Test of η1 = η2 vs η1 ≠ η2 is significant at 0.0000
The test is significant at 0.0000 (adjusted for ties)
```

Test and CI for Two Variances: CGR (mpy) Field with 6 cutouts, ILI to ILI Master

```
Method

Null hypothesis         σ(CGR (mpy) Field with 6 cutouts) / σ(ILI to ILI Master) = 1
Alternative hypothesis  σ(CGR (mpy) Field with 6 cutouts) / σ(ILI to ILI Master) ≠ 1
Significance level      α = 0.05


Statistics

                                                          95% CI for
Variable                           N  StDev  Variance      StDevs
```

CGR (mpy) Field with 6 cutouts	106	7.365	54.236	(6.428, 8.597)
ILI to ILI Master	3742	2.751	7.568	(2.625, 2.885)

Ratio of standard deviations = 2.519
Ratio of variances = 7.167

95% Confidence Intervals

Method	CI for StDev Ratio	CI for Variance Ratio
Bonett	(2.043, 3.595)	(4.173, 12.923)
Levene	(2.480, 3.860)	(6.152, 14.897)

Tests

Method	DF1	DF2	Test Statistic	P-Value
Bonett	—	—	—	0.000
Levene	1	3846	285.70	0.000

ABOUT DNV GL

Driven by our purpose of safeguarding life, property, and the environment, DNV GL enables organizations to advance the safety and sustainability of their business. We provide classification and technical assurance along with software and independent expert advisory services to the maritime, oil and gas, and energy industries. We also provide certification services to customers across a wide range of industries. Operating in more than 100 countries, our 16,000 professionals are dedicated to helping our customers make the world safer, smarter, and greener.